

Numerical Simulation of a Lean Premixed Hydrogen Combustor for Aero Engines

F. Veiga López

Numerical Simulation of a Lean Premixed Hydrogen Combustor for Aero Engines

009#16#MT#FPP

By

F. Veiga López

in partial fulfilment of the requirements for the degree of

Master of Science

in Aerospace Engineering

at the Delft University of Technology,

to be defended publicly on Tuesday November 15, 2016 at 09:00 AM.

Supervisor:	Prof. Dr. A. Gangoli Rao and André A.V. Perpignan
Thesis committee:	Prof. Dr. A. Gangoli Rao, TU Delft
	André A.V. Perpignan, TU Delft
	Prof. Dr. D.J.E.M. Roekaerts, TU Delft
	Dr. Ir. M.I. Gerritsma, TU Delft

This thesis is confidential and cannot be made public until December 31, 2016.

An electronic version of this thesis is available at <http://repository.tudelft.nl/>.

Summary

The effect of aviation emissions on human-induced climate change has become a major concern in the last decades. The reduction of emissions, such as CO₂ and NO_x, is an important matter because of the predicted increase of the aviation market in the future years. The application of alternative fuels, such as hydrogen, and new combustion methods (e.g. lean premixed) are two of the main trends in order to reduce civil aviation emissions.

The AHEAD (Advanced Hybrid Engines for Aircraft Development) project presented a novel hybrid engine concept. The proposed innovative design uses two combustion chambers. The first is a cryogenic fuel combustor, conceived to operate with liquid hydrogen or liquid natural gas, followed by an inter-turbine flameless biofuel combustor.

In the present thesis, the lean premixed hydrogen combustor designed in the AHEAD project was simulated by applying a Computational Fluid Dynamics (CFD) method. The main objective of the present study is to find a set of CFD models which better characterize the named combustor, using exclusively the RANS (Reynolds Averaged Navier-Stokes) approach. Both a reactive and non-reactive approaches were followed. The results obtained were analysed and compared with experimental data.

The RANS $k-\epsilon$ realizable turbulence model provided satisfactory qualitative results for the non-reactive case. The model predicted the characteristic features of the flow field obtained at swirling premixed combustors, such as the central and outer recirculation zones, the vortex breakdown, etc.

The reactive flow field was not well characterized by the selected combustion models (e.g. Flamelet-Generated Manifold, Eddy Dissipation Concept). The main problem was found to be the mixing pattern predicted by the set of models used in the study. The RANS turbulence models applied were not accurate enough to obtain a satisfactory hydrogen-air distribution at the mixing area of the combustor. Further analysis is advised, adding a more detailed CFD approach such as the Large Eddy Simulation.

Acknowledgements

First, I would like to thank all the people that have supported me to achieve this final thesis document, both from the University and my personal background.

Thank you to my family, who were always there at the stressful and very difficult moments of this year.

Thank you to André, who gave me very good advises to complete this MSc thesis. His close supervision and help is much more than appreciated!

Finally, say thanks to Arvind Gangoli Rao for his supervision during this Master degree thesis.

Contents

List of figures	9
List of tables	13
Introduction	14
Background.....	16
2.1. Combustion modelling	16
2.2. Hydrogen as future fuel and novel combustion systems; the AHEAD project	27
2.3. Literature review	33
Numerical setup	42
3.1. Meshes	42
3.2. Solving methods, boundary conditions and mesh study	46
Results and discussion	52
4.1. Isothermal flow	52
4.2. Reactive flow.....	56
Conclusions.....	74
Future work	76
Bibliography	77

List of figures

Figure 1. Classification of flames [1].	17
Figure 2. Difference of the temperature evolution using different computational approaches [1].	17
Figure 3. Subdivisions of the region close to the walls [12].	22
Figure 4. FGM method schematic [33].	26
Figure 5. Flammability range of hydrogen and kerosene [46].	28
Figure 6. NO _x emissions comparison for different fuels and combustion methods [46].	28
Figure 7. Effect of tank volume increase on aircraft characteristics [46].	29
Figure 8. AHEAD hybrid engine schematic [56].	29
Figure 9. Variation of hydrogen and methane adiabatic flame temperature with equivalence ratio for different inlet temperatures [54].	30
Figure 10. Variation of NO _x emissions in ppm at 15%O ₂ with equivalence ratio for different inlet temperatures, swirl numbers and axial air injection mass flow [54].	31
Figure 11. Schematic of the AHEAD burner [55].	32
Figure 12. Time-averaged OH PLIF images for air-fuel flow rate of 700slm and adiabatic flame temperature of 1570K for different hydrogen mole fraction [68].	33
Figure 13. Variation of lean blow-off limits of the flame with combustion chamber pressure for different amounts of hydrogen in the fuel mixture [70].	34
Figure 14. Time-averaged OH-PLIF images for different amounts of hydrogen in the fuel mixture [71]. Intensities are multiplied by a factor in order to use the same scale.	35
Figure 15. Velocity distribution at the premixing zone and burner nozzle for different axial mass flow at a swirl number of 0.9 and with a long mixing tube ($u_0 = 70\text{m/s}$) [65].	36
Figure 16. Spatial distribution of time-averaged, normalized concentration of the fuel for different amounts of axial air injection ($D_{or} = 0\text{mm}, 8\text{mm}$ and 8.8mm respectively) [65].	36
Figure 17. Experimental setup schematic for PIV and chemiluminescence measurements [58]	37

Figure 18. Equivalence ratio effect on the reactive flow field ($u_0 = 70\text{m/s}$) [58].	38
Figure 19. Flame probability for different equivalence ratios at a Reynolds number of 75000 [55].	38
Figure 20. ABEL-deconvoluted OH^* images. They are normalized with the maximum intensity at the highest equivalence ratio [58].	38
Figure 21. Mean OH signal probability (top) and instant OH PLIF shoots (bottom) for an inlet temperature of 453K [67].	39
Figure 22. Temperature distribution in the combustion chamber for different amounts of hydrogen [76].	40
Figure 23. Spatial distribution of the time-averaged, normalized concentration of the fuel at the combustion chamber inlet obtained in RANS, LES and the experiments respectively [77].	41
Figure 24. Premix tube 2D geometry simplification.	43
Figure 25. 2D mesh.	44
Figure 26. Isometric (left) and detailed (right) view of the simplified geometry used for the 3D model.	45
Figure 27. Tridimensional mesh.	46
Figure 28. Variation of the swirl number (S) at the premixer outlet with swirler inlet angle for the 2D and 3D case.	49
Figure 29. Measured (symbols) and modeled (lines) fuel temperature variation with equivalence ratio and preheat air temperature [67].	50
Figure 30. Two-dimensional mesh study for 9000, 14000 and 22000 nodes ($u_0 = 70\text{m/s}$; $v_0 = 20\text{m/s}$; $D = 34\text{mm}$).	51
Figure 31. Three-dimensional mesh study for 140000, 250000, 500000 and 700000 nodes ($u_0 = 70\text{m/s}$; $v_0 = 20\text{m/s}$; $D = 34\text{mm}$).	51
Figure 32. Velocity distribution in the combustion chamber obtained with CFD 2D RANS standard and realizable $k-\epsilon$ models ($u_0 = 70\text{m/s}$; $v_0 = 20\text{m/s}$; $D = 34\text{mm}$).	53
Figure 33. Axial (top) and radial (bottom) velocity contours obtained with CFD 2D RANS standard $k-\epsilon$ model (left) and with experiments (right) [58].	53
Figure 34. Velocity distribution in the combustion chamber obtained with CFD 3D RANS realizable $k-\epsilon$ models applying an inlet angle of 35° at the swirl inlet ($u_0 = 70\text{m/s}$; $v_0 = 20\text{m/s}$; $D = 34\text{mm}$).	54

Figure 35. Velocity distribution in the combustion chamber obtained with CFD 3D RANS standard and realizable k- ϵ models ($u_0 = 70\text{m/s}$; $v_0 = 20\text{m/s}$; $D = 34\text{mm}$).	55
Figure 36. Stagnation point location comparison for the studied meshes ($u_0 = 70\text{m/s}$; $D = 34\text{mm}$).	56
Figure 37. Temperature distribution obtained with the 2D approach, EDC model, Li et al. chemistry reaction mechanism and realizable k- ϵ turbulence model ($T_{\text{max}} = 1666\text{K}$).	57
Figure 38. Axial velocity distribution obtained with the 2D approach, EDC model, Li et al. chemistry reaction mechanism and realizable k- ϵ turbulence model ($u_0 = 70\text{m/s}$).	57
Figure 39. Variation of resultant swirl number and different vortex breakdown types with geometrical swirl number and axial air injection [81].	58
Figure 40. Mass fraction of hydrogen normalized with the stoichiometric value obtained with the 2D approach, EDC model, Li et al. chemistry reaction mechanism and realizable k- ϵ turbulence model.	59
Figure 41. Streamlines of hydrogen and air at the mixing section obtained with the 2D approach, EDC model, Li et al. chemistry reaction mechanism and realizable k- ϵ turbulence model.	60
Figure 42. OH mass fraction normalized with the value of 0.004, obtained with the 2D approach, EDC model, Li et al. chemistry reaction mechanism and realizable k- ϵ turbulence model.	61
Figure 43. Normalized heat release (left) obtained with the 2D approach, EDC model, Li et al. chemistry reaction mechanism and realizable k- ϵ turbulence model and normalized experimental OH* (right) [58].	61
Figure 44. Normalized OH distribution at the mid-plane of the analyzed combustor, obtained with the standard (left) and the realizable (right) k- ϵ turbulence model, EDC and Li et al. chemical reaction mechanism.	62
Figure 45: OH mass fraction axial variation predicted with the realizable k- ϵ turbulence model, EDC and Li et al. chemical reaction mechanism.	63
Figure 46. OH mass fraction obtained with different mean source term variance modelling; Transport equation (left) and Algebraic (right) approaches. Results obtained with the k- ϵ realizable turbulence model, Li et al. [17] chemical mechanism and FGM.	65
Figure 47. Temperature distribution normalized with the maximum value at stoichiometric conditions ($T_{\text{max}} = 2460\text{K}$) at the combustion chamber for different equivalence ratios obtained with the 3D approach, FGM model, Li et al. chemical reaction mechanism and realizable k- ϵ turbulence model.	66

Figure 48. Swirl number variation with equivalence ratio at the combustion chamber inlet obtained with the 3D approach, FGM model, Li et al. chemistry reaction mechanism and realizable k-ε turbulence model.67

Figure 49. Normalized OH distribution at the combustion chamber for an equivalence ratio of 0.4 obtained with the 3D approach, FGM model, Li et al. chemistry reaction mechanism and realizable k-ε turbulence model.67

Figure 50. Finite Rate (left) and Turbulent Flame Speed (right) source term at the combustion chamber for an equivalence ratio of 0.4 obtained with the 3D approach, FGM model, Li et al. chemistry reaction mechanism and realizable k-ε turbulence model.68

Figure 51. Normalized mixture fraction at the combustion chamber inlet for an equivalence ratio of 0.4 obtained with the 3D approach, FGM model, Li et al. chemical reaction mechanism and realizable k-ε turbulence model.69

Figure 52. Temperature distribution normalized with the maximum value at stoichiometric conditions ($T_{max} = 2455K$) at the combustion chamber for different equivalence ratios obtained with the 3D approach, EDC model, Li et al. chemistry reaction mechanism and realizable k-ε turbulence model.70

Figure 53. Normalized OH distribution at the combustion chamber for an equivalence ratio of 0.4 obtained with the 3D approach, EDC model, Li et al. chemical reaction mechanism and realizable k-ε turbulence model.71

Figure 54. Normalized heat release (left) obtained with the 3D approach, EDC model, Li et al. chemistry reaction mechanism and realizable k-ε turbulence model and normalized experimental OH* (right) [58].71

Figure 55. Normalized hydrogen mass fraction at the combustion chamber inlet for an equivalence ratio of 0.4 obtained with the 3D approach, EDC model, Li et al. chemical reaction mechanism and realizable k-ε turbulence model.72

Figure 56. Hydrogen streamline calculated from the fuel inlets at the mixing section obtained with the 3D approach, EDC model, Li et al. chemistry reaction mechanism and realizable k-ε turbulence model.72

List of tables

Table 1. Comparison between RANS, LES and DNS [1].	18
Table 2. Reaction mechanism for hydrogen and oxygen [17] in the form $k = AT^n \exp(-E/RT)$ for nitrogen as the main bath (units are cm, moles, s, cal and K).	23
Table 3. Revised H ₂ /O ₂ Reaction Mechanism [18], units are cm ³ , mol, s, kcal, K.	24
Table 4. Parameters (Inlet temperature, mass flow, swirl number and axial mass flow percentage) used for the calculation of NO _x emissions in the cases presented in Figure 9	31
Table 5. 2D mesh quality report.	44
Table 6. 3D mesh quality report.	46
Table 7. Summary of the boundary conditions for the non-reactive case.	47
Table 8. Fuel mass flow for the studied cases.	49
Table 9. Axial flame position predicted by the experiments [67] and the 3D approach with the standard and the realizable k-ε turbulence model, EDC and Li et al. chemical reaction mechanism.	63
Table 10. Summary of the Flamelet Generated Manifold parameters chosen for the case at hand.	64
Table 11. Axial flame position predicted by the experiments [67] and the 3D approach with the realizable k-ε turbulence model, Li et al. chemical reaction mechanism and EDC/FGM.	69

1

Introduction

Human-induced climate change has become a major concern in the last decades. The impact on climate of aerospace emissions cannot be neglected, which represents an important part of the total anthropogenic radiative forcing. Aviation is and will be a noteworthy part of the problem due to the expected growth of this sector in the next years.

One of the approaches in order to reduce civil aviation emissions is the design and development of innovative propulsion systems. New engine configurations are being developed because of the increasing demand for less polluting and more fuel efficient aircraft. The AHEAD (Advanced Hybrid Engines for Aircraft Development) project presented a novel hybrid engine concept. The proposed innovative design uses two combustion chambers. The first is a cryogenic fuel combustor, conceived to operate with liquid hydrogen or liquid natural gas. This is followed by an inter-turbine flameless biofuel combustor. The main challenges faced during the design of the cryogenic combustor were the high reactivity of hydrogen, which can become a problem when using it as premixed fuel, and its tendency to cause flashback.

Alternative fuels, such as hydrogen and biofuels, are an option to replace current fossil fuels. Moreover, the implementation of new combustion methods (e.g. lean premixed and flameless combustion) potentially improves the overall performance and reduces the emissions of undesired products such as CO₂ and NO_x.

Numerical analysis is a common tool in the design of combustion chambers, which can provide a lot of information about a particular matter with a relatively low cost. Numerical analysis is widely applied in industry and academia because it provides approximate but fairly precise solutions to difficult problems. Computational Fluid Dynamics (CFD) is a numerical analysis method in which the well-known finite volume approach is applied to solve the Navier-Stokes equations. CFD can also be used to solve combustion problems. Simulating reactive flows is a challenging task. Different scientific fields such as fluid dynamics, chemistry and heat transfer are involved thus making these studies multidisciplinary and complex.

The main objective of the present study is to find a set of CFD models which better characterize the lean premixed cryogenic combustor developed for the AHEAD project, using exclusively the RANS (Reynolds Averaged Navier-Stokes)

approach. The results obtained are compared to the available experimental data regarding the same combustor. The simulations performed will provide a set of models suited to this type of combustion. It could be used as a reference for future hydrogen-air premixed combustion studies, as well as within the AHEAD project for further research.

In the remainder of the present report, essential theory related to combustion CFD is provided. Then, an overview of the AHEAD project is given, focusing on the first stage combustor of the hybrid engine. Furthermore, the state of the art concerning experimental and numerical hydrogen combustion is presented. Next, the models used to perform the calculation as well as the results obtained for different studies are introduced. Additionally, these results are discussed and compared to the available experimental data. Finally, the conclusions of the study are drawn, followed by recommendations for future work.

2

Background

In this chapter, a review of the literature regarding hydrogen combustion computational simulations is presented. The objective of this chapter is to give a general insight on the current developments in this area. This will position the present project in a larger framework and show the gap which will be covered.

First, a basic theoretical survey regarding the numerical models applied during the simulations is given. Next, a general outlook of the AHEAD project is provided; the feasibility of using hydrogen as fuel, the influence of different parameters in the combustor design, and the lean premixed hydrogen combustor are analysed. Finally, similar cases to the problem investigated in this report are studied.

2.1. Combustion modelling

Combustion is a complex process that englobes different disciplines, such as fluid dynamics, chemistry and heat transfer. Flames can be divided into four different types, depending on the mixing and the flow regimen (Figure 1). The problem at hand is a turbulent premixed case.

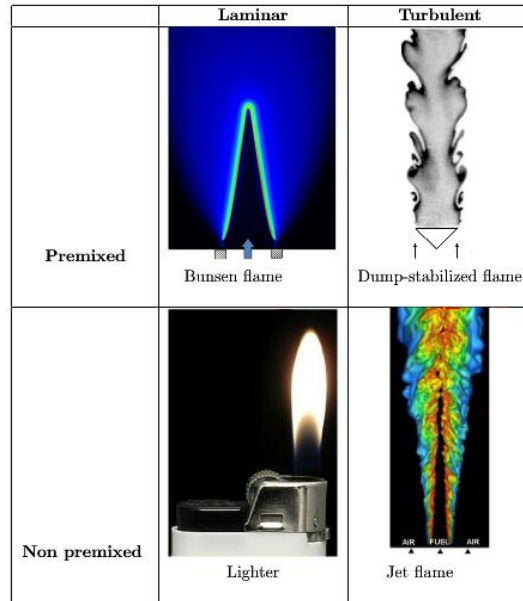


Figure 1. Classification of flames [1].

Furthermore, when describing a problem using Computational Fluid Dynamics (CFD), three computational levels can be used [1]:

- Reynolds Averaged Navier-Stokes (RANS). This technique was developed to solve for the mean values of all quantities. The averaged equations require closure rules.
- Large Eddy Simulations (LES). The turbulent large scales are explicitly calculated whereas the effects of smaller ones are modeled using sub grid closure rules.
- Direct Numerical Simulations (DNS). The full instantaneous Navier-Stokes equations are solved without any model for turbulent motion.

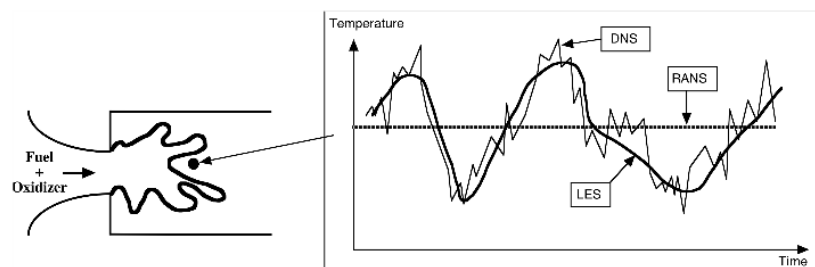


Figure 2. Difference of the temperature evolution using different computational approaches [1].

The following table (Table 1) compares the three approaches, providing all the advantages and disadvantages of each particular one. For the hydrogen combustor of the AHEAD engine, the Reynolds Averaged Navier Stokes (RANS) modelling was used, mainly because of the limited computational power available.

Table 1. Comparison between RANS, LES and DNS [1].

Approach	Advantages	Drawbacks
RANS	<ul style="list-style-type: none"> - "Coarse" numerical grid - Geometrical simplification (2D flows, symmetry, etc.) - "Reduced" numerical costs 	<ul style="list-style-type: none"> - Only mean flow field - Models required
LES	<ul style="list-style-type: none"> - Unsteady features - Reduced modelling impact (compared to RANS) 	<ul style="list-style-type: none"> - Models required - 3D simulations required - Needs precise codes - Numerical costs
DNS	<ul style="list-style-type: none"> - No models needed for turbulence/combustion interaction - Tool to study models 	<ul style="list-style-type: none"> - Prohibitive numerical costs (fine grids, precise codes) - Limited to academic problems

Regarding turbulent premixed combustion, these type of problems are treated as an interaction between a flame front and turbulent "eddies" with sizes and characteristic speeds that go from the integral to the Kolmogorov scale. Dimensionless parameters as the Damköhler and the Karlovitz numbers can be defined to ease its study [1]. Also different diagrams, such as the one proposed by Peters [2], were created to characterize this type of flames with reference to the aforementioned dimensionless parameters.

Combustion modelling mainly concerns the study of turbulence, chemical kinetics and the interaction between these two. In this chapter, the models used during the present study are introduced. First, the turbulence models considered are explained. Next, the chemical reaction mechanisms employed are described. Then, the chemistry-turbulence interaction models are presented.

- **Turbulence models**

When averaging the Navier-Stokes equations using the Favre (i.e. mass-weighted) approach, some terms have to be modelled to close the system. Turbulence models provide approximations for the Reynolds stress tensor. These can be divided into two main categories: Eddy Viscosity Models (EVM) and Reynolds Stress Models (RSM).

Boussinesq [3] introduced the concept of eddy viscosity in order to model the momentum transfer caused by turbulent eddies. Applying this hypothesis, different approaches regarding turbulence modelling appeared in history. First, an algebraic model was proposed by Prandtl, followed by other "zero-equations" formulations [4]. Then, one [5] or more transport equations [6]–[8] were suggested. The standard k-ε [6] and the realizable k-ε [7] will be used in the CFD model, thus a more detailed analysis of these will be done.

In the Reynolds Stress Model [9]–[11], the system is closed by calculating the Reynolds stresses and the turbulent dissipation rate using transport equations. The Reynolds Stress Model is supposed to provide better results for complex flow configurations. However, in the present project was not considered because of its high computational time. Additionally, the k-ε approach provided valid results for the non-reactive case with much lower computational requirements.

Standard k-ε

The standard k-ε [6] is a two-equation eddy viscosity turbulence model. These models obtain turbulence length and time scale by solving two separate equations. The standard k-ε solves these equations for turbulence kinetic energy (k) and turbulence dissipation rate (ε). It is a semi-empirical model; thus the equations of the model are derived from different phenomenological considerations and experimentation. Furthermore, this model assumes fully turbulent flow.

The following transport equations are used to obtain the turbulence kinetic energy (1) and turbulence dissipation rate (2) [12].

$$\frac{\partial}{\partial t}(\rho k) + \frac{\partial}{\partial x_i}(\rho k u_i) = \frac{\partial}{\partial x_j} \left[\left(\mu + \frac{\mu_t}{\sigma_k} \right) \frac{\partial k}{\partial x_j} \right] + G_k + G_b - \rho \varepsilon - Y_M + S_k \quad (1)$$

$$\frac{\partial}{\partial t}(\rho \varepsilon) + \frac{\partial}{\partial x_i}(\rho \varepsilon u_i) = \frac{\partial}{\partial x_j} \left[\left(\mu + \frac{\mu_t}{\sigma_\varepsilon} \right) \frac{\partial \varepsilon}{\partial x_j} \right] + C_{1\varepsilon} \frac{\varepsilon}{k} (G_k + C_{3\varepsilon} G_b) - C_{2\varepsilon} \rho \frac{\varepsilon^2}{k} + S_\varepsilon \quad (2)$$

Where G_k (3) represents the generation of turbulence kinetic energy due to the mean velocity gradients.

$$G_k = -\rho \overline{u_i' u_j'} \frac{\delta u_j}{\delta x_i} = \mu_t S^2 \quad (3)$$

With $S = \sqrt{2S_{ij}S_{ij}}$, which represents the modulus of the mean rate-of-strain tensor.

G_b (4) is the generation of k due to buoyancy, and for ideal gases the following expression is used.

$$G_b = -g_i \frac{\mu_t}{\rho Pr_t} \frac{\partial \rho}{\partial x_i} \quad (4)$$

Where g_i refers to the gravity component and Pr_t (turbulent Prandtl number) is 0.85.

Y_M (5) is the contribution of fluctuating dilatation in compressible turbulence to the dissipation rate.

$$Y_M = 2\rho\varepsilon M_t^2 \quad (5)$$

With M_t (turbulent Mach number) = $\sqrt{\frac{k}{a^2}}$ where a is the speed of sound.

Turbulent viscosity is computed from (6) for every eddy viscosity model.

$$\mu_t = \rho C_\mu \frac{k^2}{\varepsilon} \quad (6)$$

S_k and S_ε are the source terms for turbulent kinetic energy and rate of dissipation respectively. These terms can be defined by the user.

The constants of the model have the following values by default

$$C_{1\varepsilon} = 1.44 ; C_{2\varepsilon} = 1.92 ; C_\mu = 0.09 ; \sigma_k = 1 ; \sigma_\varepsilon = 1.3$$

Being σ_k and σ_ε the turbulent Prandtl numbers for turbulent kinetic energy and rate of dissipation respectively. The possibility of modifying the constants of the model was assessed in some studies [13]. It has to be mentioned that modifying the constants of any model has to be done carefully. The possibility of obtaining unrealistic flow fields is high. On the present report, only the results obtained using the default constant values are reported.

Realizable k- ε

The realizable k- ε model [7] is a variant of the previous model. Realizability [14] is defined as the absence of negative turbulent normal stresses and the positivity of the Schwarz inequality. This principle should be obeyed by any turbulence model in order to prevent it from producing non-physical results. The main differences from the standard model are the alternative formulation for the turbulent viscosity and a revised transport equation for the dissipation rate, based on the dynamic equation of the mean-square vorticity fluctuation [12]. The realizable k- ε model has been validated in several complex flows, such as confined or swirl dominated flows [7], [15].

Following the same nomenclature as for the standard model, the transport equation for the turbulent kinetic energy (7) and the revised transport equation for the eddy dissipation (8) are:

$$\frac{\partial}{\partial t}(\rho k) + \frac{\partial}{\partial x_j}(\rho k u_j) = \frac{\partial}{\partial x_j} \left[\left(\mu + \frac{\mu_t}{\sigma_k} \right) \frac{\partial k}{\partial x_j} \right] + G_k + G_b - \rho\varepsilon - Y_M + S_k \quad (7)$$

$$\frac{\partial}{\partial t}(\rho\varepsilon) + \frac{\partial}{\partial x_j}(\rho\varepsilon u_j) = \frac{\partial}{\partial x_j} \left[\left(\mu + \frac{\mu_t}{\sigma_\varepsilon} \right) \frac{\partial \varepsilon}{\partial x_j} \right] + \rho C_{1\varepsilon} S_\varepsilon - \rho C_{2\varepsilon} \frac{\varepsilon^2}{k + \sqrt{v\varepsilon}} + C_{1\varepsilon} \frac{\varepsilon}{k} C_{3\varepsilon} G_b + S_\varepsilon \quad (8)$$

Where $C_1 = \max \left[0.43, \frac{\eta}{\eta + 5} \right]$, with $\eta = S \frac{k}{\varepsilon}$.

In this model, turbulent viscosity is calculated using the same procedure as in every eddy viscosity model (6). However, the constant C_μ is now a function of the rotation and mean strain rates. It is calculated using the following expression (9).

$$C_\mu = \frac{1}{A_0 + A_s \frac{kU^*}{\varepsilon}} \quad (9)$$

Where $U^* = \sqrt{S_{ij}S_{ij} + \widetilde{\Omega}_{ij}\widetilde{\Omega}_{ij}}$ with $\widetilde{\Omega}_{ij} = \overline{\Omega}_{ij} - 3\varepsilon_{ijk}\omega_k$, $A_0 = 4.04$ and $A_s = \sqrt{6} \cos\phi$. The parameter ϕ can be obtained from (10)

$$\phi = \frac{1}{3} \cos^{-1}(\sqrt{6}W) \quad (10)$$

Where $W = \frac{S_{ij}S_{jk}S_{ki}}{S^3}$, $S = \sqrt{S_{ij}S_{ij}}$ and $S_{ij} = \frac{1}{2} \left(\frac{\partial u_j}{\partial x_i} + \frac{\partial u_i}{\partial x_j} \right)$. Finally, the default constants of the model used in Fluent[®] are:

$$C_{1\varepsilon} = 1.44 ; C_{2\varepsilon} = 1.9 ; \sigma_k = 1 ; \sigma_\varepsilon = 1.2$$

Wall treatment

The near-wall region can be subdivided into three layers (Figure 3). The viscous sublayer, where the flow is almost laminar. An intermediate sublayer, where the effects of viscosity and turbulence are of similar importance. And the outer layer, where turbulence plays a major role. Y^+ (11) determines the position of a node in relation to the subdivisions.

$$Y^+ = \frac{\rho u_\tau y}{\mu_t} \text{ with } u_\tau = \sqrt{\frac{\tau_w}{\rho}} \quad (11)$$

Two approaches are traditionally followed to model the region close to the walls. Applying wall functions, the viscous sublayer is not resolved but estimated by different developed functions [12]. Y^+ values higher than 15 would provide errors to the simulation results. Or using the near-wall model, which resolves the whole domain, all the way down to the wall. This approach requires very refined meshes at the area (Y^+ values around 1), leading to high computational cost.

For the turbulence models presented above, Fluent[®] provides a near wall treatment that combines a two-layer model with enhanced wall functions [12]. This provides a Y^+ independent model to the user. This model is applied in the present project.

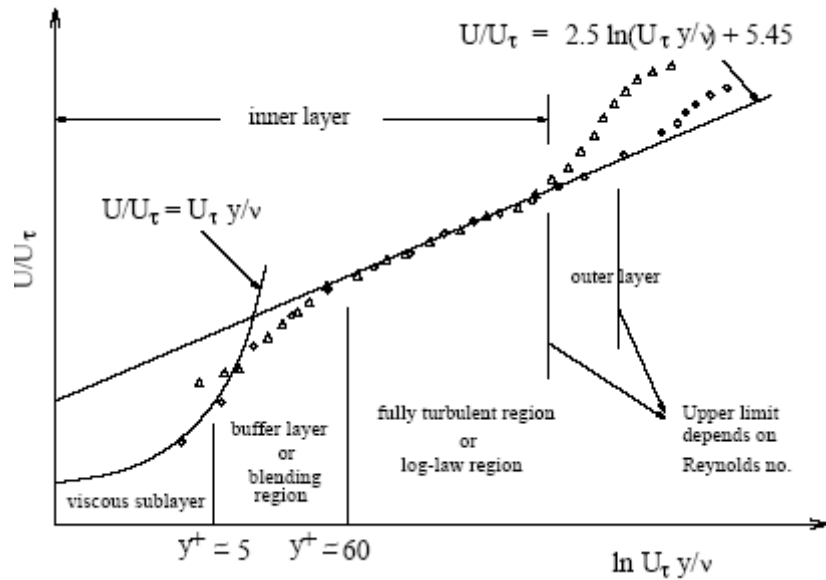


Figure 3. Subdivisions of the region close to the walls [12].

▪ Chemical reaction mechanisms

Chemical kinetics is a capital point when modelling a combustion problem. In this section, the hydrogen combustion kinetics applied to the model are introduced.

In the present study, only detailed mechanisms are used to have more accurate results when applying them directly and are not simplified as in the Flamelet Generated Manifold turbulence-chemistry interaction model. This is because they provide a high degree of detail. Ströhle and Myhrvold [16] defended the use of the mechanisms proposed by Li et al. (Table 2) and Ó Conaire et al. (Table 3) because of the good agreement with the data taken from combustion experiments under gas turbine conditions.

Table 2. Reaction mechanism for hydrogen and oxygen [17] in the form $k = AT^n \exp(-E/RT)$ for nitrogen as the main bath (units are cm, moles, s, cal and K).

No.	Reaction	A	n	E
1	$H + O_2 = O + OH$	3.547×10^{15}	-0.406	16.599
2	$O + H_2 = H + OH$	0.508×10^{05}	2.67	6290
3	$H_2 + OH = H_2O + H$	0.216×10^{09}	1.51	3430
4	$O + H_2O = OH + OH$	2.970×10^{06}	2.02	13.400
5	$H_2 + M = H + H + M^a$	4.577×10^{19}	-1.40	104.380
6	$O + O + M = O_2 + M^a$	6.165×10^{15}	-0.50	0
7	$O + H + M = OH + M^a$	4.417×10^{18}	-1.00	0
8	$H + OH + M = H_2O + M^a$	3.800×10^{22}	-2.00	0
9	$H + O_2 + M = HO_2 + M^b$	k_∞ 1.475×10^{12}	0.60	0
		k_0 6.366×10^{20}	-1.72	524.8
10	$HO_2 + H = H_2 + O_2$	1.660×10^{13}	0.0	823
11	$HO_2 + H = OH + OH$	7.079×10^{13}	0.0	295
12	$HO_2 + O = O_2 + OH$	0.325×10^{14}	0.0	0
13	$HO_2 + OH = H_2O + O_2$	2.890×10^{13}	0.0	-497
14	$HO_2 + HO_2 = H_2O_2 + O_2$	4.200×10^{14}	0.0	11.982
		1.300×10^{11}	0.0	-1629.3
15	$H_2O_2 + M = OH + OH + M^c$	k_∞ 2.951×10^{14}	0.0	48.430
		k_0 1.202×10^{17}	0.0	45.500
16	$H_2O_2 + H = H_2O + OH$	0.241×10^{14}	0.0	3970
17	$H_2O_2 + H = HO_2 + H_2$	0.482×10^{14}	0.0	7950
18	$H_2O_2 + O = OH + HO_2$	9.550×10^{06}	2.0	3970
19	$H_2O_2 + OH = HO_2 + H_2O$	1.000×10^{12}	0.0	0
		5.800×10^{14}	0.0	9557
a	Third body enhancement factor: $H_2 = 2.5$, $H_2O = 12$.			
b	Third body enhancement factor: $H_2 = 2$, $H_2O = 11$, $O_2 = 0.78$. Troe parameter: 0.8.			
c	Third body enhancement factor: $H_2 = 2$, $H_2O = 11$. Troe parameter: 0.5.			

Table 3. Revised H₂/O₂ Reaction Mechanism [18], units are cm³, mol, s, kcal, K.

	Reaction	A	n	E _a
H ₂ /O ₂ chain reactions				
1	H + O ₂ = O + OH	1.91 x 10 ¹⁴	0.00	16.44
2	O + H ₂ = H + OH	5.08 x 10 ⁰⁴	2.67	6.292
3	OH + H ₂ = H + H ₂ O	2.16 x 10 ⁰⁸	1.51	3.43
4	O + H ₂ O = OH + OH	2.97 x 10 ⁰⁶	2.02	13.4
H ₂ /O ₂ dissociation/recombination reactions				
5 ^a	H ₂ + M = H + H + M	4.57 x 10 ¹⁹	-1.40	105.1
6 ^b	O + O + M = O ₂ + M	6.17 x 10 ¹⁵	-0.50	0
7 ^c	O + H + M = OH + M	4.72 x 10 ¹⁸	-1.00	0
8 ^{d, e}	H + OH + M = H ₂ O + M	4.50 x 10 ²²	-2.00	0
Formation and consumption of HO ₂				
9 ^{f, g}	H + O ₂ + M = HO ₂ + M	3.48 x 10 ¹⁶	-0.41	-1.12
	H + O ₂ = HO ₂	1.48 x 10 ¹²	0.60	0.00
10	HO ₂ + H = H ₂ + O ₂	1.66 x 10 ¹³	0.00	0.82
11	HO ₂ + H = OH + OH	7.08 x 10 ¹³	0.00	0.30
12	HO ₂ + O = OH + O ₂	3.25 x 10 ¹³	0.00	0.00
13	HO ₂ + OH = H ₂ O + O ₂	2.89 x 10 ¹³	0.00	-0.50
Formation and consumption of H ₂ O ₂				
14 ^h	HO ₂ + HO ₂ = H ₂ O ₂ + O ₂	4.2 x 10 ¹⁴	0.00	11.98
	HO ₂ + HO ₂ = H ₂ O ₂ + O ₂	1.3 x 10 ¹¹	0.00	-1.629
15 ^{i, f}	H ₂ O ₂ + M = OH + OH + M	1.27 x 10 ¹⁷	0.00	45.5
	H ₂ O ₂ = OH + OH	2.95 x 10 ¹⁴	0.00	48.4
16	H ₂ O ₂ + H = H ₂ O + OH	2.41 x 10 ¹³	0.00	3.97
17	H ₂ O ₂ + H = H ₂ + HO ₂	6.03 x 10 ¹³	0.00	7.95
18	H ₂ O ₂ + O = OH + HO ₂	9.55 x 10 ⁰⁶	2.00	3.97
19 ^h	H ₂ O ₂ + OH = H ₂ O + HO ₂	1.0 x 10 ¹²	0.00	0.00
	H ₂ O ₂ + OH = H ₂ O + HO ₂	5.8 x 10 ¹⁴	0.00	9.56
a	Efficiency factors are H ₂ O = 12.0; H ₂ = 2.5.			
b	Efficiency factors are H ₂ O = 12.0; H ₂ = 2.5; Ar = 0.83; He = 0.83.			
c	Efficiency factors are H ₂ O = 12.0; H ₂ = 2.5; Ar = 0.75; He = 0.75.			
d	Original pre-exponential A factor is multiplied by 2 here.			
e	Efficiency factors are H ₂ O = 12.0; H ₂ = 0.73; Ar = 0.38; He = 0.38.			
f	Troe parameters: reaction 9, a = 0.5, T*** = 1.0 x 10 ⁻³⁰ , T* 1.0 x 10 ³⁰ , T*** = 1.0 x 10 ¹⁰⁰ ; reaction 15, a = 0.5, T*** = 1.0 x 10 ⁻³⁰ , T* = 1.0 x 10 ³⁰ .			
g	Efficiency factors are H ₂ O = 14.0; H ₂ = 1.3; Ar = 0.67; He = 0.67.			
h	Reactions 14 and 19 are expressed as the sum of the two rate expressions.			
i	Efficiency factors are H ₂ O = 12.0; H ₂ = 2.5; Ar = 0.45; He = 0.45.			

Furthermore, the same authors [16] recommended to apply the Li et al. reaction mechanism because it presents more up-to date data for high pressure condition when comparing it to the Ó Conaire mechanism. The chemical reaction mechanism proposed by Li et al. was used for the current study. Additional reactions should be considered in order to take NO_x into account [19].

• Turbulence-chemistry interaction models

Modelling the interaction between chemical reactions and turbulence. Scientists developed different concepts to solve this problem. The laminar flamelet approach [1], [20], [21], the probability density function (PDF) technique [1], [22]–[24], the Flamelet-Generated Manifold (FGM) method [25], [26] and the Eddy Dissipation Concept (EDC) [27]–[29] are some of the approaches. In the present report, a survey of the FGM and EDC models is given as these are the turbulence - chemistry interaction models applied in the CFD calculation.

Flamelet-Generated Manifold (FGM)

The Flamelet Generated Manifold [25] can be seen as a combination of a manifold, such as the ILDM [30], and a flamelet [20] approach. It follows the idea of the flamelet models that a multi-dimensional flame can be considered as an ensemble of one-dimensional flames. The chemical compositions in 1-D flames are used to construct a manifold, based on the chosen reaction mechanism.

The flamelet equations [31], [32] used to construct the manifold in the reaction-progress space in Fluent[®] are (12-13). It is important to mention the assumption of negligible differential diffusion in the following expressions.

$$\rho \frac{\partial Y_k}{\partial t} + \frac{\partial Y_k}{\partial c} \dot{\omega}_c = \rho \chi_c \frac{\partial^2 Y_k}{\partial c^2} + \dot{\omega}_k \quad (12)$$

$$\rho \frac{\partial T}{\partial t} + \frac{\partial T}{\partial c} \dot{\omega}_c = \rho \chi_c \frac{\partial^2 T}{\partial c^2} - \frac{1}{c_p} \sum_k h_k \dot{\omega}_k + \frac{\rho \chi_c}{c_p} \left(\frac{\partial c_p}{\partial c} + \sum_k c_{p,k} \frac{\partial Y_k}{\partial c} \right) \frac{\partial T}{\partial c} \quad (13)$$

Where Y_k refers to a determined species mass fraction, T is the temperature, t is time, ρ is the density, $\dot{\omega}_k$ refers to a determined species mass reaction rate, h_k is the total enthalpy and $c_{p,k}$ is a determined species specific heat at constant pressure. The scalar dissipation rate as a function of mixture fraction (f) and progress variable (c) is given by (14)

$$\chi_c(f, c) = \chi_{max}^{sto} \exp \left(-2 \left(\operatorname{erfc}^{-1} \left(\frac{f}{f_{sto}} \right) \right)^2 \right) \exp \left(-2 \left(\operatorname{erfc}^{-1}(2c) \right)^2 \right) \quad (14)$$

Where χ_{max}^{sto} indicates the maximum scalar dissipation at stoichiometric mixture fraction. In Fluent[®], this parameter has a default value of 1000Hz.

The model is incorporated in the CFD by solving the transport equations for the control variables. In this case, Fluent[®] uses a progress variable (c) and mixture fraction (f) as control variables. Every iteration, the program consults the previously generated look-up table and obtains the values of all the thermo-chemical variables for a determined c and f . The effect of turbulence is considered by combining the FGM method with the aforementioned turbulence models. The interaction between chemistry and turbulences is taken into account by presumed shape probability density functions [26].

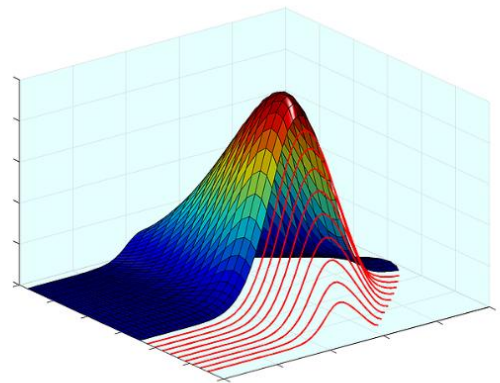
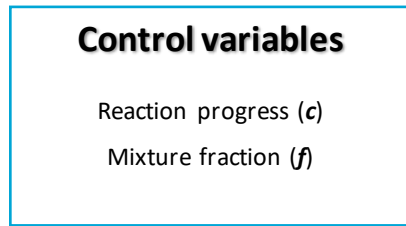


Figure 4. FGM method schematic [33].

Eddy Dissipation Concept (EDC)

The Eddy Dissipation Concept [27] assumes that reactants are homogeneously mixed within “fine structures”. These fine structures have a characteristic dimension of the same magnitude as the Kolmogorov scale and are responsible for turbulence dissipation into heat. The chemical reactions are assumed to happen in these fine structures and are locally characterized as adiabatic, isobaric, Perfectly Stirred Reactors (PSR). The ratio between the Kolmogorov scale and the large scale is used to determine the scaling factor in the reaction rate. This approach requires a very high computational capability when combined with a detailed chemical reaction mechanism. The EDC method is one of the most detailed turbulence-chemistry reaction mechanisms because a transport equation for each species is solved during the CFD calculation.

In Fluent[®], the length fraction of the fine scales is given by (15)

$$\xi^* = C_\xi \left(\frac{\nu \varepsilon}{k^2} \right)^{\frac{1}{4}} \quad (15)$$

With $C_\xi = 2.1377$. Additionally, the species are assumed to react in the fine structures over a time scaled obtained by (16)

$$\tau^* = C_\tau \left(\frac{\nu}{\varepsilon} \right)^{\frac{1}{2}} \quad (16)$$

With $C_\tau = 0.4082$. The source term of a determined species is given by the following expression (17), which combines the previous parameters.

$$R_i = \frac{\rho(\xi^*)^2}{\tau^*[1-(\xi^*)^3]} [Y_i^* - Y_i] \quad (17)$$

In order to make this model computationally cheaper, Fluent[®] implements In Situ Adaptive Tabulation [12], [34]. This approach dynamically generates a look-up table during the calculations. Only the compositional region, that is appropriate to the flow field is created, saved and accessed at every iteration. The compositional space is given by the mass fraction of the species considered in the chemical reaction mechanism chosen and the enthalpy at a determined position of the domain [35].

2.2. Hydrogen as future fuel and novel combustion systems; the AHEAD project

The possibility of developing fuel innovative designs for aero-engines has arisen to reduce the amount of emissions from civil aerospace vehicles. The option of using hydrogen fueled systems has become a potential solution to the problem [36]–[38]. The feasibility of applying this technology to the aeronautical industry was examined in the past [39], mainly after the oil crisis of 1973 [40], [41]. Even flight tests using liquid hydrogen as fuel were performed in the late eighties [42] obtaining promising results.

Hydrogen guarantees low emissions as an aircraft fuel [37]. This is because when hydrogen reacts with air, mostly water vapor (H_2O) is emitted. Furthermore, oxides of nitrogen (NO_x) are present in smaller amounts. The complete elimination of carbon dioxide from the exhaust gases is one of its best attractions. On the other hand, the significant amount of water vapor formed contributes to the generation of contrails, thus contributing to global warming. Nevertheless, the impact of H_2O on global warming was found to be lower than that of CO_2 [43].

The production of NO_x can be significantly lowered by applying innovative combustor designs [38], [44]. The idea is to obtain the leanest combustion possible. Rich and lean combustion refers respectively to an excess or lack of fuel in the reactants when compared to the stoichiometric ratio. The wider flammability range of hydrogen as compared to kerosene allows leaner combustion (Figure 5). Mainly due to this fact, a potential reduction of NO_x emissions was found when changing from kerosene to H_2 (Figure 6). Ziemann et al. [45], Boggia and Jackson [44], Brand et al. [46] and Hanglind and Singh [47] considered lean premixed combustion as the best alternative to reduce NO_x emissions when compared to other techniques such as Lean Direct Injection [48], [49] or Micro-mix combustion [50]. The emissions reduction of lean premixed combustion when compared to these techniques counteracts the stability problems that may appear when applying a premixed approach (e.g. auto-ignition).

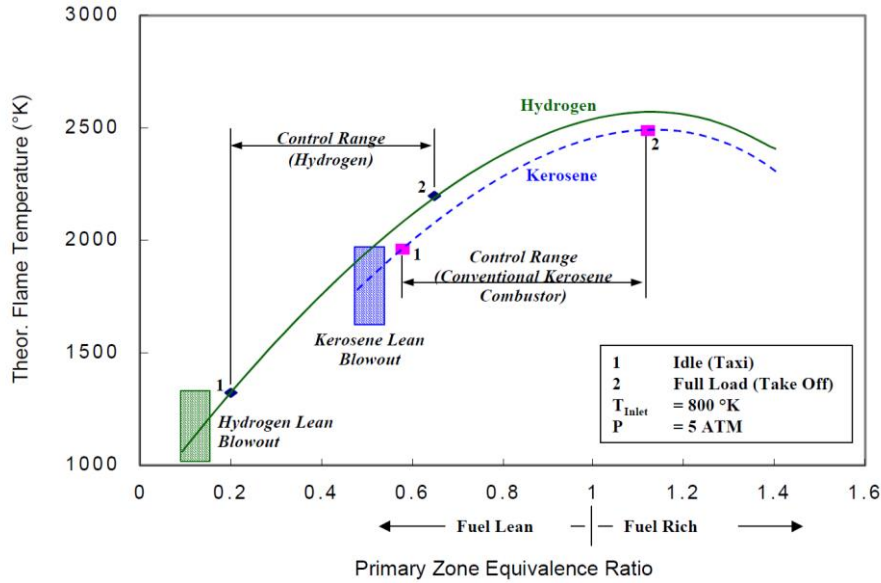


Figure 5. Flammability range of hydrogen and kerosene [46].

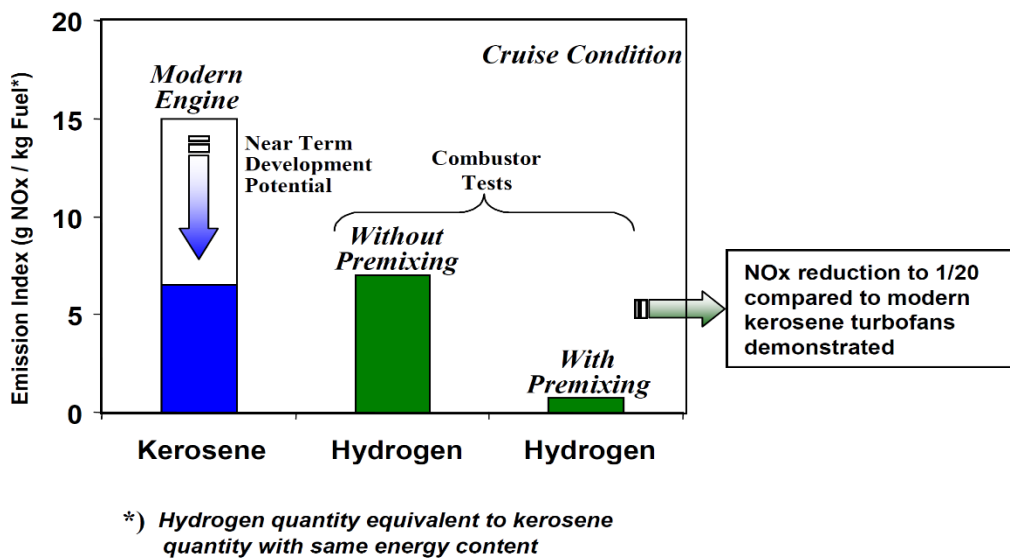


Figure 6. NO_x emissions comparison for different fuels and combustion methods [46].

Moreover, Haglind & Singh [47] and Corchero & Montañés [51] concluded that there is also room for performance improvement (e.g. specific fuel and energy consumption) when changing the fuel from kerosene to hydrogen [47], [51]. However, engine performance and combustion are not the only important parameters to be analyzed when assessing the possibility of using this fuel in future aircraft. Fuel production [52], technical development of hydrogen systems, security, handling methods and the need of novel aircraft designs also have to be considered [38], [53].

Considering all the different design parameters, several approaches were followed by different designers when developing a hydrogen fueled propulsion system. Fuel storage (Figure 7) and engine configuration are critical points of the design process [38], [44]. Boggia and Jackson [44] investigated the use of conventional aero gas turbines adapted for hydrogen, which would lead to major modifications of the base system.

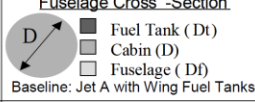
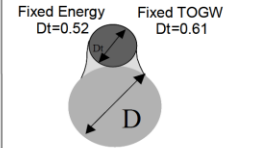
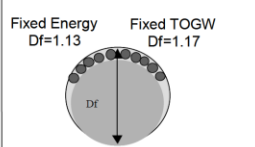
Fuel	Fuselage Cross -Section 	Lift to Drag Ratio (%)		Weight Impact	Range Impacts due to H2 (%)		TRL
		Fixed Energy	Fixed TOGW		Fixed Energy	Fixed TOGW	
LH ₂	Fixed Energy Dt=0.52 Fixed TOGW Dt=0.61 	-16.0%	-17.7%	Tankage Impact: FE: +626 lbs, FTOGW: +922 lbs; Fuselage Weight Impacts FE: +1723 lbs, FTOGW: +2229lbs Corrected Mass Ratio Impact: FE: -2.5% FTOGW: +27.2% <small>Note: Minimum Boil-off Configuration; Fewer Fuel Reserves Necessary.</small>	-18.3%	+4.5%	2
LH ₂	Fixed Energy Df=1.13 Fixed TOGW Df=1.17 	-5.0%	-6.3%	Tankage Impacts: FE: +1620 lbs, FTOGW: +2259lbs Fuselage Weight Impacts: FE: +483 lbs, FTOGW: +269 lbs Corrected Mass Ratio Impact: FE: -1.5% FTOGW: +27.3% <small>Note: Higher Weight Due to larger Tank Surface Area to Volume Ratio</small>	-6.46%	+19.2%	2

Figure 7. Effect of tank volume increase on aircraft characteristics [46].

The concept proposed by the AHEAD project team was a contra-rotating turbfan hybrid engine [54], [55]. This engine would have dual combustors. The first part was conceived as a low NO_x cryogenic fuel combustor, able to operate with liquid hydrogen or liquid natural gas. The second stage was designed as an inter-turbine flameless biofuel burner.

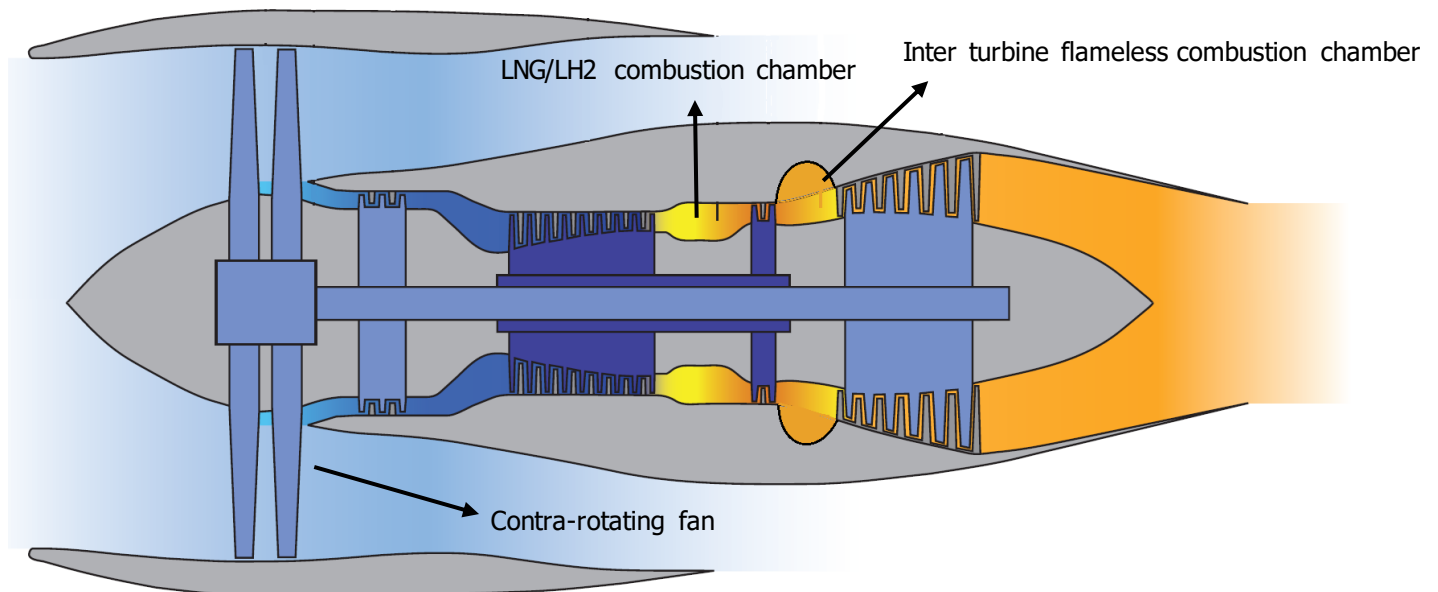


Figure 8. AHEAD hybrid engine schematic [56].

Focusing on the first combustor, the project designers analyzed the most important parameters when developing a premixed combustor: adiabatic flame temperature [54], laminar burning velocity [19], [54], [57], [58] and auto-ignition time [58]–[60]. Once all the parameters were examined, they decided to implement lean premixed combustion in the first stage of the combustion chamber. This would reduce the adiabatic flame temperature of the reaction and, consequently NO_x emissions. Nevertheless, it was necessary to consider flashback when at surge or other off-design conditions [60]. Additionally, it was also important to contemplate a safety margin for the residence time of the mixture in the premixing zone to avoid auto-ignition [59].

The combustor was designed to correctly operate at a control range defined by the equivalence ratio. This control range was chosen for an equivalence ratio from 0.4 to 0.55. Within this range, enough security for the combustion process while still being in the low NO_x emission window is provided. Different experiments were performed by Levy et al. [54] during the AHEAD project in order to determine this control range. They studied different inlet temperatures, swirl numbers, mass flows, etc. On the one hand, the lower limit was selected because the adiabatic flame temperature at leaner conditions would be lower than that required for the correct engine operation (Figure 9). On the other hand, the upper limit permits NO_x emissions to be below 10ppm (Figure 10).

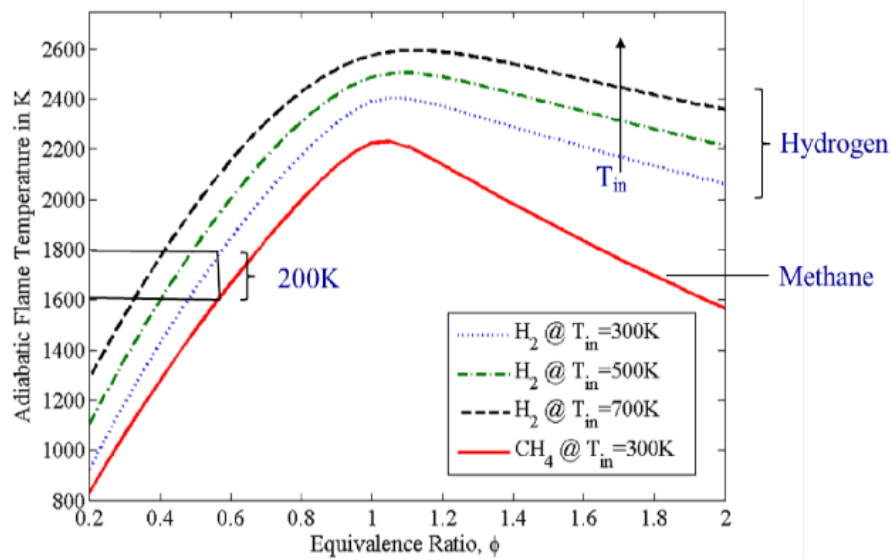


Figure 9. Variation of hydrogen and methane adiabatic flame temperature with equivalence ratio for different inlet temperatures [54].

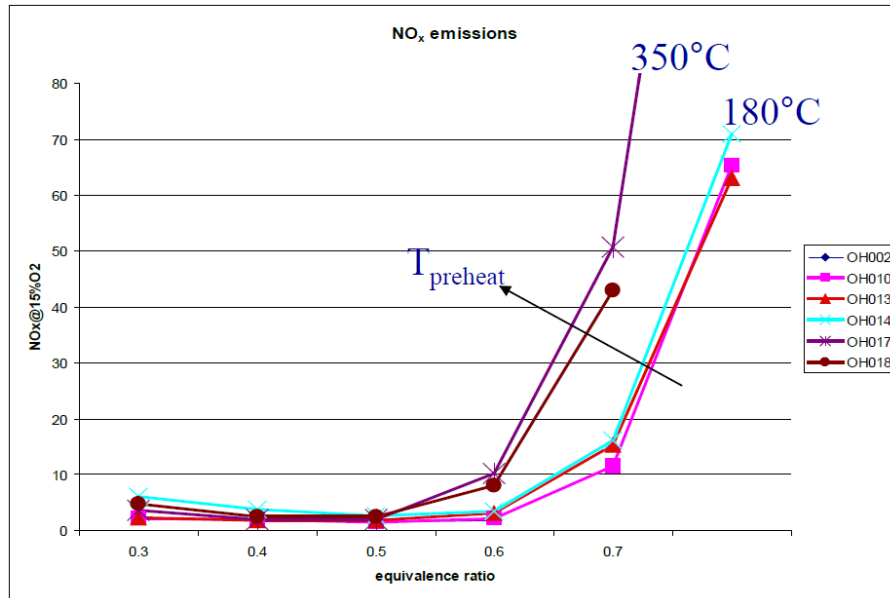


Figure 10. Variation of NO_x emissions in ppm at 15% O_2 with equivalence ratio for different inlet temperatures, swirl numbers and axial air injection mass flow [54].

Table 4. Parameters (Inlet temperature, mass flow, swirl number and axial mass flow percentage) used for the calculation of NO_x emissions in the cases presented in Figure 10.

Case	Inlet temperature [°C]	Mass flow [kg/h]	Swirl number	Axial mass flow [%]
OH002	180	200	0.9	9
OH010	180	180	0.9	12.5
OH013	180	180	0.7	12.5
OH014	180	180	0.7	7.5
OH017	350	130	0.7	12.5
OH018	350	130	0.9	12.5

As mentioned before, the main problem that could appear in the chosen design was flashback due to the low blow-out limit and high burning velocity of the fuel [61]. Flashback can mainly be caused by four independent phenomena or a

combination of them [62]: combustion instabilities, boundary layer flashback [63], flame propagation in the core flow and combustion induced vortex breakdown. Two main measures can be taken in order to lower the risk of flashback [55]: increase the bulk air velocity or reduce the swirl intensity of the burner. However, both solutions cause an increase in pressure losses, thus lowering the efficiency. Likewise, worse fuel-air mixing might be obtained, which negatively influences NO_x emissions [64].

In the particular case of the AHEAD project, Reichel and Levy [55] studied the flashback problem in detail and tested different measures in order to avoid it. They implemented axial air injection to obtain a non-swirling flow pattern at the nozzle axis and shifting the stagnation point downstream. Furthermore, they introduced the injection of air at the mixing tube walls to obtain a leaner mixture and destruct the boundary layer at this position, reducing flashback probability at the boundary layer.

All these points together lead to the following burner design (Figure 11), which was chosen by the AHEAD project team.

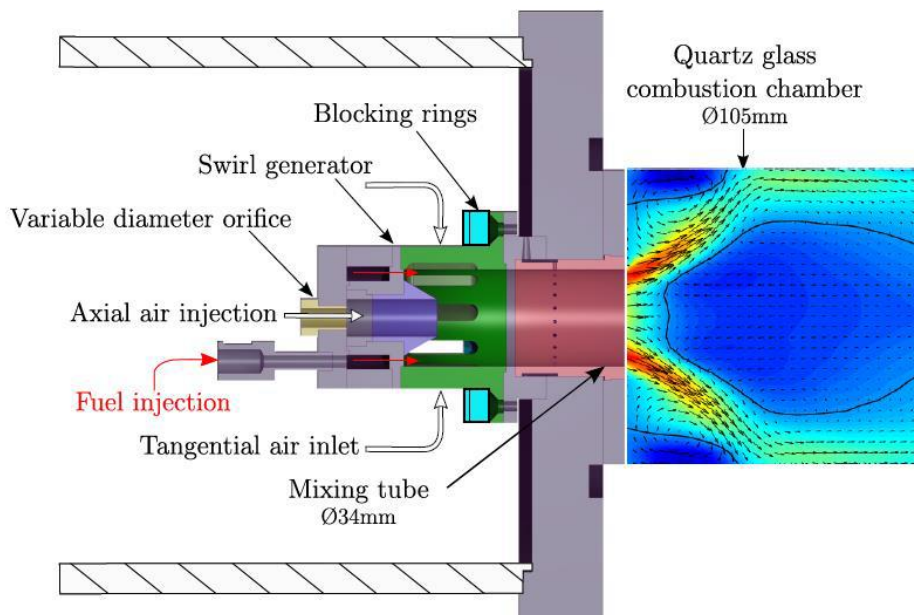


Figure 11. Schematic of the AHEAD burner [55].

There are two possibilities in this burner concept for the air to reach the mixing tube. Through eight radial swirl generators, which inlet area (and thus the swirl number) can be modified by the blocking rings, or across the axial air injection hole. This injector has a varying geometry to control the amount of axial air flow. There are sixteen fuel injectors located in an annular pattern around the axial injector. Both air and fuel are mixed in the mixing tube. The length of this part was designed based on the auto-ignition delay time. It presents a cylindrical shape because it is better than a converging nozzle to relocate the flame in case of flashback.

Finally, several experiments were performed at TU Berlin [65]–[67]. They obtained different results depending on the amount of axial mass flow as well as the selected swirl number for both reactive and isothermal flows. The data acquired during the experimental campaign, which are partially presented in the next section, will be compared to the CFD results.

2.3. Literature review

In this point, a brief review of previous researches related to the topics of the present is given. Most of them employed methane and hydrogen mixtures, instead of pure H₂. Nevertheless, the results obtained and the methods used in their studies are comparable and interesting for the project at hand. Both experimental and numerical cases are considered.

▪ Experimental cases

Schefer et al. [68] studied the characteristics of a lean premixed swirl-stabilized flame. The fuel used was a mixture of methane and hydrogen. In this experimental study, OH PLIF (Planar Laser-Induced Fluorescence) images were used to obtain the flame characteristics under these conditions (Figure 12). They investigated different parameters of the flame, such as flame stability and lean blowout limits, up to a determined amount of hydrogen present in the mixture (mole fraction $X_{H_2} = 0.29$). Furthermore, CO and NO_x emissions were studied. On this matter, they found out a significant reduction in CO emissions with hydrogen addition, while NO_x emissions were almost unaffected.

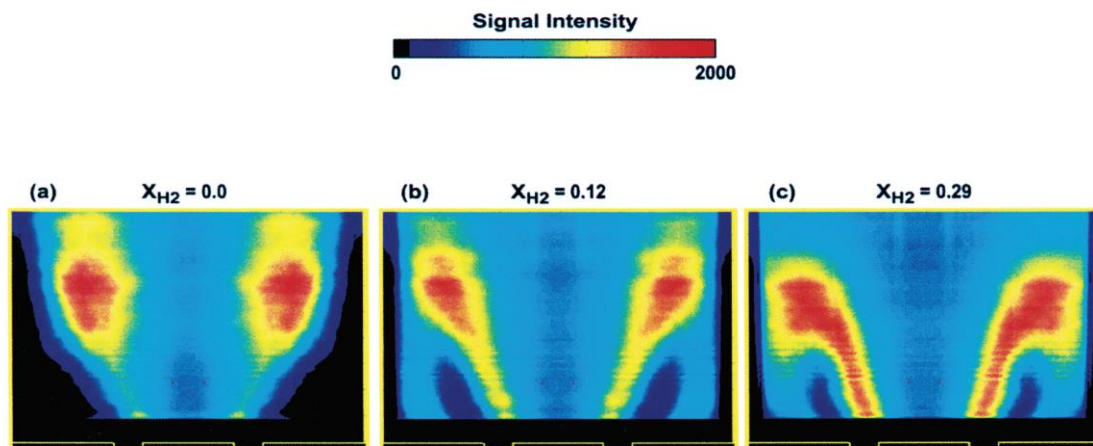


Figure 12. Time-averaged OH PLIF images for air-fuel flow rate of 700slm and adiabatic flame temperature of 1570K for different hydrogen mole fraction [68].

The flame structure was modified by the addition of hydrogen to the fuel, which significantly increased the OH radical concentrations. The flame characteristics were mainly modified at the corner toroidal zone.

More authors followed a similar line of investigation [69]–[71]. Kim et al. [69] also examined the effect of hydrogen addition in a methane-air flame. They used a swirl-stabilized burner under confined conditions. The main objective of their research was to analyze flame stability and the effect of swirl strength, as well as studying the emissions for

different amounts of hydrogen in the fuel mixture. They used Particle Image Velocimetry (PIV) and micro-thermocouples to obtain the velocity and thermal field respectively. Moreover, OH chemiluminescence was utilized to capture the OH concentration in the flame. Emissions were studied by using a gas analyzer at the burner exit.

Their main conclusion was that the lean stability limit is extended by hydrogen addition, as expected. Additionally, NO_x emission increased when adding hydrogen to the fuel mixture. However, this fact could be overcome by increasing either the excess air or swirl intensity. Furthermore, they compared the emissions of premixed and diffusion flames under the same conditions. NO_x emissions were found to be lower in the premixed burner.

Emadi et al. [70] performed an analysis on how hydrogen addition modifies methane flame dynamics. The experiments were carried out in a low-swirl burner for different combustion chamber pressures; from atmospheric conditions, up to 3atm. OH radical images were got applying the PLIF technique to characterize the flame.

Their main finding was also that lean blow-off limits broaden with the addition of H₂ (Figure 13), confirming the approach followed during the AHEAD project regarding the use of hydrogen as fuel. A lower lean blow-off limit permits leaner mixtures to react without instabilities (e.g. auto-ignition), which is favorable for premixed flames. Furthermore, hydrogen addition decreased the radius of curvature and increased wrinkling of the flame front.

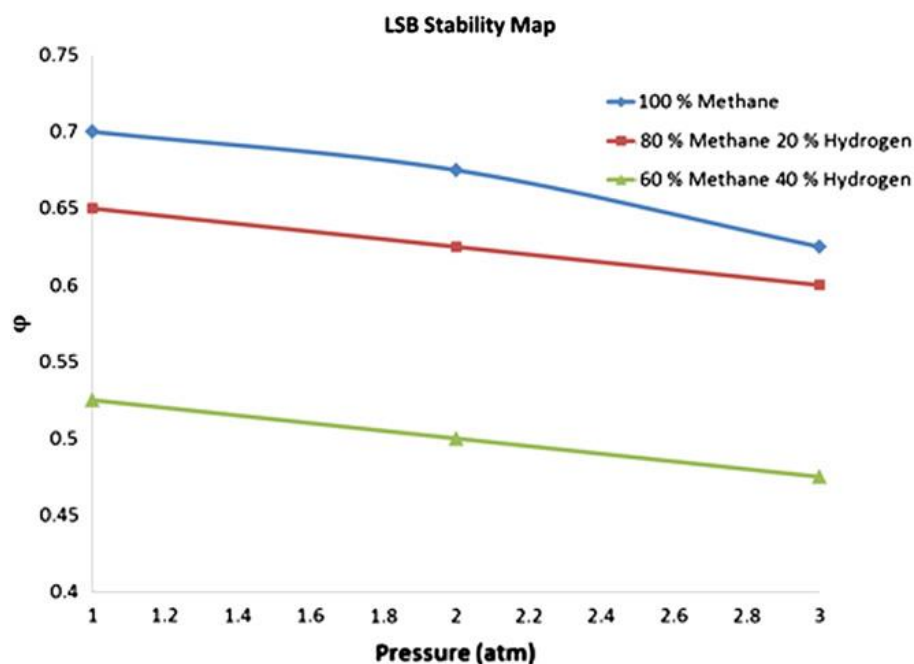


Figure 13. Variation of lean blow-off limits of the flame with combustion chamber pressure for different amounts of hydrogen in the fuel mixture [70].

Lantz et al. [71] investigated the effect of hydrogen enrichment (up to 80% of volume fraction) to natural gas flames. Due to the high percentage of hydrogen in the mixture and other conditions (premixed swirl-stabilized flame), this is a case of particular interest for the present work. They used the OH PLIF technique and flame chemiluminescence imaging

to characterize the flame. The burner used for the experiments was the dry low emission (DLE) found in industrial gas turbines manufactured by Siemens [72].

They concluded that hydrogen addition clearly affects the flame shape and size, becoming shorter and narrower the higher the amount of H_2 . Flashback appeared for 60% and 80% of hydrogen (Figure 14).

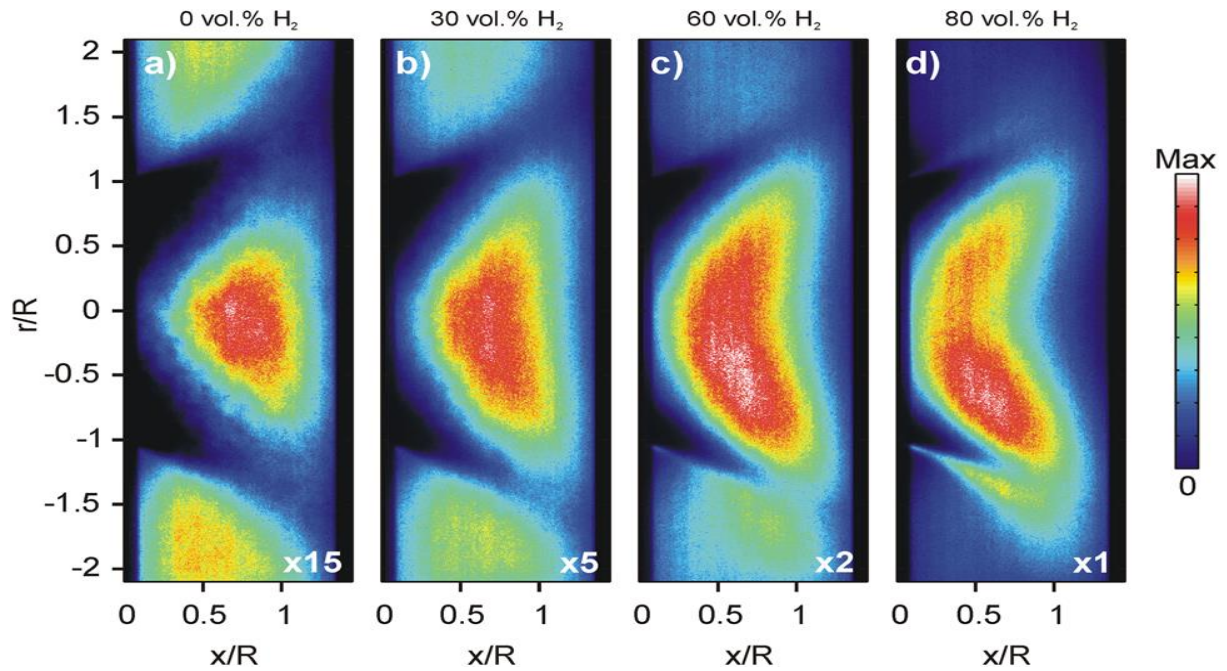


Figure 14. Time-averaged OH-PLIF images for different amounts of hydrogen in the fuel mixture [71]. Intensities are multiplied by a factor to use the same scale.

The experiments related to the AHEAD combustor presented in the previous chapter are of particular interest [58], [65], [67]. These documents provide a more detailed analysis of the lean premixed hydrogen combustor.

Reichel et al. [65] studied how the flow field of the swirl-stabilized hydrogen premixed combustor behaves when applying different amounts of axial air injection. The axial injection of air would allow to have flashback-proof combustion of premixed hydrogen. They proved that with this flow configuration, flashback-free operation of the burner is achieved for the whole operational range of the combustor when a "high" axial injection is used. The amount of axial air is directly controlled by the diameter of the axial inlet present in the combustor (Figure 11). Additionally, the effect of axial injection in the mixing quality [73] was assessed.

To determine the velocity field, they used a high-speed PIV camera in a water tunnel testing facility. The Reynolds number of the experiments was set to 40000, using the diameter of the mixing tube ($D = 34\text{mm}$) as characteristic length. For the mixing quality, they used a PLIF method and the same tunnel. They added Rhodamine G6 dye to the water representing the fuel.

The effect of axial air injection in the mixing tube flow field is presented (Figure 15).

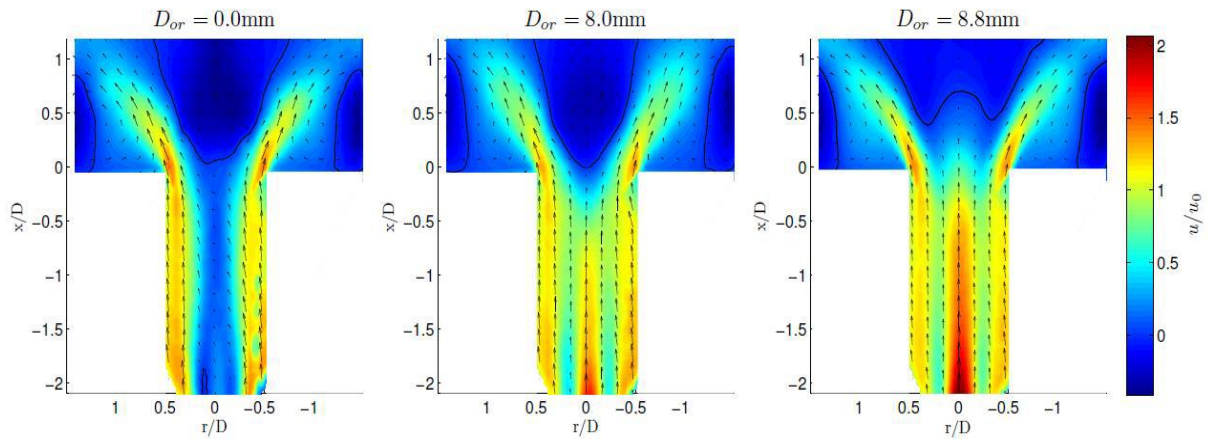


Figure 15. Velocity distribution at the premixing zone and burner nozzle for different axial mass flow at a swirl number of 0.9 and with a long mixing tube ($u_0 = 70\text{m/s}$) [65].

For the case of the long mixing tube, only a high amount of axial mass flow ($D_{or} = 8.8\text{mm}$) provided flashback safety. This case was the one simulated in the CFD model. Further increase in axial injection would have a bad effect in the mixing quality.

Regarding the mixing quality experiments, the following results were obtained for a long mixing tube and a geometrical swirl number (S) of 0.9 (Figure 16).

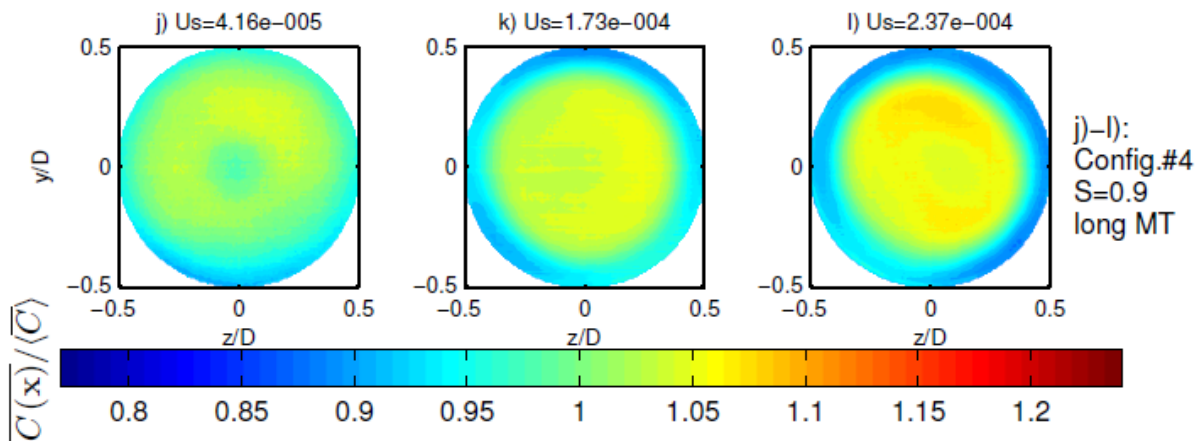


Figure 16. Spatial distribution of time-averaged, normalized concentration of the fuel for different amounts of axial air injection ($D_{or} = 0\text{mm}, 8\text{mm}$ and 8.8mm respectively) [65].

Considering this results, they concluded that axial air injection would not have a major effect in the mixing quality, thus not increasing NO_x emissions.

In their second publication, Reichel et al. [58] analyzed the main modifications in the flow field and the flashback limits in a combustion test rig operated at atmospheric pressure (Figure 17). They characterized the flame structure using OH* chemiluminescence imaging. Moreover, the flow field was analyzed with PIV and the flame probability assessed by means of the qualitative light sheet (QLS) [74].

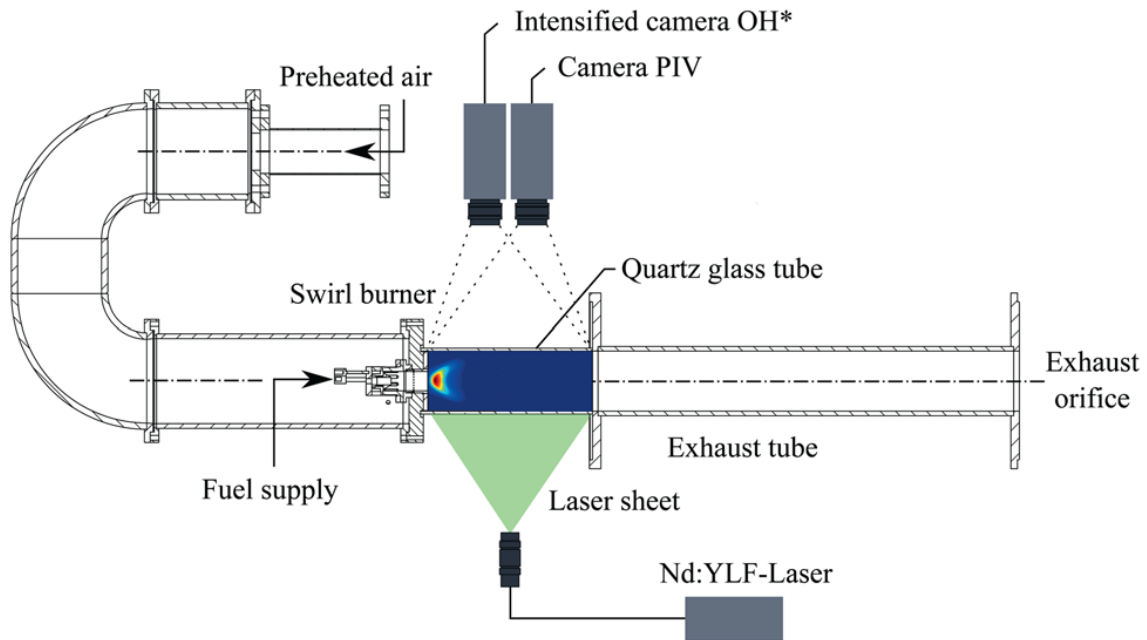


Figure 17. Experimental setup schematic for PIV and chemiluminescence measurements [58]

In the present paper, only the results for the case of interest are discussed ($S = 0.9$, long mixing tube). The impact of the equivalence ratio on the flow field was investigated (Figure 18). They found that the stagnation point moved downstream with increasing equivalence ratio. This is due to the additional axial momentum imposed by the fuel jet, which counteracts the effect of a higher turbulent flame speed. A higher turbulent flame speed moves the stagnation point, thus the flame location, upstream. Furthermore, the flame probability was given (Figure 19), showing that the flame is prone to attach to the inlet corner. This effect is more important at higher equivalence ratios.

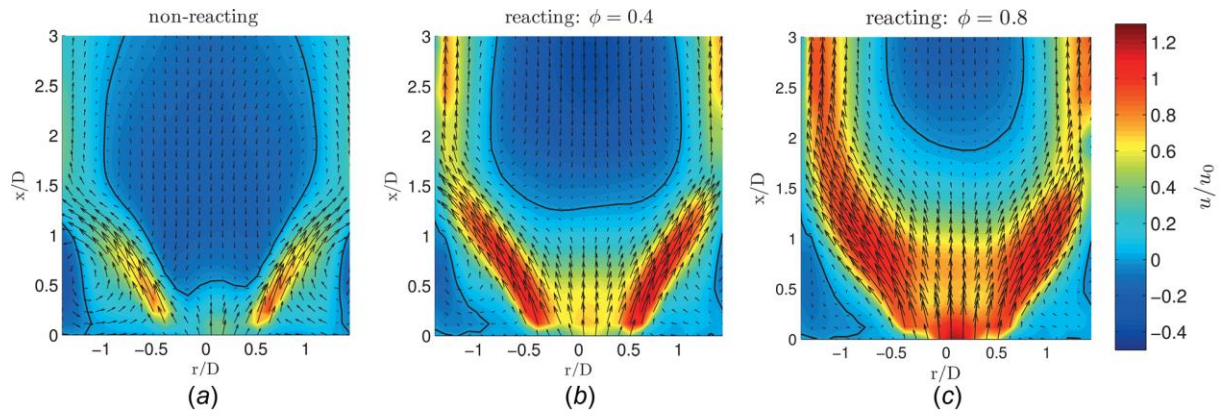


Figure 18. Equivalence ratio effect on the reactive flow field ($u_0 = 70\text{m/s}$) [58].

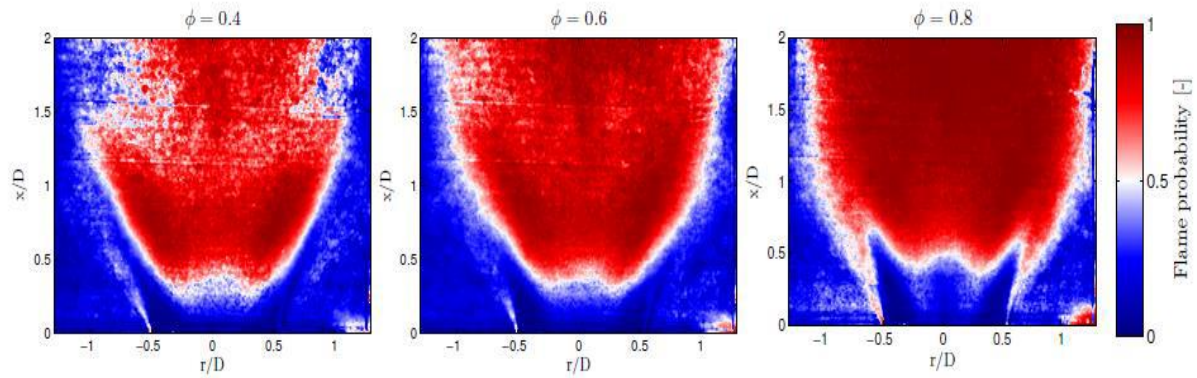


Figure 19. Flame probability for different equivalence ratios at a Reynolds number of 75000 [55].

Furthermore, OH^* chemiluminescence was checked in order to know the flame location (Figure 20). They concluded that no flashback appeared for a high amount of axial injection.

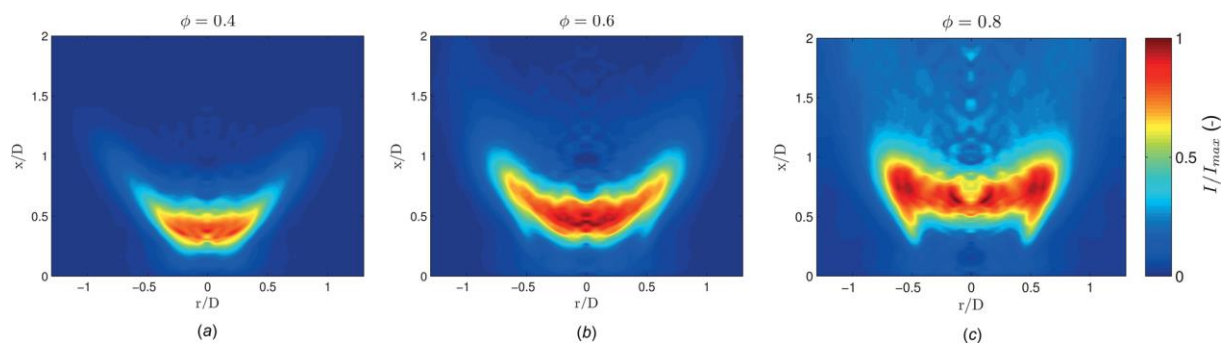


Figure 20. ABEL-deconvoluted OH^* images. They are normalized with the maximum intensity at the highest equivalence ratio [58].

In their latest experimental study regarding the AHEAD combustor, Reichel et al. [67] applied the OH PLIF technique to locate the flame anchoring and assess flashback probability of the burner. The results obtained showed the following OH distribution for the case of interest ($S = 0.9$, long mixing tube, $D_{or} = 8.8\text{mm}$) (Figure 21).

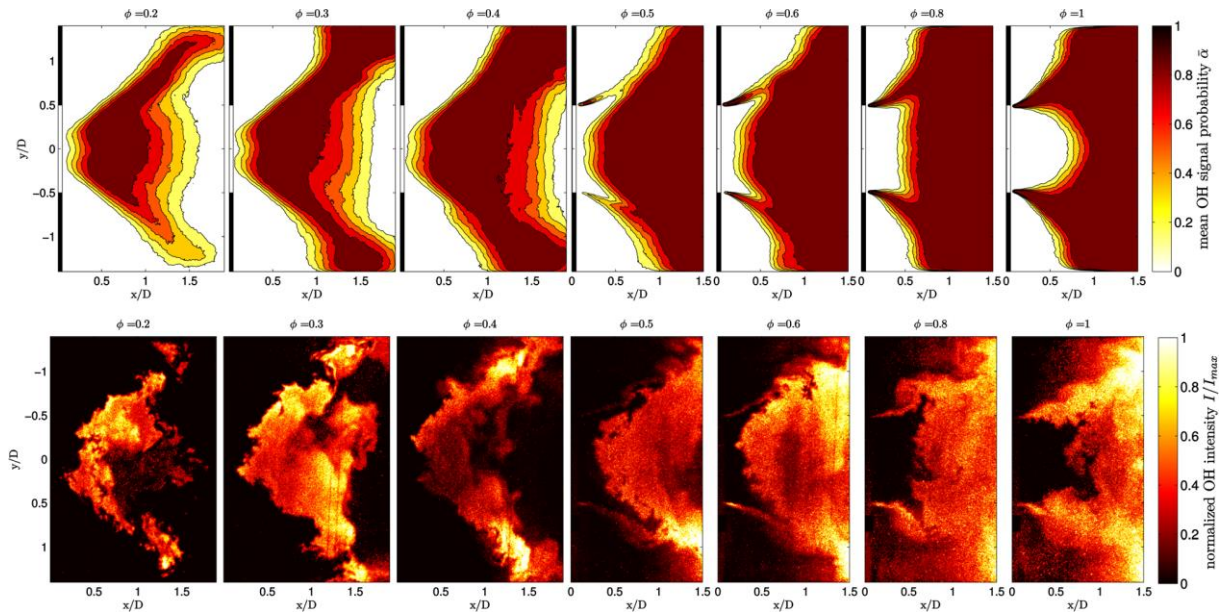


Figure 21. Mean OH signal probability (top) and instant OH PLIF shoots (bottom) for an inlet temperature of 453K [67].

They applied an algorithm to the OH images to obtain the maximum flame front probability (X_F). They concluded that X_F is moved downstream with equivalence ratio, mainly due to the added momentum of the hydrogen jet. The effect of the increasing momentum due to fuel injection is higher than the increment of turbulent flame speed with equivalence ratio. There is a direct relation between the equivalence ratio and the fuel jet momentum because the air mass flow was kept constant.

▪ Numerical simulations

Some examples of similar numerical simulations were selected in order to give an overview of the main models normally used in the field and the expected results from the CFD analysis [75], [76]. Furthermore, a previous non-reactive numerical analysis of the AHEAD hydrogen combustor is assessed [77].

AbdelGayed et al. [75] performed a numerical investigation about the flow characteristics of a lean premixed swirl stabilized combustor. They used the realizable $k-\epsilon$ and the Detached Eddy Simulation (DES) approach. Applying the realizable $k-\epsilon$ approach, they could simulate the central recirculation zone of the combustor, which is a major point for flame stabilization. This makes the realizable $k-\epsilon$ turbulence model likely to predict the flow field of the lean premixed hydrogen combustor designed in the AHEAD project.

Mansouri et al. [76] carried out a RANS numerical simulation using Fluent[®]. They assessed the effects of adding hydrogen (up to 80% volumetric fraction) to a premixed propane burner [78]. They used the realizable k- ϵ turbulence model and a three-step global reaction mechanism. The turbulence-chemistry interaction was considered by applying the Finite-Rate/Eddy Dissipation approach provided by Fluent[®] [12]. In addition, they performed a study regarding differential diffusion. They concluded that ignoring this effect could provide nonrealistic effects. The effect of differential diffusion was checked in the thesis.

The temperature results of their simulations for a high swirl number are presented in the following figure (Figure 22). The behavior found in this simulation was similar to that obtained in the thesis at hand. Regarding the flame configurations, Mansouri et al. found that it had a M-shape and was located at the CRZ for all the cases considered. Furthermore, in the whole study the flame was attached to the inlet corner and showed no tendency of lift-off.

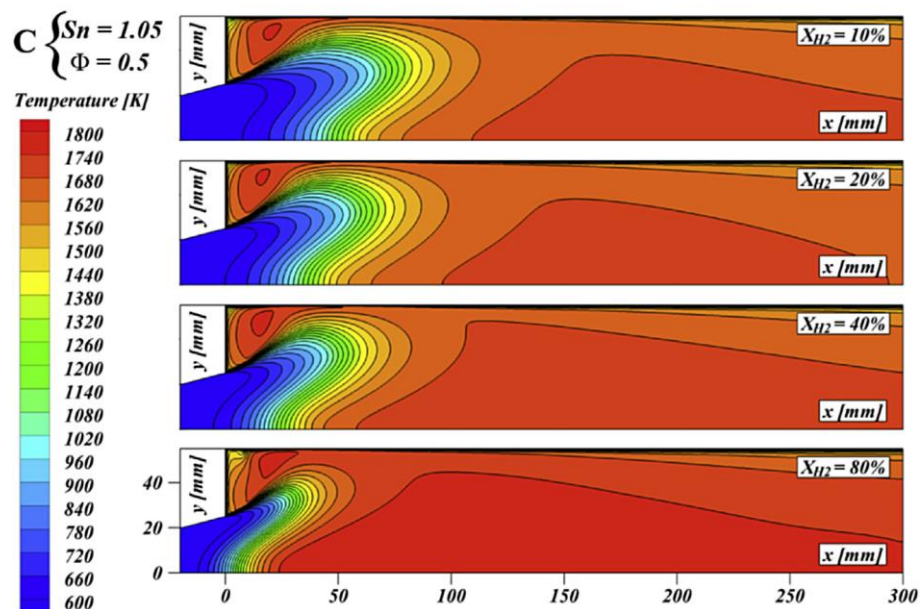


Figure 22. Temperature distribution in the combustion chamber for different amounts of hydrogen [76].

Tanneberger et al. [77] performed a non-reactive numerical study of the AHEAD combustor. They used water as fluid in order to compare the results with the experimental tests carried out in the water tunnel [65]. For the steady state flow, a RANS k- ϵ realizable model was used obtaining good results. Additionally, they did a dynamic flow field simulation using LES. Furthermore, they compared the mixing quality of the two simulated cases (RANS and LES) and the experimental data (Figure 23). They found out that the mixing predicted by the RANS model was not realistic using water as fluid. The high diffusivity of hydrogen could provide a different mixing pattern. Furthermore, the relation between the mixing pattern and other parameters of the reactive flow field (e.g. flame position, temperature) was not simulated.

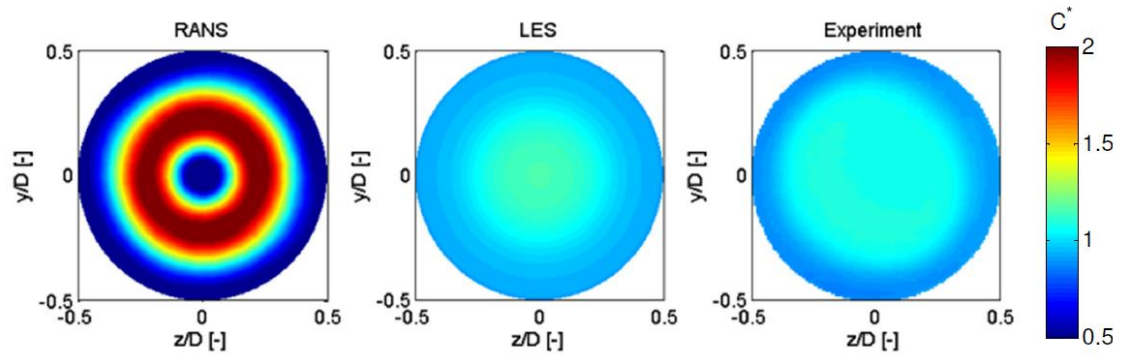


Figure 23. Spatial distribution of the time-averaged, normalized concentration of the fuel at the combustion chamber inlet obtained in RANS, LES and the experiments respectively [77].

3

Numerical setup

In this chapter, the numerical setup used for the analysis of the lean premixed hydrogen combustor designed in the AHEAD project is presented. ANSYS Fluent[®] v16.1 was used for the complete study. In the following points, the two dimensional and three dimensional approaches are introduced. For each case, the mesh and boundary conditions are given.

3.1. Meshes

In this point, the meshes constructed for the 2D and 3D approaches using ANSYS ICEM CFD v16.1 are presented. In both cases, special care was taken to obtain a valid mesh for isothermal and reactive cases. Moreover, the use of an unstructured mesh was avoided. Both meshes were based on a previous internal study performed at TU Delft.

- *2D Mesh*

The first approach to the problem was to simplify it as much as possible. This would provide a fast CFD model with a small number of cells, which could fairly represent the combustor. Under this consideration, a two-dimensional approach was created. This approach was considered because of the axisymmetric nature of the fully developed flow in the combustion chamber.

To develop the two-dimensional mesh, two main simplifications in the geometry were done. The radial swirl generator and the fuel injection had to be carefully modeled. The common problem of these two parts is that they are not axisymmetric. The logical solution to this problem is to create an annulus for the fuel inlet and a cylinder (without its top and bottom faces) for the swirl inlet (Figure 24), keeping the total inlet area ($A_{\text{swirl}} = 584\text{mm}^2$).

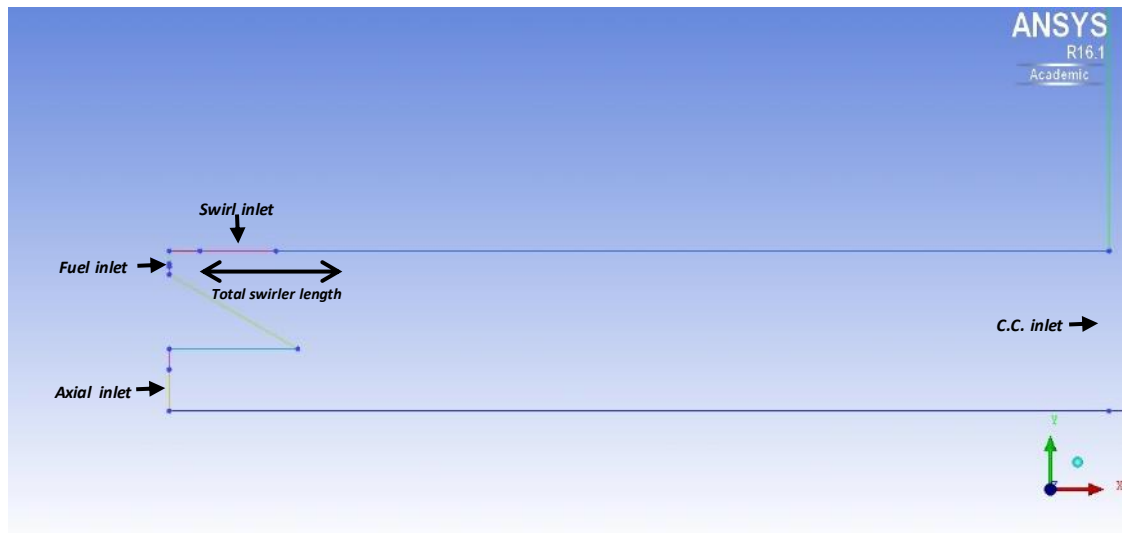


Figure 24. Premix tube 2D geometry simplification.

For the swirl inlet, different axial positions of the created cylinder were assessed. This was done placing it throughout the total axial length of the 3D swirler. With this approach in mind and beginning from the left, the simplified geometry was placed at the beginning, at the center and at the end of the actual swirler. Moreover, a distributed inlet was also considered. This was done by discretizing the cylinder into eight parts and placing them throughout the total axial length of the swirler. In the present report, only the results regarding the first position are given (Figure 24). This was chosen to reduce the interaction between the swirling and the axial jet due to the presence of a wall in between. Due to the axisymmetric nature of the model, the interaction between these two was found to be too intense when placing it at other positions, where no wall is present.

Moreover, the experimental combustion chamber has a total length of 600mm. In the numerical domain, this was reduced to around 300mm to diminish the total mesh size. The combustion chamber has a radius of 52.5mm. Furthermore, the premix cylinder diameter was set to 34mm, which was used as the reference value for all the length dimensionless parameters. The created mesh using ANSYS ICEM CFD v16.1 is a two-dimensional structured mesh. It has around 9350 nodes and 9000 quadrilateral cells (Figure 25).

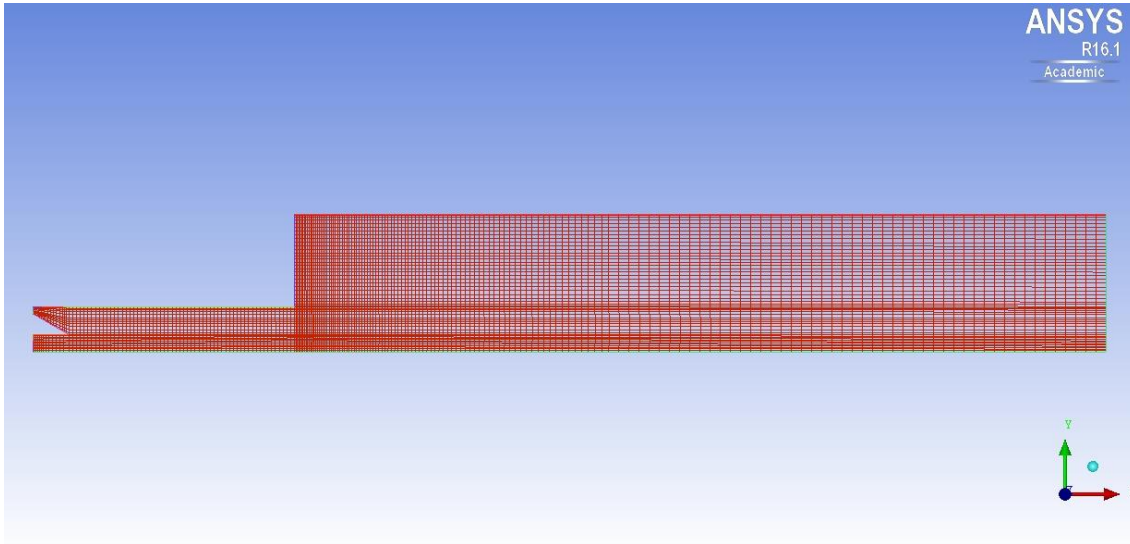


Figure 25. 2D mesh.

The mesh quality obtained is presented in the following table (Table 5). A very high quality of the mesh was achieved. In the 2D case, the quality parameter of the mesh is calculated as the determinant (2x2x2).

Table 5. 2D mesh quality report.

Parameter [min. – max.]	Values
Quality [0 – 1]	> 0.876
Angle [0° – 90°]	> 59.76°

- **3D Mesh**

In this point, the mesh constructed for the tridimensional case using ANSYS ICEM CFD v16.1 is presented. As for the two-dimensional approach, several simplifications were implemented to the combustor geometry. The following figures give an overview of the selected geometry (Figure 26).

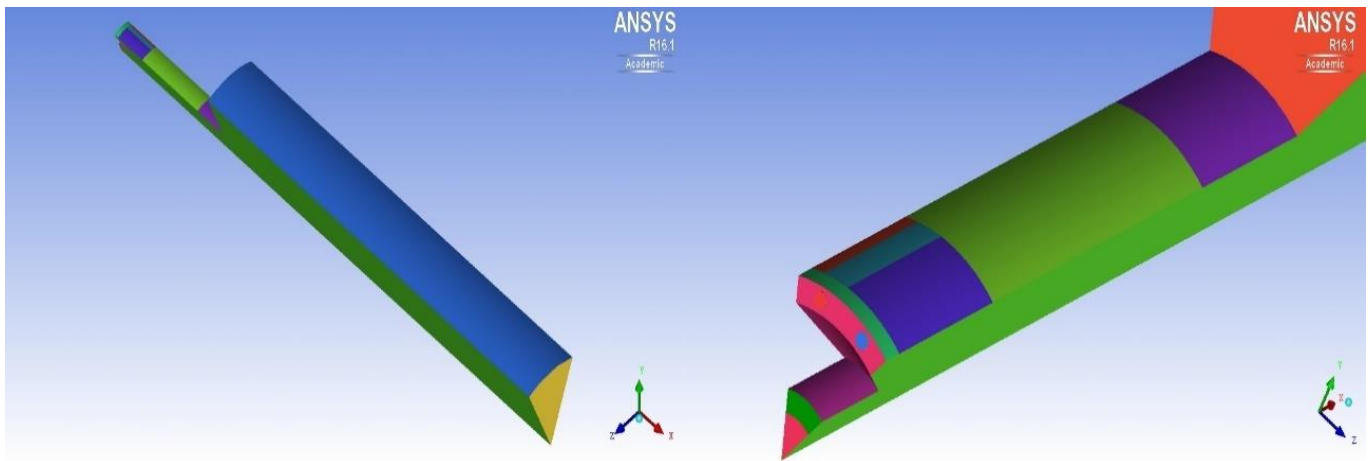


Figure 26. Isometric (left) and detailed (right) view of the simplified geometry used for the 3D model.

Taking advantage of the periodical configuration of the combustor design, a section of 45° was considered. For this section, one of the eight swirl inlets was assigned. The sector presents two fuel inlets (there are 16 in total), which have a diameter of 1.6mm. Applying the periodic condition, the number of required computational cells is highly reduced.

The swirl inlet presents a simplified geometry. The swirler duct joins the plenum with the mixing tube. The actual swirler duct has a complex geometry with rounded corners (Figure 11). A simple quadrilateral inlet with the same area ($A_{\text{swirl}_i} = 72\text{mm}^2$) was considered. Additionally, in the 3D approach only the outlet of the actual duct was taken.

Furthermore, the fuel inlets were considered as small cylinders. The most important approach in relation to the fuel inlets was the implementation of the interface option, provided by ANSYS Fluent[®], between the cylinder outlets and the external annulus of the pre-mixer. The interface option was chosen because it is an easy way of connecting the fuel injectors to the mixing tube keeping the hexahedral mesh configuration. When applying this condition, Fluent[®] creates new faces produced from the overlapping of the two regions [12]. The values of the different parameters required for the calculation are obtained for these new faces, ignoring the previous mesh configuration.

In addition, the combustion chamber domain was reduced as well as for the two-dimensional case, from around 600mm to 300mm. The mixing zone was divided into two different parts at $x/D = -0.7$ (Figure 11). This was done to consider the boundary layer destruction (slip wall condition) in this area since no mass flow data through this holes were available. This condition was only applied for the reactive cases.

The designed mesh was a tridimensional hexahedral structured mesh. It presents around 140000 nodes and 128000 hexahedral cells (Figure 27).

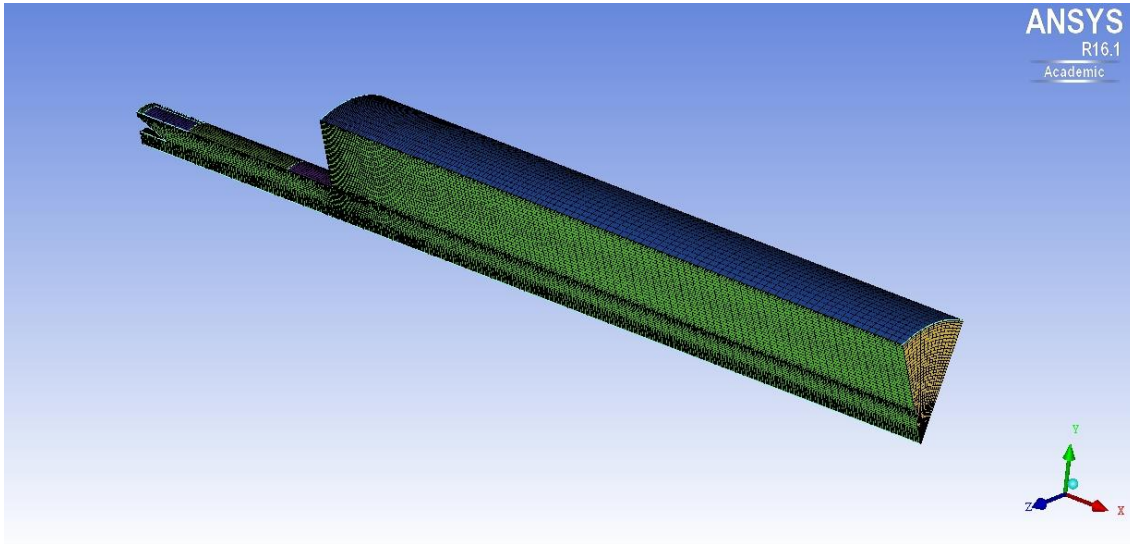


Figure 27. Tridimensional mesh.

The values presented in the following table (Table 6) were obtained for the different mesh quality parameters. A high quality of the mesh was also achieved for this case. For the 3D approach, the quality parameter is calculated as a weight diagnostic between the determinant, maximum orthogonality and maximum warps of the faces comprising the element. The warp of each face is calculated as the maximum angle between the triangles connected at the diagonals of the face.

Table 6. 3D mesh quality report.

Parameter [min. – max.]	Values
Quality [0 – 1]	> 0.7
Determinant (3x3x3) [0 – 1]	> 0.7
Angle [0° – 90°]	> 40°

3.2. Solving methods, boundary conditions and mesh study

In this point, an overview regarding the flow solving methods is provided. Then, the boundary conditions applied for the calculations are given. Additionally, a mesh study for both cases is presented.

- **Solver methods**

For all the simulations performed, a second order upwind scheme was used to solve most of the equations: momentum, turbulence, energy and species. The PRESTO! method was applied to the pressure equation and the SIMPLE scheme to the pressure-velocity coupling. Furthermore, the Least Squares Cell Based approach was used for the evaluation of gradients.

Regarding the turbulence models, the standard and realizable k-ε were applied and compared for both the 2D and 3D case. Likewise, the presented Li et al. was tested as chemical reaction mechanisms. Moreover, the FGM and EDC approaches are used for the reactive flow cases.

- **Boundary conditions for the isothermal case**

At first, the following table gives an overview of the boundary conditions imposed to the domain (Table 7). The total values are given, i.e. the mass flow has to be divide by 8 in the 3D case because of the imposed periodical condition.

Table 7. Summary of the boundary conditions for the non-reactive case.

	2D		3D	
	<i>Axial air inlet</i>	<i>Swirl air inlet</i>	<i>Axial air inlet</i>	<i>Swirl air inlet</i>
<i>Mass flow [kg/h]</i>	32.4	147.6	32.4	147.6
<i>Inlet temperature [K]</i>	450	450	450	450
<i>Turbulence intensity [%]</i>	5	5	5	5
<i>Direction vector</i>	\vec{i}	42.5° with respect to the radial direction	\vec{i}	31° with respect to the radial direction
<i>Walls</i>	No slip condition and adiabatic			
<i>Outlet</i>	Outflow			

Regarding the axial air injection, the actual amount was not assessed during the experiments [58]. They only adjusted it by the pressure loss ratio between the swirler and the axial injection hole. For a high amount of axial air injection, they considered the axial volumetric flow to be a 12.5% of the total flow. For the present study, a value of 18% was used as proposed by the previous internal report. The axial air inlet diameter was kept at 8.8mm as the design parameter to control the amount of axial flow.

Additionally, a turbulence intensity of 5% was selected due to the lack of information regarding this point. In any case, this parameter is supposed not to modify the outcome in an important fashion.

The swirl number at the premixer outlet is the only available information regarding the swirler inlet angle in the literature. Due to this, a swirl number study is presented to choose the correct angle for the swirl inlet. The swirl number [79] is a dimensionless parameter which characterizes swirling flows. It is defined as the ratio between the axial flux of angular momentum and the axial flux of linear momentum. A simplified formula [80] is given here (17).

$$S = \frac{G_{tan}}{RG_{as}} = \frac{\int_0^R wu r^2 dr}{R \int_0^R u^2 r dr} \quad (17)$$

With the experimental configuration, a geometrical swirl number of 0.9 was obtained. The axial air injection introduces additional axial momentum to the flow and the tangential momentum produced by the swirler is reduced as the total mass flow is kept constant. A resultant swirl number of around 0.55 was found for a high amount of axial air injection [81].

In relation to the direction vector of the swirler in the 3D, a value of 35° was suggested in the previous study. Applying this boundary condition, an overestimation of the radial velocity was found (Figure 34). This was because the swirl number obtained at the premixer outlet was 0.6 (Figure 28), while an experimental value of 0.55 was reported. To obtain a flow field closer to the actual experiment, a swirl number study was used to select the inlet angle in the 3D case as done for the two dimensional one.

The following figure provides the variation of the swirl number at the combustor chamber inlet, where the swirling flow pattern is completely developed, with the angle imposed at the swirler (with respect to the radial direction) (Figure 28). The results presented were obtained with the k-ε realizable model. However, these were found to be valid for the k-ε standard. Almost no variation was found in the swirl number calculation between both models. An inlet angle of 42.5° and 31° was selected for the 2D and 3D mesh respectively.

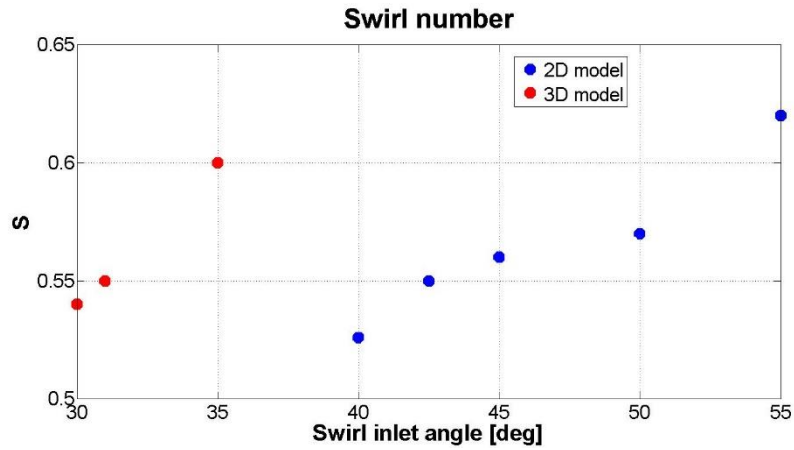


Figure 28. Variation of the swirl number (S) at the premixer outlet with swirler inlet angle for the 2D and 3D case.

▪ Boundary conditions for the reactive case

The only added feature in the reactive cases is the fuel flow, which was calculated for the different equivalence ratios studied during the experiments (from 0.2 to 1). The following table shows the total hydrogen mass flow for each studied case (Table 8). It is important to remark that for the 3D case there are 16 fuel injection ports, i.e. the values shown at the table have to be divided by 16. The fuel is injected following the X direction, providing additional axial momentum to the flow field.

Table 8. Fuel mass flow for the studied cases.

Equivalence ratio	H₂ mass flow [kg/h]
0.2	1.05
0.4	2.10
0.6	3.15
0.8	4.21
1	5.26

Heat transfer through the walls due to convection and conduction was not considered. Experimental data regarding this was not available. Thus, major assumptions should be made to consider this effect, leading to important errors.

Additionally, the slip wall condition was applied at the premixer tube at $x/D = -0.7$ to simulate boundary layer destruction before entering the combustion chamber. Regarding the turbulence intensity, a value of 5% was also applied for the fuel injectors. Experimental data in relation to this parameter was not available.

Finally, studies regarding the fuel inlet temperature were done during the experimental campaign [67]. They designed an analytical model based on the Fourier law of heat transfer to consider the influence of heat transfer between the fuel pipe and the preheated air. The following figure provides the results obtained for hydrogen and methane for different preheat air temperatures (Figure 29). For the present project, only an inlet air temperature of 450K was considered.

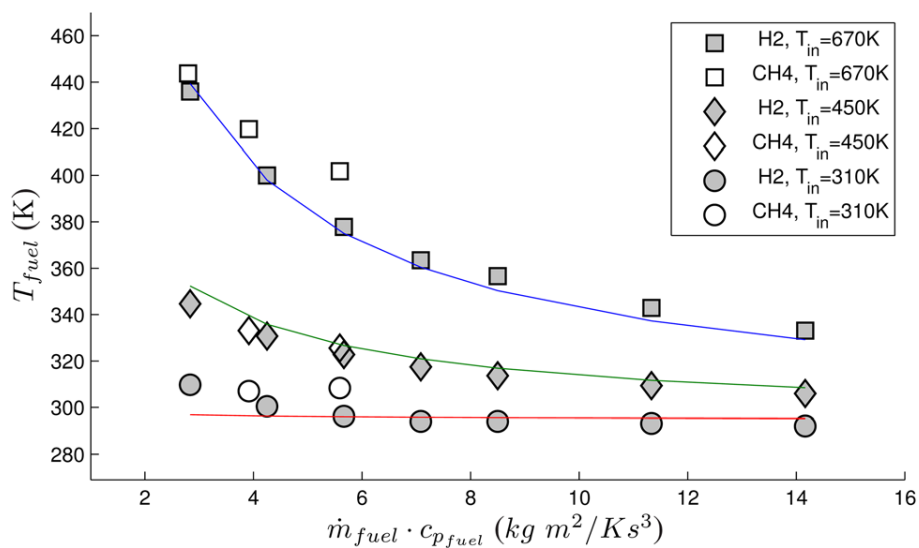


Figure 29. Measured (symbols) and modeled (lines) fuel temperature variation with equivalence ratio and preheat air temperature [67].

For all the cases considered in this report, a fuel temperature value of 320K was used as the variation with equivalence ratio is not very important.

▪ Mesh study

A mesh study was performed to guarantee mesh independent simulations. For the whole study, the coordinate origin was placed at the combustion chamber inlet. The mesh study was performed applying the realizable k- ϵ turbulence model under isothermal flow conditions. Major variations are not expected for the rest of the cases (standard k- ϵ model and reactive flow), thus its validity for all the cases was assumed. It can be seen in the following figures (Figure 30- Figure 31) that the results do not show major discrepancies at the region of interest (C.C.) when refining the mesh. Considering this results, the smallest meshes were used for the 2D (9000 nodes) and 3D (140000 nodes) case.

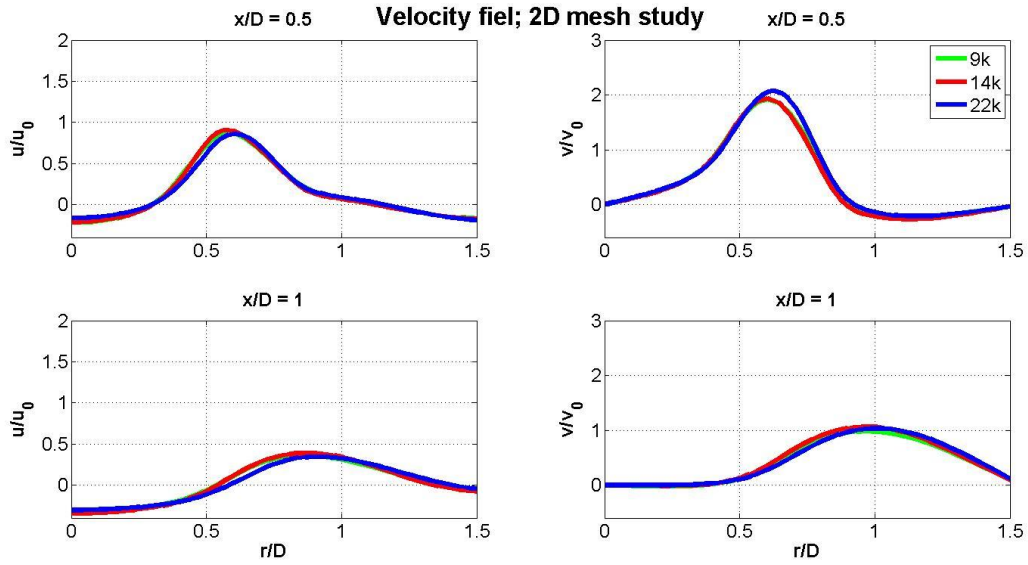


Figure 30. Two-dimensional mesh study for 9000, 14000 and 22000 nodes ($u_0 = 70\text{m/s}$; $v_0 = 20\text{m/s}$; $D = 34\text{mm}$).

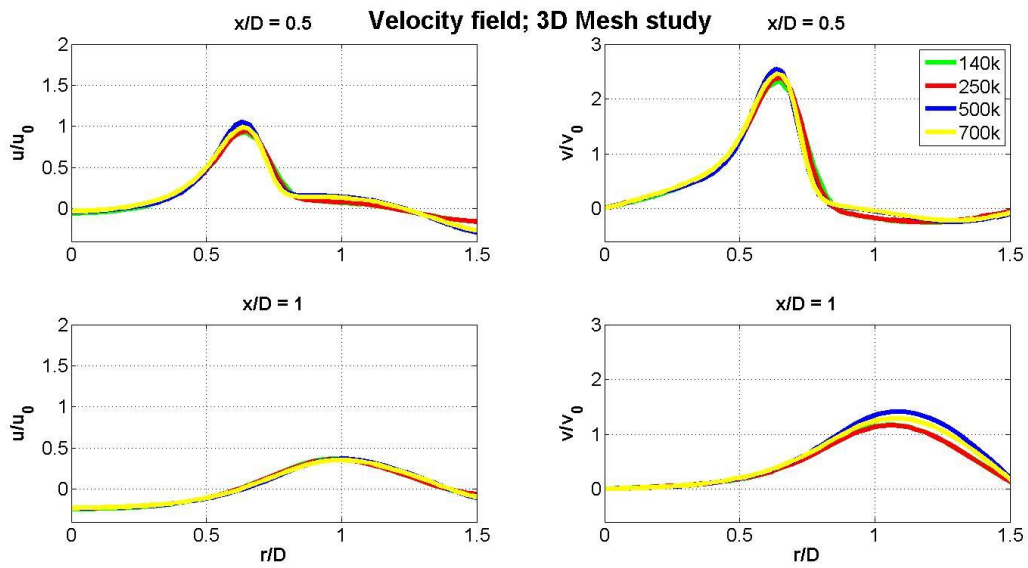


Figure 31. Three-dimensional mesh study for 140000, 250000, 500000 and 700000 nodes ($u_0 = 70\text{m/s}$; $v_0 = 20\text{m/s}$; $D = 34\text{mm}$).

Results and discussion

In this chapter the results obtained after the numerical study of the lean premixed hydrogen combustor design in the AHEAD project are given. The CFD results are analyzed and compared to the available experimental data.

4.1. Isothermal flow

In this section, the results regarding the non-reactive flow analysis of the presented models are given. All the calculations were performed using ANSYS Fluent[®] v16.1 [12]. The main scope of this section is to find out the turbulence model that better characterizes the flow at the combustor. Additionally, the validity of both approaches is assessed.

- *2D case*

Applying the boundary conditions presented before, the following velocity profiles at the combustion chamber were obtained with the standard and realizable k - ϵ turbulence model (Figure 32). Better results are expected with the realizable model as it was validated for similar cases [76], [77]. Also, the standard k - ϵ was considered due to the low swirling nature of the developed flow. The k - ϵ turbulence models were used because of its lower computational cost when compared to more detailed approaches, such as the RSM.

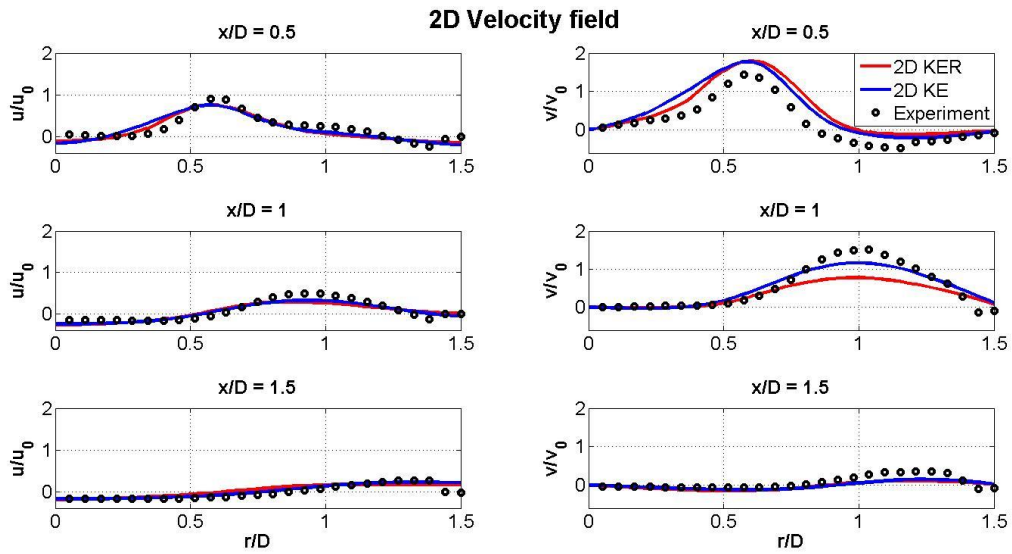


Figure 32. Velocity distribution in the combustion chamber obtained with CFD 2D RANS standard and realizable $k-\epsilon$ models ($u_0 = 70\text{m/s}$; $v_0 = 20\text{m/s}$; $D = 34\text{mm}$).

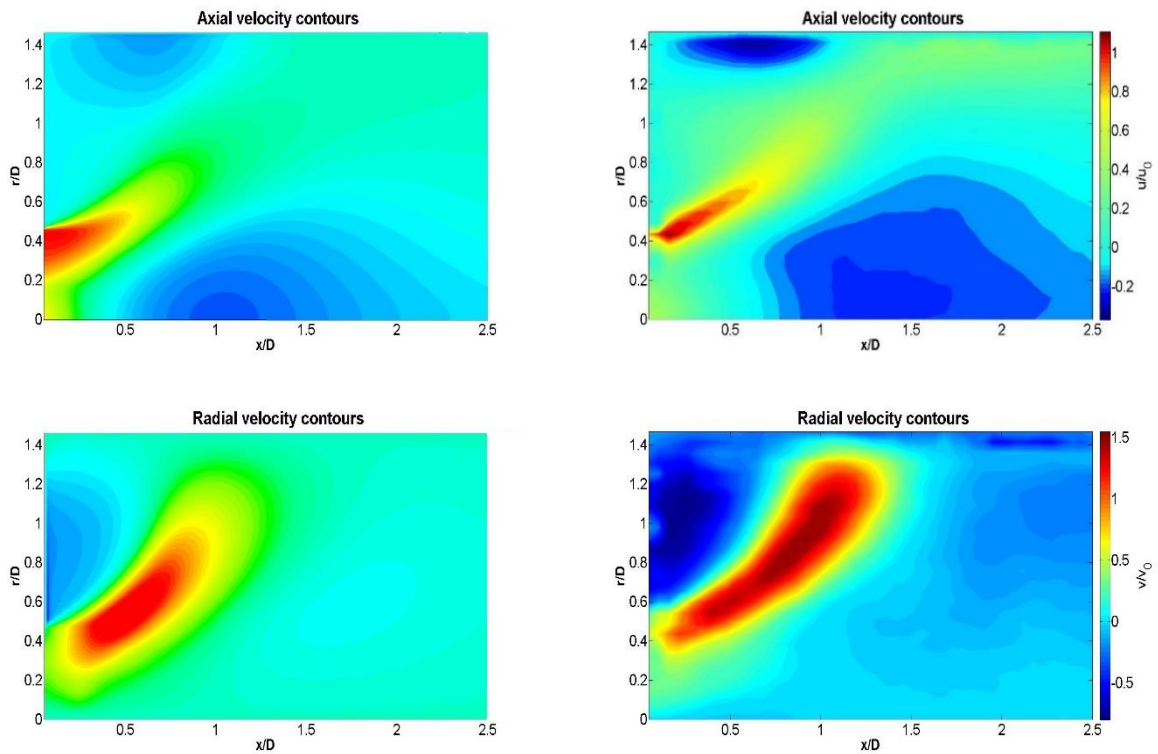


Figure 33. Axial (top) and radial (bottom) velocity contours obtained with CFD 2D RANS standard $k-\epsilon$ model (left) and with experiments (right) [58].

The results obtained show a fairly good agreement with the experimental data given the number of assumptions. The main trend of the velocity curves is captured with this model. Additionally, the central and the outer recirculation zones, which are important characteristics of this type of flows, are well predicted (Figure 33). However, the quantitative results show some disagreement, mostly in the radial velocity. Moreover, the fuel inlets were also modeled. The mixing pattern of circular jets is not the same as for an annular inlet, providing additional modelling errors to the 2D approach. The effect of the fuel inlet is assessed in reactive simulations.

- **3D case**

The same study was performed for a more detailed tridimensional model. At first, the results applying the swirler angle proposed in the previous internal study are presented (Figure 34). The calculation was performed with the realizable $k-\epsilon$ turbulence model.

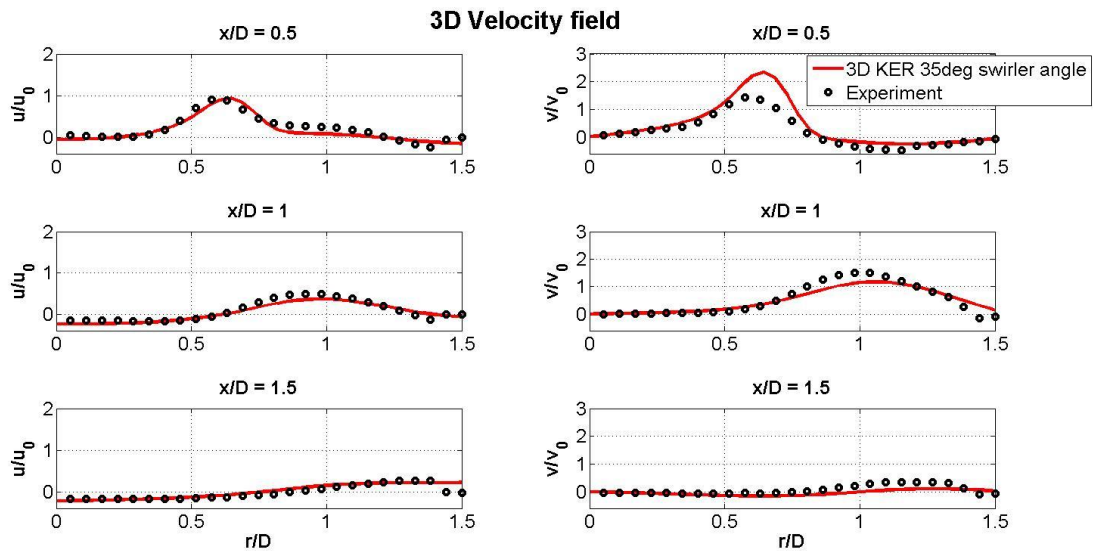


Figure 34. Velocity distribution in the combustion chamber obtained with CFD 3D RANS realizable $k-\epsilon$ models applying an inlet angle of 35° at the swirl inlet ($u_0 = 70\text{m/s}$; $v_0 = 20\text{m/s}$; $D = 34\text{mm}$).

As said, the radial velocity applying these boundary conditions is overestimated, mainly at the combustion chamber inlet. This is due to the higher swirl number obtained when comparing it to the experiment. The following velocity field at the burner was obtained after the swirl number study (Figure 35).

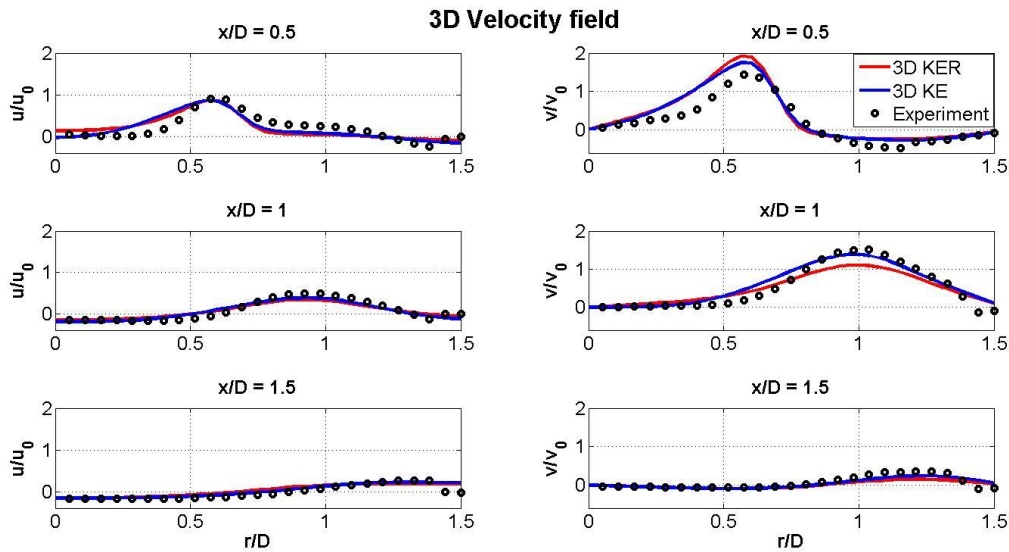


Figure 35. Velocity distribution in the combustion chamber obtained with CFD 3D RANS standard and realizable $k-\epsilon$ models ($u_0 = 70\text{m/s}$; $v_0 = 20\text{m/s}$; $D = 34\text{mm}$).

The simulations using the 3D approach show better agreement with the experimental data than the 2D configuration. However, the computational cost of the 3D approach is higher. Again, the main trend of the velocity radial distributed is obtained with this configuration. Moreover, the central (CRZ) and the outer recirculation zones (ORZ) are also well predicted.

- **Stagnation point comparison**

A more detailed comparison between all the approaches presented is given. One of the most important characteristics of the CFD configuration is its ability to predict the stagnation point and thus the CRZ position. This is important for predicting the flame position, thus assessing flashback. The following figure (Figure 36) provides a comparison between the four approaches.

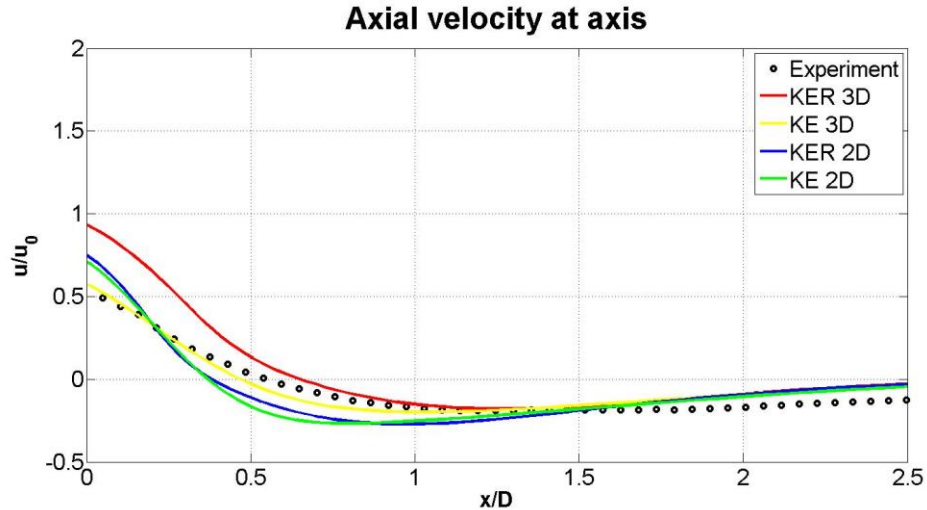


Figure 36. Stagnation point location comparison for the studied meshes ($u_0 = 70\text{m/s}$; $D = 34\text{mm}$).

From the previous figure, it can be concluded that the 2D meshes underestimate the stagnation point position. This might be a drawback when predicting flashback at the burner. The 3D approach has a good prediction of the stagnation point, in particular the standard k- ϵ . Likewise, the big difference between the 2D fuel inlet and the actual burner fuel injection ports can provide additional errors.

Because of these reasons, the 3D mesh is supposed to better represent the reactive flow in this combustor. The difference between the two turbulence models is almost negligible. Nevertheless, the standard k- ϵ shows better performance for the isothermal flow. Both models are kept for further study, as the realizable k- ϵ was recommended by similar studies and shows good results.

4.2. Reactive flow

In this section, the results regarding the reactive study are introduced. First, a brief study of the 2D model is performed to evaluate the effect of the assumptions made. Next, a detailed analysis of the 3D model is given.

▪ 2D case

The results obtained with the Eddy Dissipation Concept chemistry-turbulence interaction model are presented in this point. The hydrogen reaction mechanism proposed by Li et al. and the realizable k- ϵ turbulence model were used for the two-dimensional case. Additionally, only an equivalence ratio of 0.4 was tested to assess the effect of the simplifications applied to the 2D case.

At first, the static temperature distribution is presented to have an overall idea of the flow field obtained (Figure 37). For the 2D case, only the results obtained with Eddy Dissipation Concept model are discussed. The results regarding the FGM turbulence-chemistry interaction model were similar and did not provide any additional information.

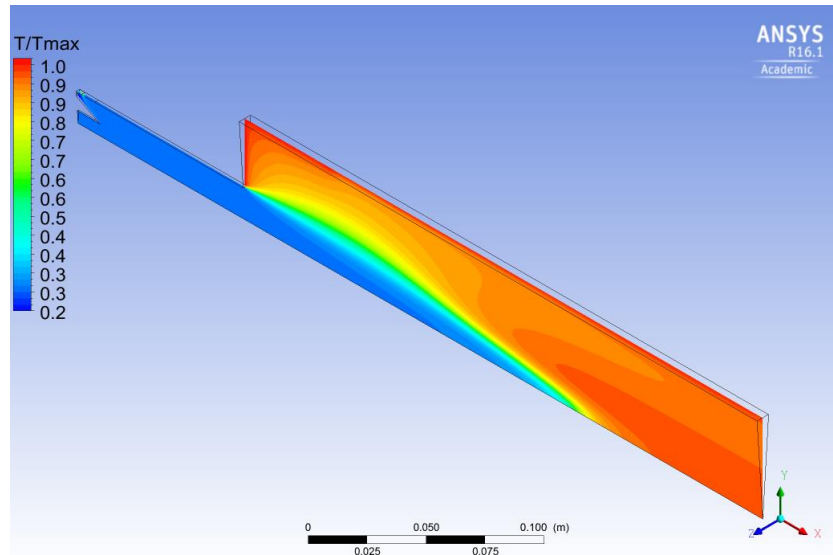


Figure 37. Temperature distribution obtained with the 2D approach, EDC model, Li et al. chemistry reaction mechanism and realizable $k-\epsilon$ turbulence model ($T_{max} = 1666K$).

The main characteristic of the case at hand is the disappearance of the vortex breakdown, thus no central recirculation zone (CRZ) was predicted. This fact was confirmed by the axial velocity distribution (Figure 38).

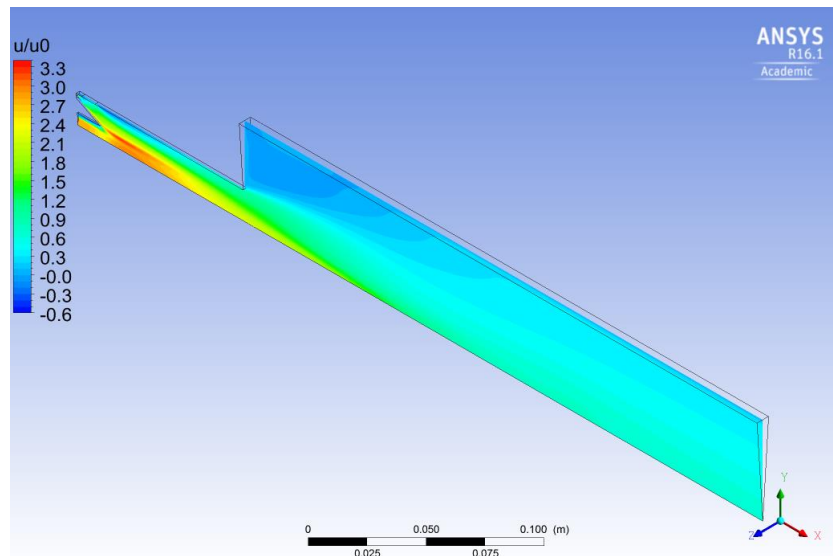


Figure 38. Axial velocity distribution obtained with the 2D approach, EDC model, Li et al. chemistry reaction mechanism and realizable $k-\epsilon$ turbulence model ($u_0 = 70m/s$).

The non-presence of the vortex breakdown, which appears for all the studied conditions in the experiments (Figure 18), was mainly caused by the over prediction of the axial momentum imposed by the fuel jet. The high level of modelling imposed to the fuel injectors played a major role. The vortex breakdown was not already predicted at very lean conditions. This effect would be worse when increasing the equivalence ratio of the mixture, because of the higher amount of fuel mass flow, thus axial momentum. The equivalence ratio and fuel mass flow have a direct relation because the air mass flow was kept constant for all equivalence ratios.

The problem studied in this report presented a high sensitivity to the extra axial momentum provided by the fuel jet. This high sensitivity is connected to the relatively low swirl number found at the mixing section, around 0.55. Terhaar et al. [81] performed an in depth study of the swirl number relation to the vortex breakdown type (e.g. bubble, cone, etc.). Regarding this study, they did some experiments with a combustor almost identical to the one at hand. They defined S_{prim} as the geometrical swirl number of the swirler. The swirl number at the premixing section was defined as S_{res} to consider the axial jet at the axis, which reduced the total swirl number. The following figure provides the resultant swirl number for different amounts of axial air flow and geometrical swirl numbers (Figure 39). Furthermore, the different vortex breakdown types are given.

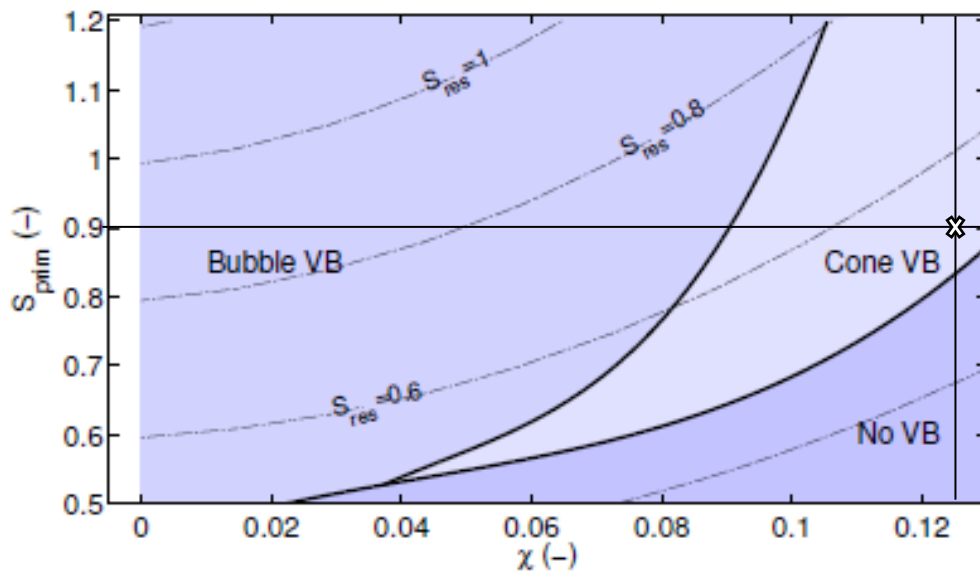


Figure 39. Variation of resultant swirl number and different vortex breakdown types with geometrical swirl number and axial air injection [81].

The characteristics of the studied case are added to the previous figure. The flow configuration studied was close to the non-presence of any kind of vortex breakdown. The over prediction of the axial fuel momentum with the 2D approach made the resultant swirl number to be below the critical value of around 0.47 [81], thus predicting a flow field without vortex breakdown.

The effect of the annulus fuel injector was further analysed. The mixing pattern at the mixing tube was incorrectly predicted. An almost homogeneous mixture was expected at the combustion chamber inlet (Figure 16 right). However, the 2D approach predicted a heterogeneous mix of air and hydrogen (Figure 40).

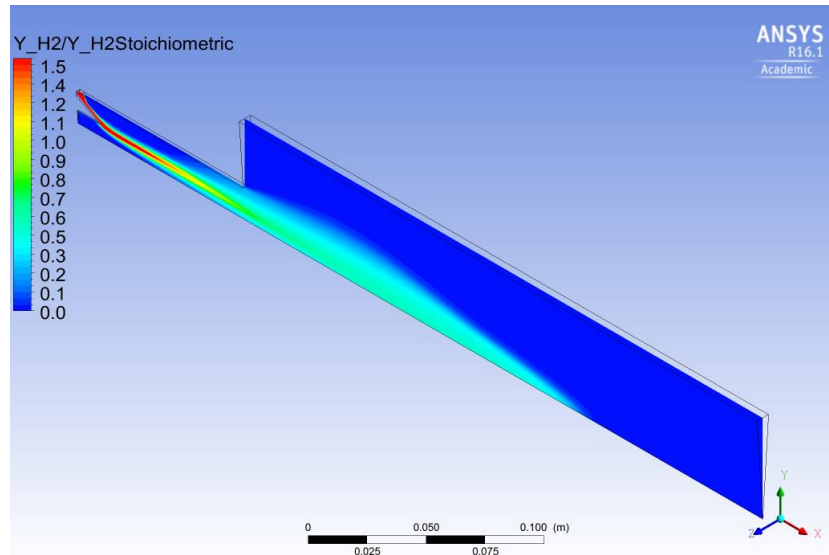


Figure 40. Mass fraction of hydrogen normalized with the stoichiometric value obtained with the 2D approach, EDC model, Li et al. chemistry reaction mechanism and realizable $k-\epsilon$ turbulence model.

At the combustion chamber inlet, some zones reached the stoichiometric and even exceeded the equivalence ratio value of 1. A homogeneous mixture with a normalized hydrogen mass fraction around 0.4 would be required to represent the actual mixing of the combustor designed in the AHEAD project. This mixing pattern can be directly related to the interaction between the fuel jet and the air streams. The following figure provides the paths followed by the hydrogen and air particles (Figure 41).

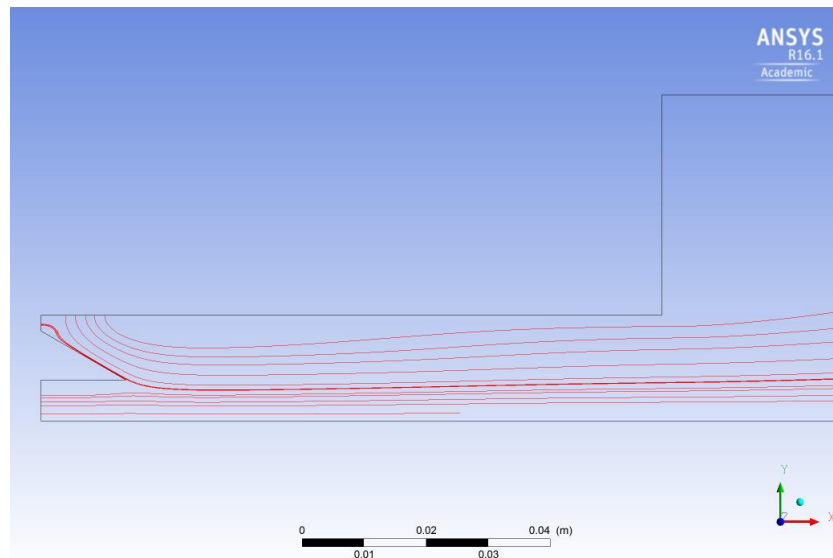


Figure 41. Streamlines of hydrogen and air at the mixing section obtained with the 2D approach, EDC model, Li et al. chemistry reaction mechanism and realizable $k-\epsilon$ turbulence model.

The swirling flow pushed the fuel jet (thick line) to the axial air stream. The high radial momentum of the swirling stream, mainly caused due to the axisymmetric configuration, provided poor mixing of the two components in the outer region of the mixing tube. The fuel-air interaction along the axis was worsened by the presence of axial flow at this region. Considering both effects, a high concentration of fuel was predicted at the interface between the axial flow and the outer swirling region.

A different flame from that of the experiments was predicted by the model, mainly due to the combination of the over predicted fuel axial momentum, thus no vortex breakdown was present, and the bad mixing quality. The following picture provides the OH distribution at the combustion chamber (Figure 42). The results obtained were completely different from that of the experiments. Moreover, the heat released by the reaction was compared to the experimental OH* images (Figure 43). This approach was suggested by Kathrotia et al. [82] for premixed methane flames. The displacement of OH* from the peak heat released was found to be less than the typical flame thickness, meaning that that both parameters are comparable without adding a big error. A similar behavior for hydrogen flames was assumed.

The 2D approach was not accurate enough to characterize the combustor at hand. The high amount of simplifications applied to this configuration caused major changes in the flow field as well as in the mixing pattern.

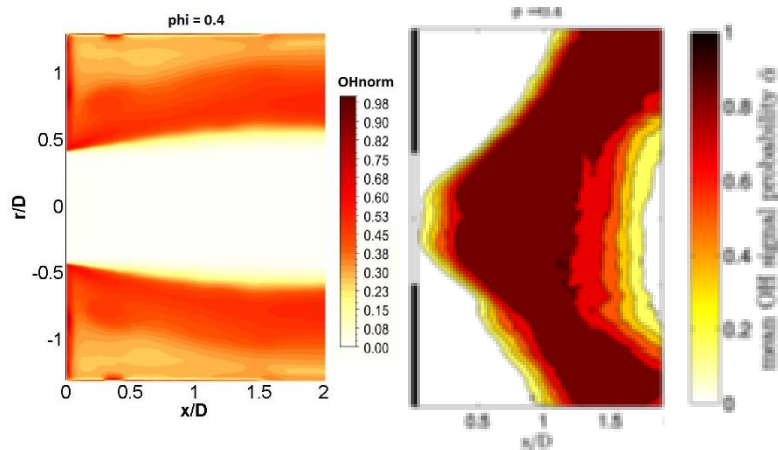


Figure 42. OH mass fraction normalized with the value of 0.004, obtained with the 2D approach, EDC model, Li et al. chemistry reaction mechanism and realizable $k-\epsilon$ turbulence model.

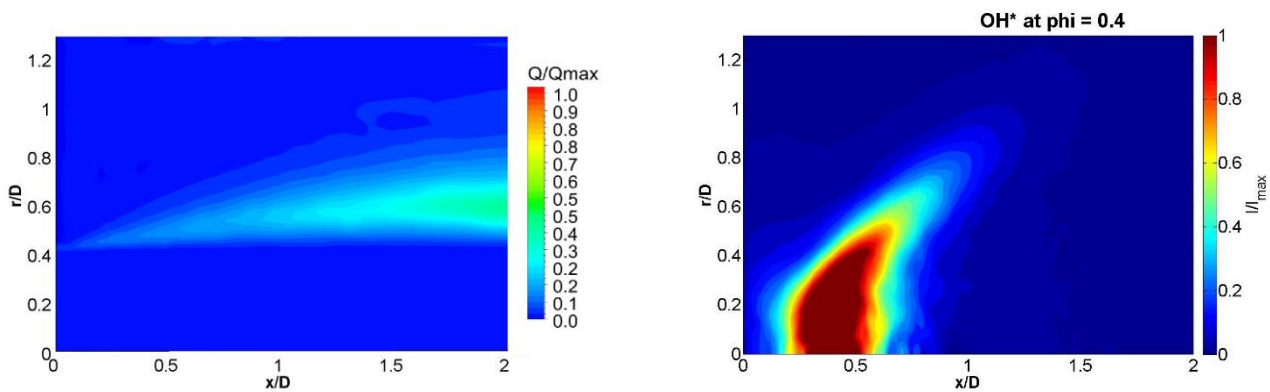


Figure 43. Normalized heat release (left) obtained with the 2D approach, EDC model, Li et al. chemistry reaction mechanism and realizable $k-\epsilon$ turbulence model and normalized experimental OH* (right) [58].

▪ 3D case

In the present point, the results regarding the 3D cases are presented. Several analyses were performed applying the three-dimensional approach. First, a comparison between the realizable and standard $k-\epsilon$ models is given. Good agreement with the experimental data was obtained with both models for the non-reactive case, thus a further study was required. Next, the results obtained with the Flamelet Generated Manifold models are presented. Then, the predictions given by the Eddy Dissipation Concept are shown.

Turbulence models comparison

The results obtained with the $k-\epsilon$ standard and $k-\epsilon$ realizable turbulence models are given in this point. This study was performed applying the Li et al. chemical reaction mechanism and the Eddy Dissipation Concept. An equivalence ratio of 0.4 was used as base for the reactive study. A similar behaviour for the rest of the models was assumed.

The following figure shows the OH distribution at the mid-plane of the combustor (Figure 44). This parameter was chosen to characterize the flame at the combustor. This species does not represent the actual flame, which will be given by the area of heat release, as OH persists in post combustion gases of premixed flames over a longer time-scale than the heat releasing reaction [67]. OH is used here because it can be directly compared with the experimental results, without applying any kind of assumption (e.g. OH* compared to the heat release region). The results were compared to the experimental results given in Figure 21 for an equivalence ratio of 0.4.

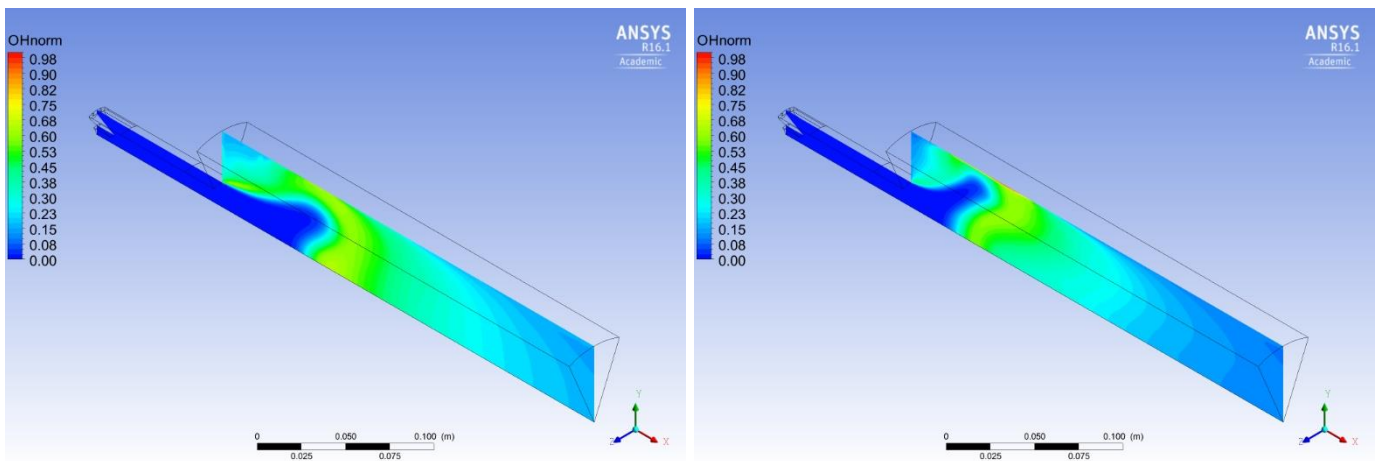


Figure 44. Normalized OH distribution at the mid-plane of the analyzed combustor, obtained with the standard (left) and the realizable (right) $k-\epsilon$ turbulence model, EDC and Li et al. chemical reaction mechanism.

The OH distribution obtained with both models is different from that given by the experimental results. The main difference is the presence of this species at the outer recirculation zone, which was predicted by the selected set of models and never appeared during the experiments. Moreover, the CFD calculations predicted flame attachment to the inlet corner of the combustor for the selected conditions. This flame attachment was captured at higher equivalence ratios in the experiments (Figure 21).

One of the most important features of the CFD simulations is its ability of predicting the actual axial flame position, thus characterizing flashback. It has been demonstrated [83] that the flame position can be identified by high OH gradients in premixed combustion. As an example, Figure 45 provides the OH mass fraction at the axis position of the combustion chamber. In this case, the flame was found at around $x/D = 1.5$, because of the high gradient of the OH concentration at this point.

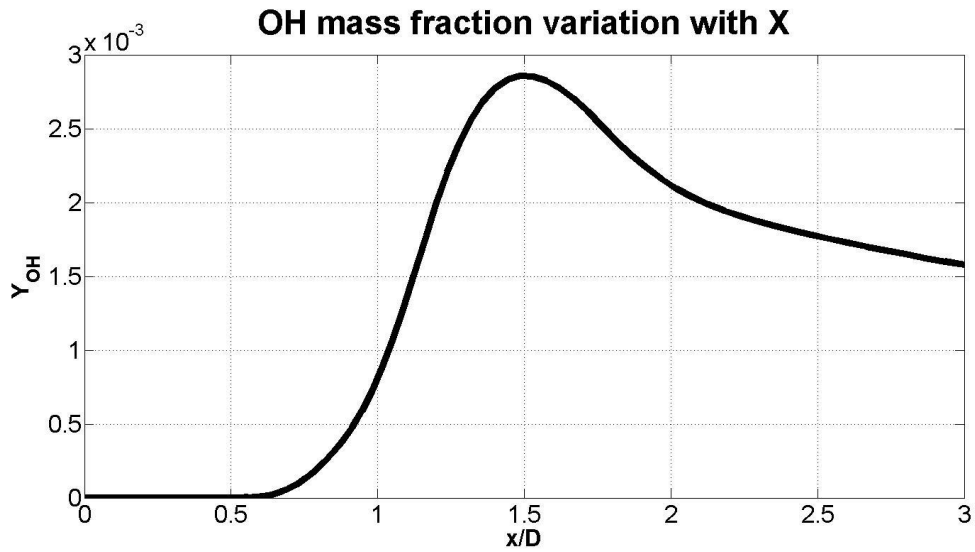


Figure 45: OH mass fraction axial variation predicted with the realizable $k-\epsilon$ turbulence model, EDC and Li et al. chemical reaction mechanism.

Following this approach, the flame position at the combustor axis was calculated for both turbulence models. The predictions obtained by the two selected turbulence models are presented in the following table (Table 9).

Table 9. Axial flame position predicted by the experiments [67] and the 3D approach with the standard and the realizable $k-\epsilon$ turbulence model, EDC and Li et al. chemical reaction mechanism.

Case	Axial flame position (x/D)
Experiment	0.25
K- ϵ Standard	2.5
K- ϵ Realizable	1.47

The flame position at the axis was over predicted by the two turbulence models in combination with the Eddy Dissipation Concept turbulence-chemistry interaction model. It was decided to perform the rest of the calculation with the realizable $k-\epsilon$ turbulence model as it provided better results and was applied in similar problems found in the literature. The reason of this flame behavior is given in upcoming points.

Flamelet Generated Manifold (FGM)

The results regarding the Flamelet Generated Manifold obtained during the simulations are compared with the experimental data and discussed in detail. As decided previously, the k- ϵ realizable turbulence model was applied to this case. The Li et al. chemical reaction mechanism was chosen for this case. The effect of the chemical reaction mechanism is not of major importance, since the chemistry is reduced by applying a look-up table approach. The results of Li et al. and O Conaire et al. were compared. No important differences in the reactive parameters (e.g. temperature, OH, etc.) were found between both chemical reaction mechanisms.

When applying the Flamelet Generated Manifold approach, Fluent[®] provides different options to calculate the Flamelets and the PDF table, regarding the turbulence-chemistry interaction. The following table summarizes all the approaches chosen for the FGM simulations (Table 10).

Table 10. Summary of the Flamelet Generated Manifold parameters chosen for the case at hand.

Parameter	Chosen configuration/value
Premixed/Diffusion flamelet	Premixed flamelet
Adiabatic/Non-adiabatic flamelet	Adiabatic flamelet
Table grid refinement [Zc]	32x32
Scalar dissipation at stoichiometric mixture fraction [Hz]	1000
Mean Source Term	Finite Rate-Turbulent Flame Speed
Variance model	Transport equation

Flamelets can be calculated applying a premixed or a diffusion approach. The premixed flamelet configuration was chosen because of the premixed nature of the case. Flamelets were calculated adiabatically. The main difference between the adiabatic and non-adiabatic approach is that the latter considers the enthalpy of the fluid when generating the look-up table. Considering the enthalpy variation at the flow field does not provide major differences in the flame location (main objective of the present study). The adiabatic approach was chosen because of its lower computational cost.

Increasing the number of points in the mixture fraction and reaction progress space provides a more refined look-up table. A more refined table could provide a better approach to the problem, giving better results. In this case, the values obtained with a refined (up to 160 points) and a coarse look-up table were very similar. Fluent® applies a linear interpolation if the value for the control variables (i.e. mixture fraction and control variable) found at a determined position of the flow field is in between two calculated points of the look-up table. Furthermore, the scalar dissipation at stoichiometric conditions (13) was set to 1000Hz. The standard value provided by the program was kept, as it is advised by the manual. This value was found to give fairly good results for most of flames [12].

The mean source term of the reaction can be calculated following three approaches: Finite Rate, Turbulent Flame Speed (Zimont or Peters) and a combination of both. All of them were tried to have an idea of the effect of this parameter in the results of the simulations. Qualitatively, all of them showed a similar behavior. It was decided to apply the combination of the Finite Rate and Turbulent Flame speed, which uses the minimum value of the two. Additionally, the mean source term variance can be calculated by a transport equation or with an algebraic approach. These two approaches gave different results (Figure 46). The application of the transport equation was chosen because the results obtained were more realistic.

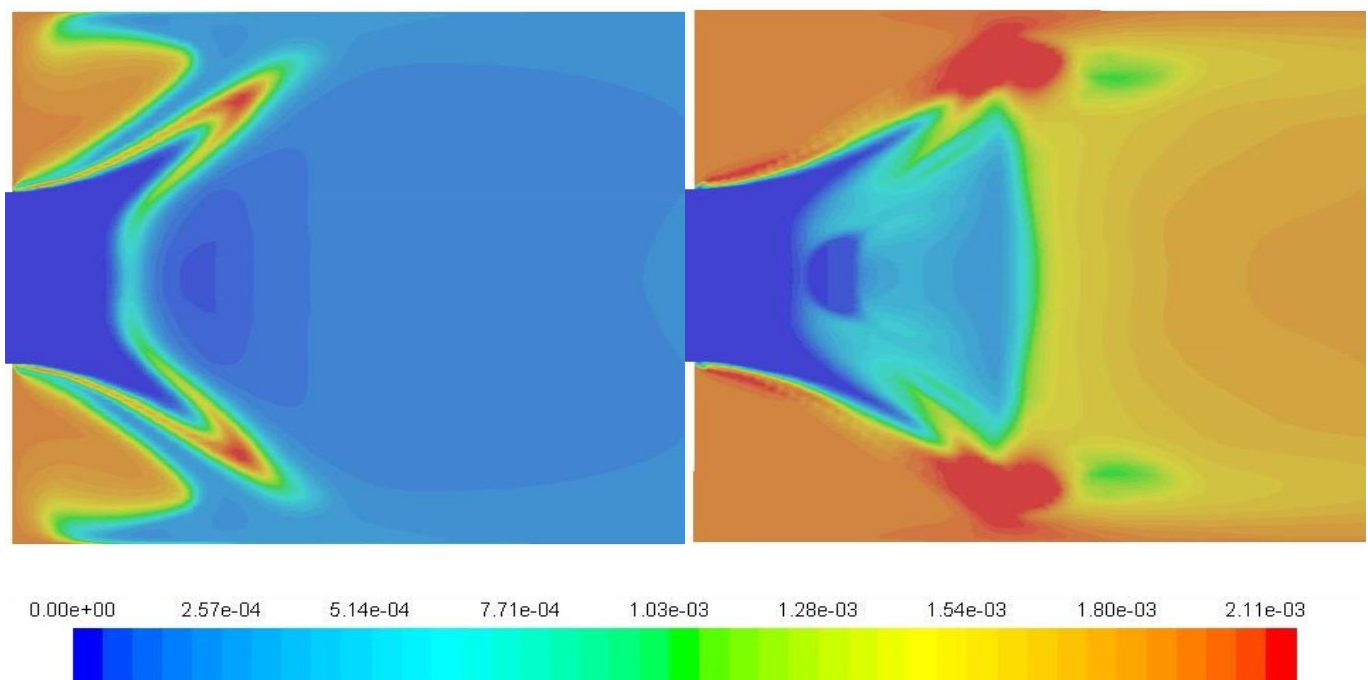


Figure 46. OH mass fraction obtained with different mean source term variance modelling; Transport equation (left) and Algebraic (right) approaches. Results obtained with the $k-\epsilon$ realizable turbulence model, Li et al. [17] chemical mechanism and FGM.

The temperature results at the mid plane obtained for different equivalence ratios are presented in the following figures (Figure 47), providing an overview of the reactive flow field for different equivalence ratios.

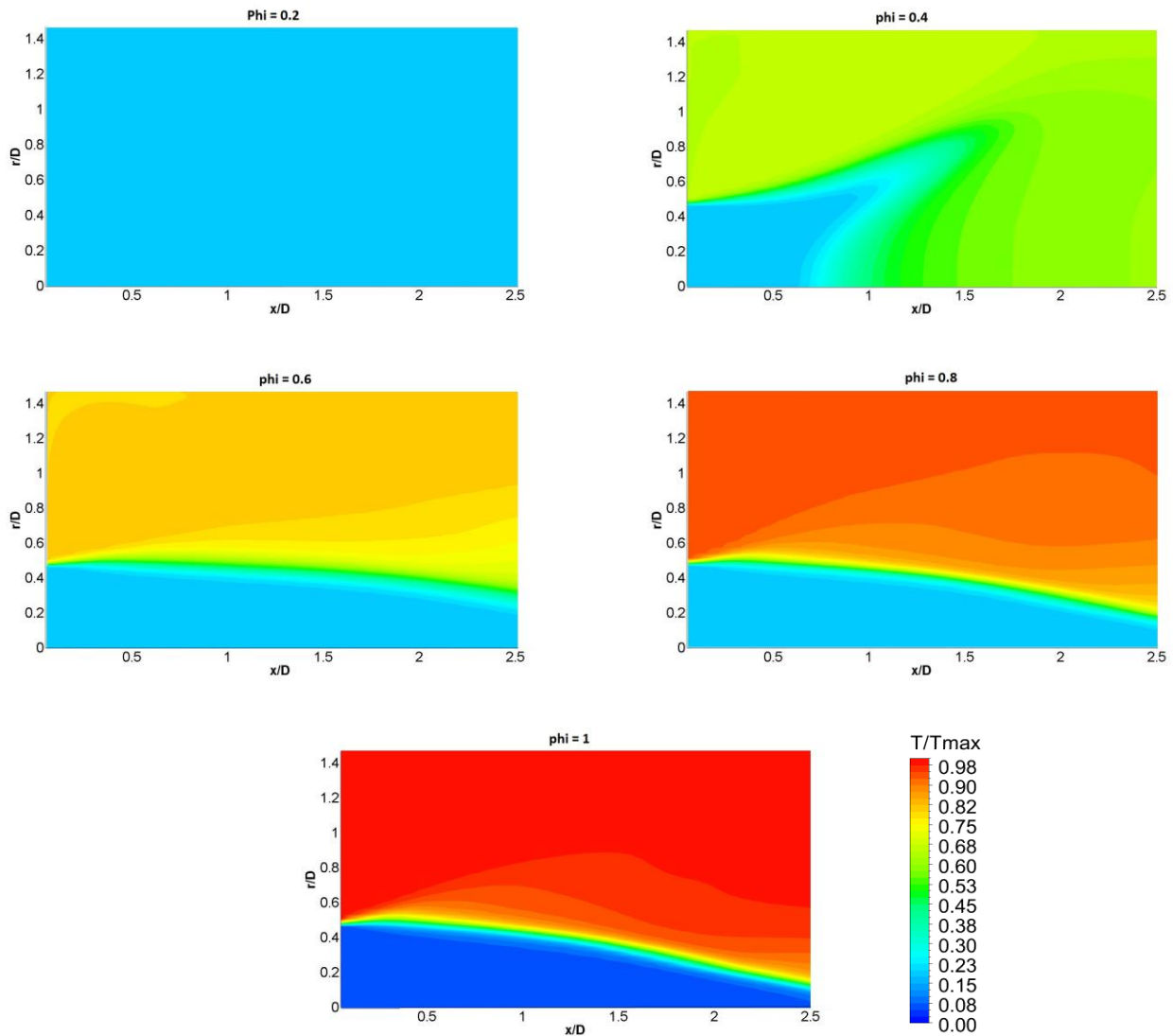


Figure 47. Temperature distribution normalized with the maximum value at stoichiometric conditions ($T_{max} = 2460K$) at the combustion chamber for different equivalence ratios obtained with the 3D approach, FGM model, Li et al. chemical reaction mechanism and realizable $k-\epsilon$ turbulence model.

At low equivalence ratios ($\phi = 0.2$), which are close to the lean blowout limit, combustion was not predicted by the selected set of models. For equivalence ratios of around 0.4, the flow field showed a fairly good qualitative behavior. Further analyses were done for this case. For higher equivalence ratios, the same problem as for the two-dimensional case appeared. The axial momentum of the fuel jet was over predicted; thus, no vortex breakdown was found in these cases.

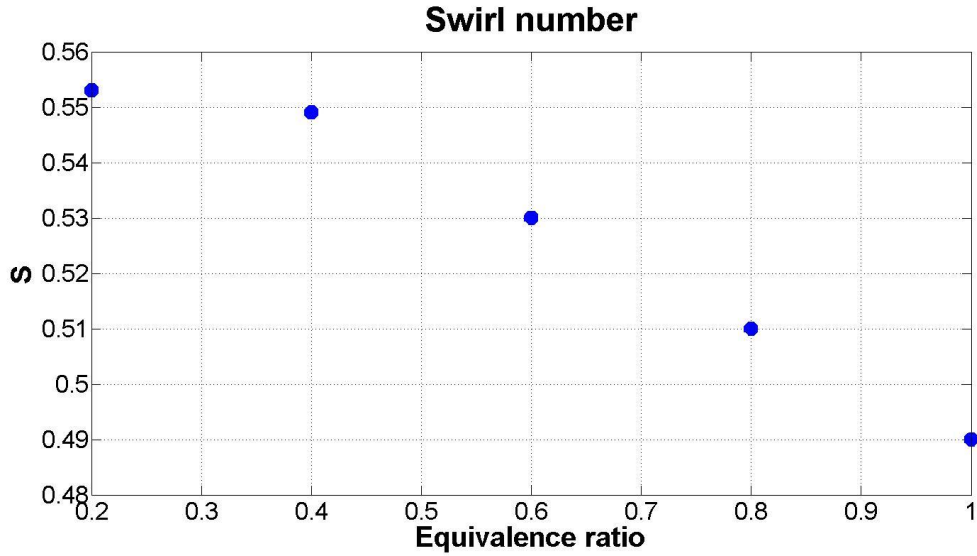


Figure 48. Swirl number variation with equivalence ratio at the combustion chamber inlet obtained with the 3D approach, FGM model, Li et al. chemistry reaction mechanism and realizable $k-\epsilon$ turbulence model.

In the figure above, the effect of the extra axial momentum given by the fuel jet was analyzed. The selected set of models predicted the transition from the cone vortex breakdown to the non-vortex breakdown to be around a swirl number of 0.53. The experimental analysis performed by Terhaar et al. [81] estimated this transition to happen at a value of around 0.47 for the swirl number. A combination of the over prediction of the fuel jet momentum and the vortex breakdown transition swirl number are responsible for the incorrect flow field estimation.

A further study of the results obtained with equivalence ratio of 0.4 was performed. The OH distribution at the mid plane obtained with the selected models was analyzed and compared to the available experimental data (Figure 49).

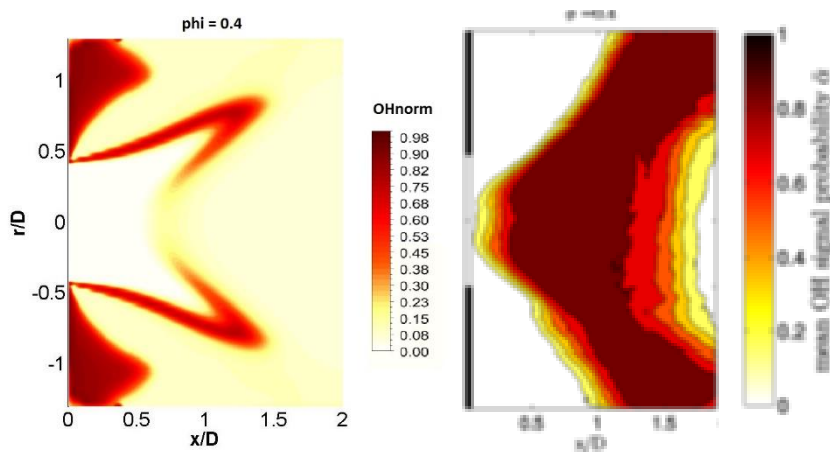


Figure 49. Normalized OH distribution at the combustion chamber for an equivalence ratio of 0.4 obtained with the 3D approach, FGM model, Li et al. chemistry reaction mechanism and realizable $k-\epsilon$ turbulence model.

The results obtained with the CFD simulations showed a different OH distribution. A high concentration of OH at the outer recirculation zone was predicted by the set of models. Additionally, in the 3D FGM results the OH distribution is anchored to the inlet corner of the combustion chamber. This behavior was found to happen for equivalence ratios higher than 0.5 during the experiments. The OH concentration at the central recirculation zone (CRZ) was under predicted by this approach, presenting almost none OH presence at this area.

One of the main differences is the position of the main reaction. The FGM method predicted the reaction to happen at the jet interface with the outer recirculation zone (Figure 50). In the following figure, the reaction area is given by the source term (S) obtained from the Finite Rate and the Turbulent Flame Speed.

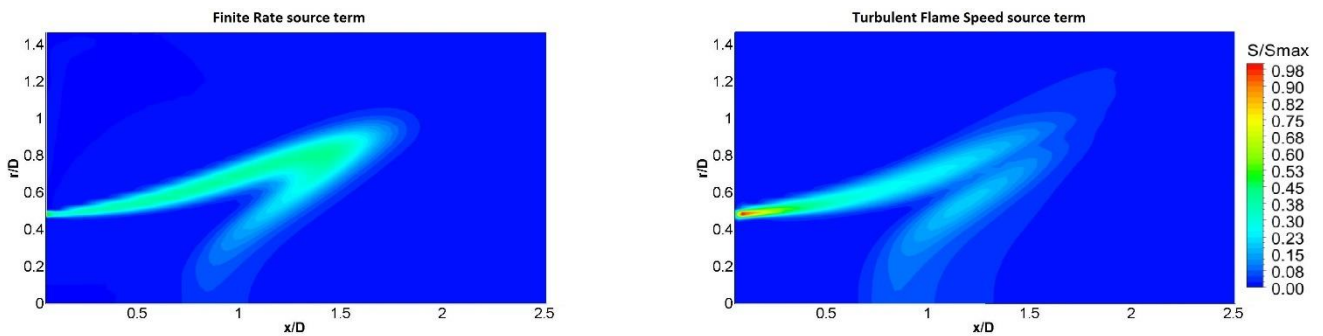


Figure 50. Finite Rate (left) and Turbulent Flame Speed (right) source term at the combustion chamber for an equivalence ratio of 0.4 obtained with the 3D approach, FGM model, Li et al. chemistry reaction mechanism and realizable $k-\epsilon$ turbulence model.

Additionally, the mixture fraction distribution obtained at the combustion chamber inlet (Figure 51 left) showed a heterogeneous mixing pattern (Figure 51 right), which influences the flame structure. The mixing obtained during the experiments (Figure 16 right) presented an almost homogeneous distribution of the fuel agent, obtaining a bit higher fuel concentration at the axis than at the premixer walls. The CFD approach predicted a heterogeneous mixing between air and fuel. Moreover, the concentration peaks were found at the walls, in disagreement with the experimental results.

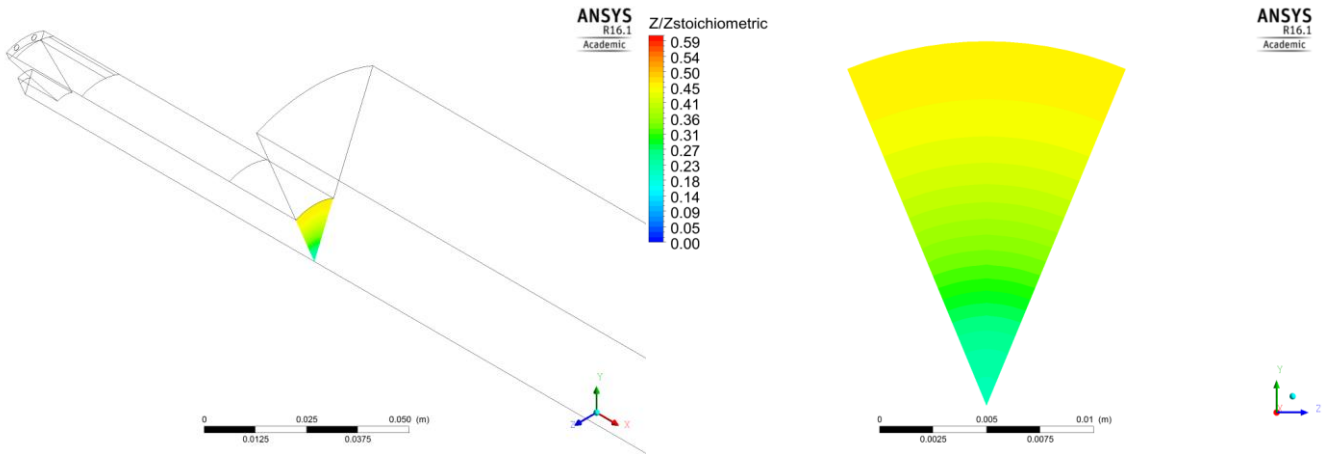


Figure 51. Normalized mixture fraction at the combustion chamber inlet for an equivalence ratio of 0.4 obtained with the 3D approach, FGM model, Li et al. chemical reaction mechanism and realizable $k-\epsilon$ turbulence model.

The flame position at the axis was calculated by applying the procedure explained previously and compared to the EDC case presented before (Table 11). The FGM model showed a flame location closer to the one found at the experiments. However, the prediction of both CFD approaches was still incorrect.

Table 11. Axial flame position predicted by the experiments [67] and the 3D approach with the realizable $k-\epsilon$ turbulence model, Li et al. chemical reaction mechanism and EDC/FGM.

Case	Axial flame position (x/D)
Experiment	0.25
FGM	0.6
EDC	1.47

The results given by the FGM approach were not accurate when simulating hydrogen combustion in the lean premixed combustor designed in the AHEAD project. Several factors might have a role in this problem. First, the FGM approach provided by Fluent[®] neglects differential diffusion, which may be of major importance when simulating hydrogen combustion. Moreover, the mixing pattern predicted by this method was found to be different than expected, thus obtaining a different flame structure. Finally, the simplifications applied to the model could also be responsible for the obtained behavior, mainly on the fuel and air jets interaction.

Eddy Dissipation Concept

In the present section, the results regarding the Eddy Dissipation Concept are given, considering adiabatic walls conditions. The $k-\epsilon$ realizable turbulence model was used. The Li et al. chemical reaction mechanism was selected as recommended by Ströhle and Myhrvold [16]. The Eddy Dissipation Concept approach is a more detailed turbulence-chemistry interaction mechanism. Furthermore, differential diffusion was considered, overcoming one of the main simplification of the previous approach (FGM).

First, the static temperature distributions at the mid plane of the combustion chamber for different equivalence ratios are presented (Figure 52).

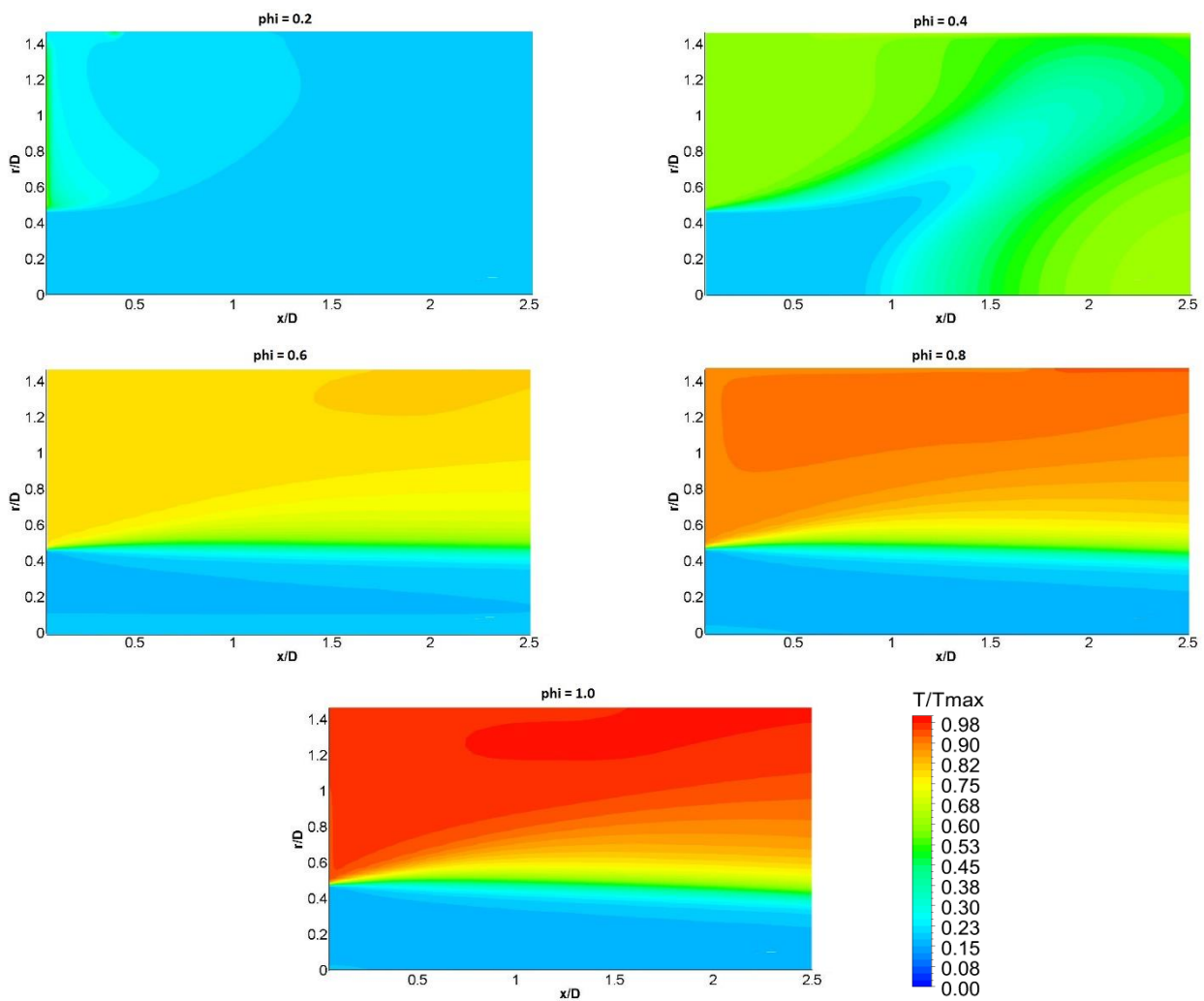


Figure 52. Temperature distribution normalized with the maximum value at stoichiometric conditions ($T_{max} = 2455K$) at the combustion chamber for different equivalence ratios obtained with the 3D approach, EDC model, Li et al. chemistry reaction mechanism and realizable $k-\epsilon$ turbulence model.

The combustion process at equivalence ratio 0.2 mainly occurs at the inlet corner, providing a non-realistic behavior of the flame when comparing it with the actual experiments. Again, for the base case of equivalence ratio 0.4, the model predicted a fairly good flow field, focusing on its qualitative characteristics. At higher equivalence ratios, the fuel axial momentum is once more over estimated. No vortex breakdown was found at these conditions by the selected set of models. Only the case of equivalence ratio 0.4 was further analyzed.

The OH distribution obtained at the mid plane of the combustor is presented and compared to the experimental results in the following figure (Figure 53). The presence of OH at the interface area between the jet and the outer recirculation zone was not captured during the experiments. The presence of this species at the central recirculation zone was predicted in this case.

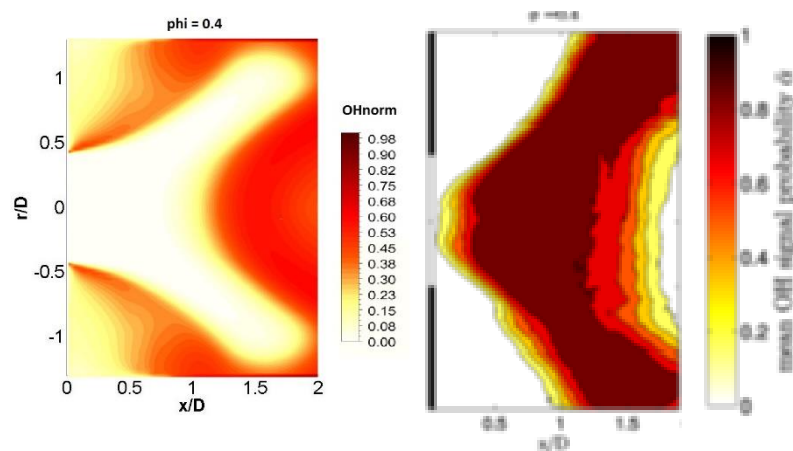


Figure 53. Normalized OH distribution at the combustion chamber for an equivalence ratio of 0.4 obtained with the 3D approach, EDC model, Li et al. chemical reaction mechanism and realizable $k-\epsilon$ turbulence model.

Moreover, the heat of reaction was compared to the OH* distribution obtained with chemiluminescence methods (Figure 54). The predicted results were not accurate enough. The maximum heat release peak was obtained close to the combustion chamber walls with the CFD approach, which was not comparable to the experimental data.

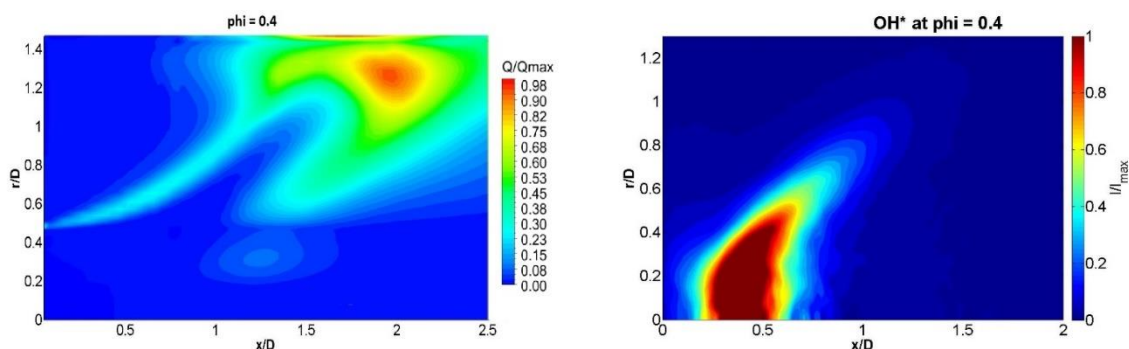


Figure 54. Normalized heat release (left) obtained with the 3D approach, EDC model, Li et al. chemistry reaction mechanism and realizable $k-\epsilon$ turbulence model and normalized experimental OH* (right) [58].

The incorrect prediction of the combustion parameters might be directly related to the erroneous calculation of the mixing pattern at the premixer. In the following figure, the hydrogen distribution found at the combustion chamber inlet is given (Figure 55). Similarities between the FGM and EDC model were found, thus differential diffusion did not play a major role in the mixing distribution at the combustor mixing zone.

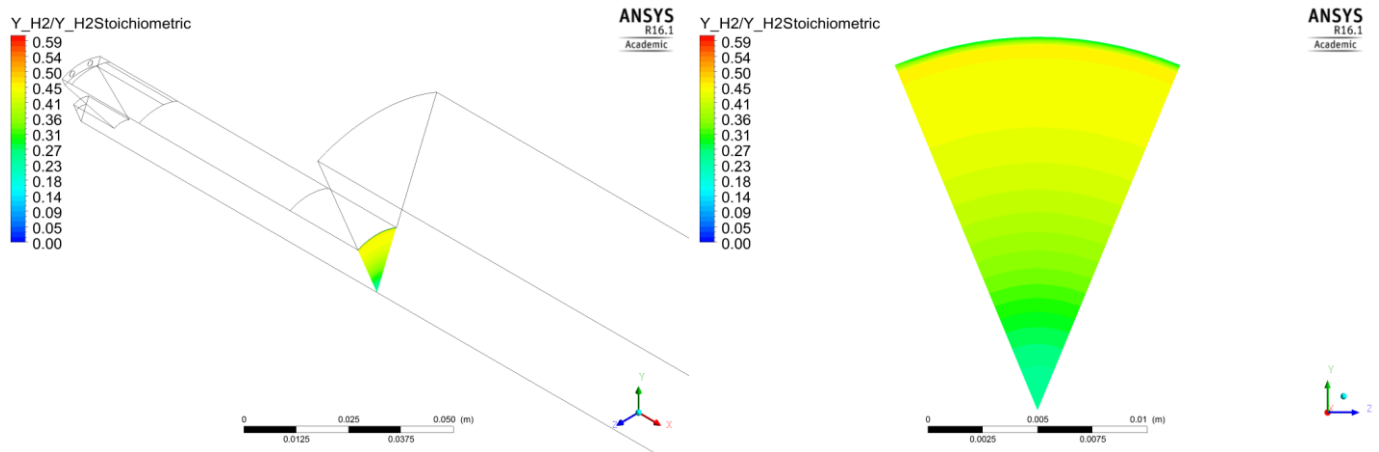


Figure 55. Normalized hydrogen mass fraction at the combustion chamber inlet for an equivalence ratio of 0.4 obtained with the 3D approach, EDC model, Li et al. chemical reaction mechanism and realizable $k-\epsilon$ turbulence model.

The selected approach predicted heterogeneous mixing between air and hydrogen. Again, the concentration peaks were found near the walls, in disagreement with the experimental results. The obtained distribution was caused by the poor mixing between the air coming from the swirler and the fuel. This might also be a reason for the over estimation of the fuel jet axial momentum, thus predicting the disappearance of the vortex breakdown at equivalence ratios higher than 0.4.

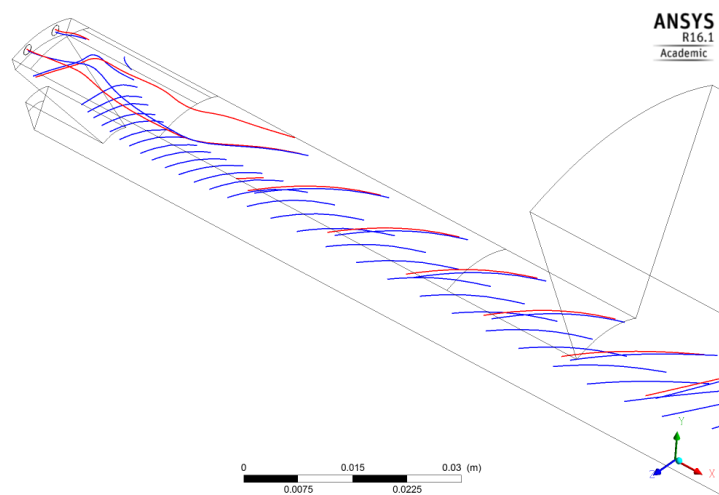


Figure 56. Hydrogen streamline calculated from the fuel inlets at the mixing section obtained with the 3D approach, EDC model, Li et al. chemistry reaction mechanism and realizable $k-\epsilon$ turbulence model.

The swirler inlet mainly interacts with the right fuel injector. The fuel jet on the left-hand side of Figure 56 was almost unaltered, increasing the hydrogen concentration at the region close to the premixer walls. The simplifications applied and the selected turbulence model might cause this behavior. Apparently, the models could not predict the mixing between the two streams.

Moreover, the direct application of the probability density function method by using the Montecarlo approach, which would provide a more complex interaction model between chemistry and turbulence, was considered. However, the available computational resources were not enough to use this method.

Important conclusions can be stated after the analysis of the simulations performed in this thesis. These are mostly related to lean premixed combustion systems and some characteristic features of the cryogenic combustor developed under the AHEAD framework.

The main difficulty of simulating a lean premixed combustor resides on the correct prediction of the mixing. The chosen RANS models, which give an averaged value of the combustion parameters at the mesh's nodes, could not represent the mixing pattern at the premixer. Furthermore, the selection of H_2 as fuel creates additional difficulties to the problem. The high diffusivity of hydrogen and flashback-prone behavior are important complications for the study and design of hydrogen combustors. The low Lewis number of hydrogen is a major factor when simulating the mixing of fuel and air. Again, the models used in the present simulations were not accurate enough to predict this behavior. Additionally, avoiding flashback while maintaining stability over a broad operational range has shown to be a challenge.

The combustor studied here, designed in the AHEAD project, presents a delicate design. It was found that the flow is very sensitive to the extra axial momentum given by the fuel jets. This effect is intensified due to the position of the fuel injectors (close to the external premixer walls, thus at the swirling region of the flow). The extra axial momentum provided by the fuel is important in relation to the swirl number at the premixer, therefore the kind of the vortex breakdown present at the combustion chamber, the mixing pattern, etc. Moreover, the combustor design is also sensitive to the relative position of its components. In particular, the location of the fuel and air injector is of capital importance, which can influence the fuel-oxidizer mixing. Special care has to be taken regarding the aforementioned design parameters of this type of combustor, and of this burner in particular.

5

Conclusions

In the present report, the lean premixed hydrogen combustor designed in the AHEAD project was simulated applying different Reynolds Averaged Navier-Stokes approaches. First, the non-reactive flow field was calculated using different turbulence models, comparing the results obtained between them and available experimental data. Next, hydrogen was added, simulating the combustor under reactive conditions. Again, different models were used to characterize these phenomena (e.g. EDC, FGM).

Regarding the non-reactive flow field, fairly good qualitative results when comparing to the experimental data were obtained, given the high amount of assumptions of some cases (e.g. 2D). All the main characteristics of the kind of flow studied in this project, such as outer recirculation zone, cone vortex breakdown, etc. were well predicted by all the selected turbulence models. The realizable k - ϵ turbulence model was chosen for its application in the reactive cases. A good characterization of the flow field including the axial stagnation point was found when using this model. Moreover, previous studies considered the realizable k - ϵ turbulence model good enough to characterize similar flows, considering the low computational cost of this approach. Furthermore, the realizable method can predict the swirling nature of the flow in a better way than the standard approach.

As an overall, the reactive problem was not well predicted by the selected approaches. The Flamelet Generated Manifold method could not predict the behavior of the combustor. This approach neglected differential diffusion, which should be included when analyzing a hydrogen fueled combustion problem. The Eddy Dissipation Concept chemical-turbulence interaction model did not either obtain good results. Finally, the direct application of the probability density function using the Montecarlo method was found to be computationally expensive.

For the base problem of equivalence ratio of 0.4, the main problem found for both methods was the predicted mixing pattern. An almost homogeneous distribution of the fuel agent was expected because of the premixed nature of the problem. During the experimental campaign, the mixing at the premixer was found to have a bit higher concentration of hydrogen at the axis of the combustor than at the walls. In the CFD calculations, the mixing pattern was found to be the opposite, presenting its peak at the walls and a leaner region at the central axis. This behavior can be explained due to the low capacity of the selected RANS models to predict mixing when considering a fuel with high diffusivity, such as hydrogen. Additionally, the interaction between the fuel and the swirler jets found to be a bit poor in half of the fuel inlets, which were almost unaffected by the presence of swirl and radial flow in the domain.

Moreover, the characterization of the reactive flow field when considering very lean conditions (around equivalence ratio of 0.2) was unrealistic with both approaches. No combustion was obtained with the FGM model and a small reactive area close to the inlet corner was found with the EDC approach.

The increase in equivalence ratio ($\phi \geq 0.6$) produced an overestimation of the axial momentum added by the fuel jets. Moreover, the transition swirl number between a conical vortex breakdown and the disappearance of this phenomenon was found to be a bit higher with the realizable $k-\epsilon$ turbulence model (around 0.53) than at the experiments (0.47). The high sensitivity of the flow at hand to this parameter can make the selected RANS approach not to be enough to characterize the problem.

It was concluded after the analysis of all the results that the studied set of models are not accurate enough to characterize the lean premixed hydrogen combustor designed in the AHEAD project. A further study of the combustor is advised, applying more detailed computational approaches.

6

Future work

The results obtained with the Reynolds Averaged Navier-Stokes approach were not satisfactory. The application of more detailed methods, such as the Large Eddy Simulation, is advised. The assumption of an averaged value for all the parameters might not be accurate enough to characterize the given problem. The high diffusivity of hydrogen could be a major problem when considering an average value for all the parameters. Moreover, previous preliminary studies showed the possibility of obtaining a better mixing pattern if a LES approach would be used.

Heat transfer through the walls by conduction, convection and radiation should be considered. This might be of major importance when characterizing some parameters, such as emissions or temperature distribution, in future studies. The presence of a realistic flame and flow field is advised in order to perform an emissions analysis.

Finally, the geometry and the simplifications made should be checked. After a detailed analysis of the results, the swirler geometry was found to be a bit different from the actual experimental setup, as the previous internal study was used as reference for the geometry. However, the difference was supposed not to be critical when characterizing this kind of combustor.

Bibliography

- [1] T. Poinso and D. Veynante, *Theoretical and Numerical Combustion*, Third ed. Bordeaux: Aquaprint, 2012.
- [2] N. Peters, "The turbulent burning velocity for large-scale and small-scale turbulence," *J. Fluid Mech.*, vol. 384, pp. 107–132, 1999.
- [3] J. Boussinesq, *Essai sur la th{e}orie des eaux courantes*. Imprimerie nationale, 1877.
- [4] B. S. Baldwin and H. Lomax, "Thin Layer Approximation and Algebraic Model for Separated Turbulent Flows," *AIAA 16th Aerosp. Sci. Meet.*, p. 9, 1978.
- [5] P. R. Spalart and S. R. Allmaras, "A one equation turbulence model for aerodynamic flows," *AIAA J.*, vol. 94, 1992.
- [6] B. E. Launder and D. B. Spalding, "The numerical computation of turbulent flows," *Comput. Methods Appl. Mech. Eng.*, vol. 3, no. 2, pp. 269–289, 1974.
- [7] T. Shih, J. Zhu, and J. L. Lumley, "Calculation of Wall-Bounded Complex Flows and Free Shear Flows," *Int. J. Numer. Methods Fluids*, vol. 23, no. February, pp. 1133–1144, 1996.
- [8] D. C. Wilcox, *Turbulence Modelling for CFD*, Third ed. La Cañada, 2006.
- [9] J. Rotta, "Statistische Theorie nichthomogener Turbulenz," *Zeitschrift für Phys.*, vol. 129, no. 6, pp. 547–572, 1951.
- [10] K. Hanjalić and B. E. Launder, "A Reynolds stress model of turbulence and its application to thin shear flows," *J. Fluid Mech.*, vol. 52, no. 4, pp. 609–638, 1972.
- [11] B. E. Launder, G. J. Reece, and W. Rodi, "Progress in the development of a Reynolds-stress turbulence closure," *J. Fluid Mech.*, vol. 68, no. 3, p. 537, 1975.
- [12] I. ANSYS, *Fluent Theory Guide*. 2015.
- [13] J. Y. Wang, G. H. Priestman, and J. R. Tippetts, "Modelling of strongly swirling flows in a complex geometry using unstructured meshes," *Int. J. Numer. Methods Heat Fluid Flow*, vol. 16, no. 7–8, pp. 910–926, 2006.
- [14] U. Schumann, "Realizability of Reynolds-stress turbulence models," *Phys. Fluids*, vol. 20, no. 5, p. 721, 1977.
- [15] S.-E. Kim, D. Choudhury, and B. Patel, "Computations of Complex Turbulent Flows Using the Commercial Code Fluent," in *Modeling Complex Turbulent Flows*, M. D. Salas, J. N. Hefner, and L. Sakell, Eds. Dordrecht: Springer Netherlands, 1999, pp. 259–276.
- [16] J. Ströhle and T. Myhrvold, "An evaluation of detailed reaction mechanisms for hydrogen combustion under gas turbine conditions," *Int. J. Hydrogen Energy*, vol. 32, no. 1, pp. 125–135, 2007.
- [17] J. Li, Z. Zhao, A. Kazakov, and F. L. Dryer, "An updated comprehensive kinetic model of hydrogen combustion," *Int. J. Chem. Kinet.*, vol. 36, no. 10, pp. 566–575, 2004.
- [18] M. Ó Conaire, H. J. Curran, J. M. Simmie, W. J. Pitz, and C. K. Westbrook, "A comprehensive modeling study of hydrogen oxidation," *Int. J. Chem. Kinet.*, vol. 36, no. 11, pp. 603–622, 2004.
- [19] M. Goswami, E. N. Volkov, A. a. Konnov, R. J. M. Bastiaans, and L. R. H. de Goey, "Updated Kinetic Mechanism for NO_x Prediction and Hydrogen Combustion," no. x, pp. 1–28, 2008.
- [20] N. Peters, "Laminar flamelet concepts in turbulent combustion," *Symp. Combust.*, vol. 21, no. 1, pp. 1231–1250,

1986.

- [21] L. P. H. De Goey and J. H. M. Ten Thijsse Boonkamp, "A flamelet description of premixed laminar flames and the relation with flame stretch," *Combust. Flame*, vol. 119, no. 3, pp. 253–271, 1999.
- [22] S. B. Pope, "The probability approach to the modelling of turbulent reacting flows," *Combust. Flame*, vol. 27, pp. 299–312, 1976.
- [23] S. B. Pope, "PDF methods for turbulent reactive flows," *Prog. Energy Combust. Sci.*, vol. 11, no. 2, pp. 119–192, 1985.
- [24] A. T. Hsu, M. S. Anand, and M. K. Razdan, "Calculation of a Premixed Swirl Combustor Using the PDF Method," *Am. Soc. Mech. Eng.*, 1997.
- [25] J. a. Van Oijen and L. P. H. De Goey, "Modelling of Premixed Laminar Flames using Flamelet-Generated Manifolds," *Combust. Sci. Technol.*, vol. 161, no. May 2016, pp. 113–137, 2000.
- [26] W. J. S. Ramaekers, B. a. Albrecht, J. a. Van Oijen, L. P. H. de Goey, and R. G. L. M. Eggels, "The application of Flamelet Generated Manifolds in modelling of turbulent partially-premixed flames," *Proc. Fluent Benelux User Gr. Meet. (pp. 3D). Belgium, Château Limelette*, pp. 1–16, 2005.
- [27] B. F. Magnussen, "On the structure of turbulence and a generalized eddy dissipation concept for chemical reaction in turbulent flow," *19th American Institute of Aeronautics and Astronautics Aerospace Science Meeting*. pp. 1–6, 1981.
- [28] I. S. Ertesvåg and B. F. Magnussen, "The Eddy Dissipation Turbulence Energy Cascade Model," *Combust. Sci. Technol.*, vol. 159, no. 1, pp. 213–235, 2000.
- [29] B. F. Magnussen, "THE EDDY DISSIPATION CONCEPT A BRIDGE BETWEEN SCIENCE AND TECHNOLOGY Invited paper at ECCOMAS Thematic Conference on Computational Combustion , Lisbon , June 21-24 , 2005 THE EDDY DISSIPATION CONCEPT A BRIDGE BETWEEN SCIENCE AND," *Eccomas*, 2005.
- [30] J. M. Powers, "Intrinsic Low-Dimensional Manifold Method for Rational Simplification of Chemical Kinetics," *Rev. Lit. Arts Am.*, 1999.
- [31] P. D. Nguyen, L. Vervisch, V. Subramanian, and P. Domingo, "Multidimensional flamelet-generated manifolds for partially premixed combustion," *Combust. Flame*, vol. 157, no. 1, pp. 43–61, 2010.
- [32] G. Lodier, L. Vervisch, V. Moureau, and P. Domingo, "Composition-space premixed flamelet solution with differential diffusion for in situ flamelet-generated manifolds," *Combust. Flame*, vol. 158, no. 10, pp. 2009–2016, 2011.
- [33] TU Eindhoven, "FGM combustion," 2015. [Online]. Available: www.fgm-combustion.org.
- [34] S. James, M. S. Anand, M. K. Razdan, and S. B. Pope, "In Situ Detailed Chemistry Calculations in Combustor Flow Analyses," *J. Eng. Gas Turbines Power*, vol. 123, no. 4, p. 747, 2001.
- [35] S. B. Pope, "Computationally efficient implementation of combustion chemistry using in situ adaptive tabulation," *Combust. Theory Model.*, vol. 1, no. 1, pp. 41–63, 1997.
- [36] D. L. Daggett, R. C. Hendricks, R. Walther, and E. Corporan, "Alternate Fuels for use in Commercial Aircraft," *Most*, no. April, pp. 2007–1196, 2007.
- [37] H. Nojumi, I. Dincer, and G. F. Naterer, "Greenhouse gas emissions assessment of hydrogen and kerosene-

- fueled aircraft propulsion," *Int. J. Hydrogen Energy*, vol. 34, no. 3, pp. 1363–1369, 2009.
- [38] B. Khandelwal, A. Karakurt, P. R. Sekaran, V. Sethi, and R. Singh, "Hydrogen powered aircraft: The future of air transport," *Prog. Aerosp. Sci.*, vol. 60, pp. 45–59, 2013.
- [39] A. Silverstein and W. H. Eldon, "Liquid Hydrogen as a Jet Fuel for High-Altitude Aircraft," Cleveland, Ohio, 1955.
- [40] S. Weiss, "The Use of Hydrogen for Aircraft Propulsion in View of the Fuel Crisis," Cleveland, Ohio, 1973.
- [41] R. O. Price, "Liquid hydrogen - an alternative aviation fuel?," *Int. J. Hydrogen Energy*, vol. 16, no. 8, pp. 557–562, 1991.
- [42] V. Sosounov and V. Orlov, "Experimental Turbofan Using Liquid Hydrogen and Liquid Natural Gas as Fuel," *AIAA 26th Jt. Propuls. Conf.*, 1990.
- [43] F. Svensson, A. Hasselrot, and J. Moldanova, "Reduced environmental impact by lowered cruise altitude for liquid hydrogen-fuelled aircraft," *Aerosp. Sci. Technol.*, vol. 8, no. 4, pp. 307–320, 2004.
- [44] S. Boggia and A. Jackson, "Some unconventional aero gas turbines using hydrogen fuel," in *ASME Turbo Expo 2002 Power for Land, Sea, and Air*, 2002, pp. 683–690.
- [45] J. Ziemann, F. Shum, M. Moore, D. Kluyskens, D. Thomaier, N. Zarzalis, and H. Eberius, "Low-NOx combustors for hydrogen fueled aero engine," *Int. J. Hydrogen Energy*, vol. 23, no. 4, pp. 281–288, 1998.
- [46] J. Brand, S. Sampath, and F. Shum, "Potential Use of Hydrogen in Air Propulsion," *AIAA/ICAS Int. Air Sp. Symp. Expo. Next 100 Years, Dayton, OH, AIAA--2003--2879*, no. July, pp. 1–11, 2003.
- [47] F. Haglind and R. Singh, "Design of Aero Gas Turbines Using Hydrogen," *J. Eng. Gas Turbines Power*, vol. 128, no. 4, pp. 754–764, 2004.
- [48] C. J. Marek, T. D. Smith, and K. Kundu, "Low Emission Hydrogen Combustors for Gas Turbines Using Lean Direct Injection," *41st AIAA/ASME/SAE/ASEE Jt. Propuls. Conf. Exhib.*, no. July, pp. 1–27, 2005.
- [49] D. Crunteany and R. Isac, "Investigation of low emission combustors using hydrogen lean direct injection," *Incas Bull.*, vol. 3, no. 3, pp. 45–52, 2011.
- [50] G. Dahl and F. Suttrop, "Engine control and low-NOx combustion for hydrogen fuelled aircraft gas turbines," *Int. J. Hydrogen Energy*, vol. 23, no. 8, pp. 695–704, 1998.
- [51] G. Corchero and J. L. Montaños, "An approach to the use of hydrogen for commercial aircraft engines," vol. 219, pp. 35–44, 2005.
- [52] A. T-Raissi and D. L. Block, "Hydrogen: Automotive fuel of the future," *IEEE Power Energy Mag.*, vol. 2, no. 6, pp. 40–45, 2004.
- [53] M. J. Sefain, "Hydrogen Aircraft Concepts & Ground Support," Cranfield University, 2000.
- [54] Y. Levy, V. Sherbaum, V. Erenburg, V. Krapp, C. O. Paschereit, T. Reichel, and J. Grey, "Chemical Kinetics of the Hybrid Combustion System," 2012.
- [55] T. Reichel and Y. Levy, "Feasibility of the hybrid combustion concept," pp. 1–15, 2014.
- [56] A. G. Rao, "AHEAD: Advanced Hybrid Engines for Aircraft Development." 2011.
- [57] M. Ilbas, A. P. Crayford, I. Yilmaz, P. J. Bowen, and N. Syred, "Laminar-burning velocities of hydrogen-air and hydrogen-methane-air mixtures: An experimental study," *Int. J. Hydrogen Energy*, vol. 31, no. 12, pp. 1768–1779, 2006.

- [58] T. G. Reichel, S. Terhaar, and O. Paschereit, "Increasing Flashback Resistance in Lean Premixed Swirl-Stabilized Hydrogen Combustion by Axial Air Injection," *J. Eng. Gas Turbines Power*, vol. 137, no. 7, p. 71503, 2015.
- [59] D. J. Beerer and V. G. McDonell, "Autoignition of Hydrogen and Air Inside a Continuous Flow Reactor With Application to Lean Premixed Combustion," *J. Eng. Gas Turbines Power*, vol. 130, no. 5, p. 51507, 2008.
- [60] J. Fritz, M. Kröner, and T. Sattelmayer, "Flashback in a Swirl Burner With Cylindrical Premixing Zone," *J. Eng. Gas Turbines Power*, vol. 126, no. 2, p. 276, 2004.
- [61] K. Döbbeling, J. Hellat, and H. Koch, "25 Years of BBC/ABB/Alstom Lean Premix Combustion Technologies," *J. Eng. Gas Turbines Power*, vol. 129, no. 1, p. 2, 2007.
- [62] T. Lieuwen, V. McDonell, E. Petersen, and D. Santavicca, "Fuel Flexibility Influences on Premixed Combustor Blowout, Flashback, Autoignition, and Stability," *J. Eng. Gas Turbines Power*, vol. 130, no. 1, p. 11506, 2008.
- [63] V. N. Kurdyumov, E. Fernández, and A. Liñán, "Flame flashback and propagation of premixed flames near a wall," *Proc. Combust. Inst.*, vol. 28, no. 2, pp. 1883–1889, 2000.
- [64] F. Biagioli and F. Güthe, "Effect of pressure and fuel-air unmixedness on NO_x emissions from industrial gas turbine burners," *Combust. Flame*, vol. 151, no. 1–2, pp. 274–288, 2007.
- [65] T. G. Reichel, S. Terhaar, and C. O. Paschereit, "Flow Field Manipulation by Axial Air Injection to Achieve Flashback Resistance and its Impact on Mixing Quality," *43rd Fluid Dyn. Conf.*, no. x, pp. 1–12, 2013.
- [66] T. Reichel and C. O. Paschereit, "Experimental Investigation of Flame Stability of Swirl-Stabilized, Lean Premixed Hydrogen Flames," 2014.
- [67] T. G. Reichel, K. Goeckeler, and O. Paschereit, "Investigation of Lean Premixed Swirl-Stabilized Hydrogen Burner With Axial Air Injection Using OH-PLIF Imaging," *J. Eng. Gas Turbines Power*, vol. 137, no. 11, p. 111513, 2015.
- [68] R. W. Schefer, D. M. Wicksall, and A. K. Agrawal, "Combustion of hydrogen-enriched methane in a lean premixed swirl-stabilized burner," *Proc. Combust. Inst.*, vol. 29, no. 1, pp. 843–851, 2002.
- [69] H. S. Kim, V. K. Arghode, M. B. Linck, and A. K. Gupta, "Hydrogen addition effects in a confined swirl-stabilized methane-air flame," *Int. J. Hydrogen Energy*, vol. 34, no. 2, pp. 1054–1062, 2009.
- [70] M. Emadi, D. Karkow, T. Salameh, A. Gohil, and A. Ratner, "Flame structure changes resulting from hydrogen-enrichment and pressurization for low-swirl premixed methane-air flames," *Int. J. Hydrogen Energy*, vol. 37, no. 13, pp. 10397–10404, 2012.
- [71] A. Lantz, R. Collin, M. Aldén, A. Lindholm, J. Larfeldt, and D. Löstad, "Investigation of Hydrogen Enriched Natural Gas Flames in a SGT-700/800 Burner Using OH PLIF and Chemiluminescence Imaging," *Proc. ASME Turbo Expo, June 16-20, Düsseldorf, Ger.*, vol. 137, no. March, pp. 1–11, 2015.
- [72] A. Lindholm, D. Löstad, P. Magnusson, P. Andersson, and T. Larsson, "Combustion stability and emissions in a lean premixed industrial gas turbine burner due to changes in the fuel profile," in *ASME Turbo Expo 2009: Power for Land, Sea, and Air*, 2009, pp. 341–350.
- [73] P. V. Danckwerts, "The definition and measurement of some characteristics of mixtures," *Appl. Sci. Res. Sect. A*, vol. 3, no. 4, pp. 279–296, 1952.
- [74] I. Roehle, R. Schodl, P. Voigt, and C. Willert, "Recent developments and applications of quantitative laser light sheet measuring techniques in turbomachinery components," *Meas. Sci. Technol.*, vol. 11, no. 7, pp. 1023–1035,

2000.

- [75] H. M. AbdelGayed, W. A. Abdelghaffar, and K. El Shorbagy, "Main flow characteristics in a lean premixed swirl stabilized gas turbine combustor – Numerical computations," *Am. J. Sci. Ind. Res.*, no. 2003, pp. 123–136, 2013.
- [76] Z. Mansouri, M. Aouissi, and T. Boushaki, "Numerical computations of premixed propane flame in a swirl-stabilized burner: Effects of hydrogen enrichment, swirl number and equivalence ratio on flame characteristics," *Int. J. Hydrogen Energy*, vol. 41, no. 22, pp. 9664–9678, 2016.
- [77] T. Tanneberger, T. G. Reichel, O. Krüger, S. Terhaar, and C. O. Paschereit, "Numerical Investigation of the Flow Field and Mixing in a Swirl-Stabilized Burner With a Non-Swirling Axial Jet," in *ASME Turbo Expo 2015: Turbine Technical Conference and Exposition*, 2015, p. V04BT04A026--V04BT04A026.
- [78] P. M. Anacleto, E. C. Fernandes, M. V. Heitor, and S. I. Shtork, "Swirl flow structure and flame characteristics in a model lean premixed combustor," *Combust. Sci. Technol.*, vol. 175, no. 8, pp. 1369–1388, 2003.
- [79] N. Syred and J. M. Beér, "Combustion in Swirling Flows : A FReview," *Combust. Flame*, vol. 201, no. 2, pp. 143–201, 1974.
- [80] H. J. Sheen, W. J. Chen, S. Y. Jeng, and T. L. Huang, "Correlation of Swirl Number for a Radial-Type Swirl Generator," *Exp. Therm. Fluid Sci.*, vol. 12, no. 4, pp. 444–451, 1996.
- [81] S. Terhaar, T. Reichel, and C. Schrödinger, "Vortex Breakdown and Global Modes in Swirling Combustor Flows with Axial Air Injection," *43rd Fluid Dyn. Conf.*, vol. 31, no. 1, pp. 1–16, 2013.
- [82] T. Kathrotia, U. Riedel, and J. Warnatz, "A numerical study on the relation of OH*, CH*, and C2* chemiluminescence and heat release in premixed methane flames," *Proc. Eur. Combust. Meet.*, no. July 2016, pp. 2–6, 2009.
- [83] R. Sadanandan, M. Stöhr, and W. Meier, "2008-Simultaneous OH-PLIF and PIV measurements in a gas turbine model combustor.pdf," vol. 90, pp. 609–618, 2008.